"In presenting the dissertation as a partial fulfillment of the requirements for an advanced degree from the Georgia Institute of Technology, I agree that the Library of the Institution shall make it available for inspection and circulation in accordance with its regulations governing materials of this type. I agree that permission to copy from, or to publish from, this dissertation may be granted by the professor under whose direction it was written, or, in his absence, by the dean of the Graduate Division when such copying or publication is solely for scholarly purposes and does not involve potential financial gain. It is understood that any copying from, or publication of, this dissertation which involves potential financial gain will not be allowed without written permission.

_____

_____"

THE INFLUENCE OF METEOR RADIANT DISTRIBUTIONS ON RADIO-ECHO RATES

A THESIS

Presented to

the Faculty of the Graduate Division

by

Jesse Clopton James

In Partial Fulfillment

of the Requirements for the Degree

Doctor of Philosophy

in Electrical Engineering

Georgia Institute of Technology

May, 1958

72
127

THE INFLUENCE OF METEOR RADIANT DISTRIBUTIONS ON RADIO-ECHO RATES

Approved:

M. L. Meeks

F. Kenneth Hurd

John Taylor

Date Approved by Chairman: May 29, 1958

DEDICATION

In return for constant
encouragement, patience,
and help, this thesis is
gratefully dedicated
to my wife, Barbara.

ACKNOWLEDGEMENTS

The work reported here was supported principally by the Office of Naval Research under Contract No. NOnr-991(02). The data presented for the Atlanta-Boston and Columbia-Boston paths were collected under Air Force Contract No. AF 19(604)-1593.

Because this research was also a thesis problem and because sufficient funds were not available to complete the theoretical analysis, a considerable amount of electronic computer time was made available without charge. The author is indeed grateful to those at the Georgia Institute of Technology who are responsible for this policy, in particular, Dr. William F. Atchison, director of the Rich Electronic Computer Center.

The work reported on here is the result of the contributions of many people over the last three years. Principally among these was Dr. M. L. Meeks who was the author's thesis adviser and to whom the author is greatly indebted. His inspiration, guidance, and assistance was invaluable to this research. The author also acknowledges the contributions of Dr. John Taylor and Mr. John S. Hollis whose suggestions and assistance materially affected the outcome of this work.

The author appreciates the suggestions and cooperation of the meteor-scatter group at the University of Tennessee. He is indebted for the splendid cooperation of the transmitter operators there in helping perform experiments.

The author also expresses thanks to his associates at the Engineering Experiment Station who helped install, operate, and repair equipment and reduce the data.

TABLE OF CONTENTS

LIST OF TABLES

LIST OF ILLUSTRATIONS

SUMMARY

The use of meteor trails as reflectors of radio waves provides a method of sending radio messages to distances beyond the horizon. For a long time the ionized layers of the upper atmosphere have been used for this purpose. However, these ionized layers are not always effective at radio frequencies greater than 15 to 40 megacycles. But meteor trails provide dense columns of ionization which will reflect radio waves of even higher frequencies for a short time. Therefore, meteor-trail communication is being increasingly studied because there is an ever increasing demand for additional channels of radio communication.

This research was concerned with certain aspects of the usefulness of these meteor trails as reflectors. Specifically, a study has been made to determine how the number of meteor signals received per unit of time varies with the time of day and the month of the year over an arbitrary meteor trail communication link. An additional result has been the development of a basis for predicting the relative number of useable meteor trails in various regions of the sky. The number of useable trails at a given region of the sky is dependent on the radiant distribution, which is the distribution of points on the celestial sphere from which the meteors appear to come. The effect of radiant distributions on meteor-trail communication was studied, and this effect was demonstrated by a number of computations based on several different radiant distributions. The computed results were compared with experimental data taken by workers at the Georgia Institute of Technology and with some experimental results of others.

Two analyses were first made on the basis of two highly idealized radiant distributions, the uniform and the ecliptic. For the uniform distribution the radiants were assumed to be evenly distributed over the entire celestial sphere, and the results essentially led to a measure of the geometrical effectiveness of various parts of the sky. However, the uniform-distribution analysis of course completely failed to predict the characteristic diurnal variations in meteor signal rate which are always observed experimentally.

For the ecliptic radiant distribution all radiants were assumed to be spread uniformly on the ecliptic. This distribution represented an approximation in much the same sense that the uniform distribution was an approximation but from an opposite point of view. This analysis led to a strong diurnal variation in meteor signal rate but did not take into account the geometrical effectiveness of various sky regions.

An analysis was also made of the effects of a single point-radiant. It was found that a point-radiant leads to a narrow band across the sky from which reflections may come. The analysis also included the computation of a measure of effectiveness along this band. Some very favorable comparisons were made between these point-radiant results and experimental data taken during meteor showers over the Atlanta-Knoxville meteor scatter link.

It was shown that the point-radiant results may be used as a basis for analyses of arbitrary radiant distributions. The procedures in such cases is to compute the effect of each point-radiant individually and then to weight and superimpose the results. An approximation to the

sporadic radiant distribution was made in this manner by using three point-radiants having equal weight. Several computations made on the basis of this three-point approximation were found to agree well with experiment.

Three meteor-scatter links operated by the author and his associates were used to obtain data for comparison with theory. These links are the Atlanta-Knoxville, Atlanta-Boston and Columbia-Boston paths. The characteristics of each link and the method of reducing the data is described.

CHAPTER I

INTRODUCTION

Many have observed a meteor as it streaks across the nighttime sky. But perhaps few have realized the part that these ephemeral events may soon play in radio communication. Each meteor produces a long thin trail of free electrons and ionized molecules that can reflect radio signals and thus permit radio communication around the curvature of the earth. As is well known, the ionized layers of the upper atmosphere which are now used to reflect radio waves toward distant points beyond the horizon are not effective at frequencies greater than about 30 megacycles per second. Meteor trails provide dense columns of ionization which will reflect even higher frequencies for the brief interval of a second or less during which time most of the trails diffuse and become ineffective as reflectors. The need for such reflected signals is rapidly increasing. Already the channels of communication at the lower radio frequencies are becoming crowded because each additional radio channel requires a small additional band in the frequency spectrum. But meteor trails can alleviate this situation by providing effective reflectors for additional frequency channels at higher frequencies.

The purpose of the research reported here is to investigate certain aspects of the usefulness of these meteor trails as reflectors. Specifically, an attempt has been made to determine how the number of meteor signals received per unit of time varies with the time of day and

the month of the year over an arbitrary meteor-scatter communication link. An additional aim has been to develop a basis for evaluating the relative number of useable meteor trails in various regions of the sky.

A meteor trail is formed by the evaporation of a meteoroid (or primary meteor particle) having typically a few milligrams of mass, as it moves rapidly through the air[1]. The subsequent collisions between evaporated meteoroid atoms and the molecules of the upper atmosphere form a trail of ionization. These trails have typical lengths of from 15 to 35 kilometers and are essentially long straight columns of ionized molecules and electrons that diffuse rapidly in the rare upper atmosphere. Trails are known to occur in a region, called the "meteor-trail zone," that lies roughly between 80 and 120 kilometers above the earth's surface[2,3].

In order to be useable as a reflector, a trail must be oriented so that the bisector of the angle formed between the directions of propagation of the incident wave from the transmitter and the reflected wave toward the receiver is perpendicular to the trail axis (non-specular reflection is of secondary importance). The orientation of a trail is determined by the coordinates of the point on the celestial sphere from which the meteor appears to have come. This point is called the "meteor radiant."

On certain dates each year many meteors can be observed that appear to radiate from the same spot, or radiant, among the stars. These events are called "meteor showers" and occur when the earth moves through a stream of meteor particles all traveling approximately along the same path around the sun. Meteor showers represent only about 5 per cent of

the total meteor influx to the earth[4]. The remainder is due to "sporadic meteors" whose radiants are distributed over the entire celestial sphere. The way in which this sporadic radiant distribution affects meteor-trail communication is the principal area of investigation of this study.

Whether or not a given meteor trail can reflect a useable signal in the desired direction depends on its orientation and position with regard to the transmitter and receiver and on the number of free electrons initially formed per unit of trail length. The arrival of meteoroids is a random process and it can be assumed that on the average the meteor flux is the same at all points over a horizontal surface above the earth in the neighborhood of a given transmitter and receiver.

The distributions of trail orientation and ionization densities are not known with precision. If the distribution of these quantities were accurately known, the usefulness of various sky regions could be determined in principle, although the calculation would be long and intricate on account of purely geometrical difficulties. The available information indicates that for sporadic meteors the radiants tend to be concentrated near the ecliptic with three strong concentrations respectively toward the apex of the earth's way and roughly toward the sun and anti-sun[4,5]. In addition, radiants of the principal meteor showers have been determined with considerable precision by visual and photographic techniques.

The distributions of free electron line densities have been measured for both shower and sporadic meteors, and the results can be fitted by an empirical expression of the form

$$N_o(q) = \frac{K}{q^k} \qquad (1)$$

where $N_o(q)$ is the number of meteor trails having electron densities greater than q which pass through unit area per second, and K and k are constants. The best fit to experimental data on sporadic meteors is obtained for $k = 1$, while for the major showers, k has been estimated to be somewhat less than 1.

For a given transmitter and receiver on the earth's surface, it is desirable to know the contribution of each region of the sky to the signal communicated by meteor-trail reflections. This investigation is both a theoretical and experimental study of this problem. The theoretical procedure is to analyze the problem for various assumed radiant distributions beginning with the simplest and most easily analyzed distribution and proceeding toward more realistic distributions. Each of these analyses affords a better understanding of the effects of various types of radiant distributions.

The results of the analyses based on the various radiant distributions are compared with experimental data taken at the Georgia Institute of Technology over three meteor scatter links and with published data of others. The experimental data are in the form of diurnal distributions of the number of times per minute that the received signal due to meteor-trail reflection rises above a threshold level. Ordinarily a burst of signal above the threshold is the result of a single meteor trail and such a burst is called a "meteor echo."

CHAPTER II

DEVELOPMENT OF EQUATIONS FOR PREDICTING METEOR ECHO RATES

The problem to be considered in this chapter is the computation of the relative rate at which meteor echoes are received as a function of time for a given transmitter and receiver. The procedure will be to determine the number of echoes observed at the receiver per unit time from a unit volume of space and then to integrate this number over the illuminated portion of the meteor-trail zone. This zone is considered relatively thin and therefore in many cases can be represented by a surface at a height of h kilometers above the earth. Initially then the problem is to determine the number of echoes received per minute that are associated with a unit area of this so-called h-surface.

The magnitude of a meteor echo is a function of the ionization density of the reflecting trail. Hence it is necessary to consider the theory of meteoric ionization. This theory was developed first by Whipple[6] and Herlofson[7] and later reviewed by Kaiser[8]. According to this theory the number q of free electrons per meter of trail length may be written as

$$q = mf(p,v) \cos \zeta, \tag{2}$$

where m is the initial meteoroid mass, ζ is the zenith angle of the trail axis, and $f(p,v)$ represents the functional dependence of q on atmospheric

pressure p and meteor velocity v. For the purposes of the present development a suitable average over p and v is made. After the averaging process this equation essentially says that the ionization density is proportional to m cos ζ. Thus an expression consistent with (1) for the distribution of meteoroid masses arriving from a given radiant point is taken to be

$$N_1(m) = \frac{\text{const.}}{m^k} \tag{3}$$

where $N_1(m)$ is the number of meteor particles with masses greater than m.

The desired expression for the meteor flux from an arbitrary radiant results from a combination of equations (2) and (3). This expression is

$$N(q) = R \left(\frac{\cos \zeta}{q} \right)^k \tag{4}$$

where $N(q)$ is the total number of trails per second per normal unit area having ionization densities exceeding q. The parameter R is assumed constant for a given radiant but its absolute value is of no consequence here since we are only interested in relative meteor rates.

Echoes of sufficient magnitude to be observed at the receiver must result from trails that have ionization densities exceeding some threshold value q_o. If this threshold value is known, then the number of echoes associated with a horizontal unit area of the h-surface and with an arbitrary radiant is given by $N(q_o) \cos \zeta$.

The value of q_o is determined by considering the amplitude of the signal received from a single trail. This received power will vary directly as the transmitted power and as the antenna gains in the

respective directions to the reflecting trail. The received signal will also be proportional to a polarization factor, S^2, given by the square of the dot product of unit vectors in the directions of the transmitted and received electric fields at the trail. The received signal is subject to the free space attenuation factor which in this case varies inversely as the square of the product of the ranges from transmitter to trail and trail to receiver. Other factors affecting the received power from a single trail are the effective reflecting area of an electron and the effective number of electrons contributing to the reflection.

As the trail diffuses all waves scattered by individual electrons do not remain in phase, and the reflected signal decreases exponentially. By assuming that only the electrons within the principal Fresnel zone contribute to the reflection, Eshleman has derived an equation embodying the above factors for the received power from a single properly-oriented trail[9]. Eshleman's equation modified to include a general polarization factor is

$$P_r = \frac{P_t}{16\pi^4}\left(\frac{\mu_o e^2}{4m}\right)^2 \frac{\lambda^3}{R_1 R_2 (R_1+R_2)} \frac{G_r\, G_t\, q^2\, S^2}{1-\cos^2\beta\sin^2\phi} \exp\left(\frac{-32\pi^2 td}{\lambda^2 \sec^2\phi}\right) \qquad (5)$$

where

P_r and P_t are the received and transmitted powers,

μ_o is the permeability of free space,

e and m are the electronic charge and mass,

λ is the wavelength,

R_1 and R_2 are ranges from trail to transmitter and receiver,

G_t and G_r are antenna gains,

2ϕ is the angle between lines along R_1 and R_2,

S is the dot product of a unit incident electric vector and a unit vector of the reflected wave in the direction of the polarization of the receiving antenna,

β is the angle between the axis of the meteor trail and the plane containing the transmitter, receiver and meteor trail,

d is the diffusion coefficient, and

t is the time elapsed since formation of the trail.

All quantities in this equation are expressed in m.k.s. units. The geometry is shown in Figure 1. In deriving this equation Eshleman assumed a meteor trail to be represented by a long circular cylinder having uniform ionization along its length and having a Gaussian distribution of ionization in cross section. Free passage of radio waves through the trail was also assumed which means that the equation holds for q less than some critical value. For values of q which exceed this critical value, total reflection occurs, and then as q is further increased the initial amplitude of the reflected signal remains constant but the time duration of the echo increases. Such trails are called "overdense" or "long-enduring" trails and as indicated by Equation (1) are relatively rare.

The expression for q_o may now be found by solving Equation (5) for q after setting $t = 0$ and $P_r = P_m$ where P_m is the minimum detectable power in the receiver. Thus q_o becomes

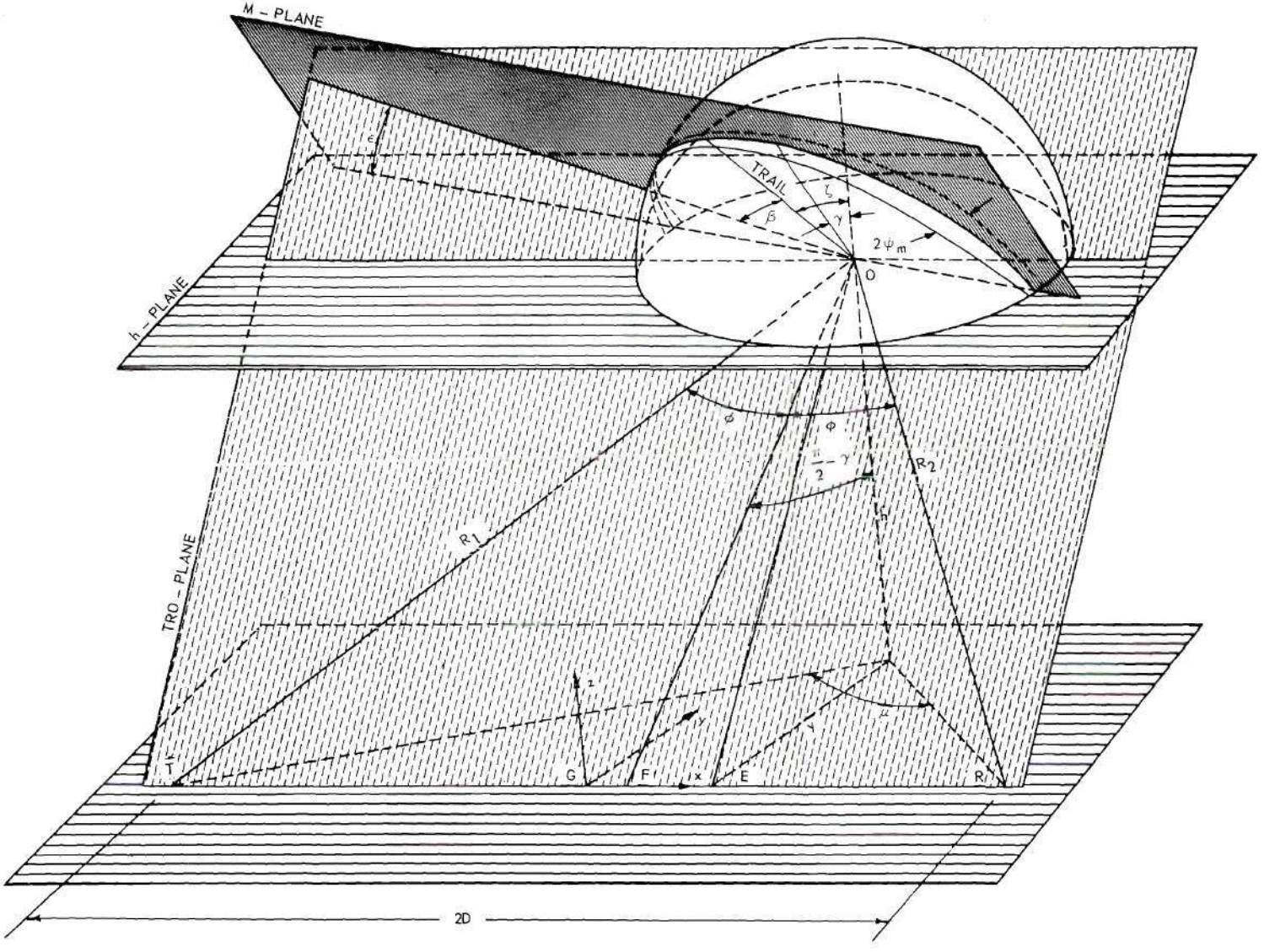

Figure 1. Geometry of the Reflection from a Meteor Trail.

$$q_o = \left[\frac{P_m}{P_t} \frac{1 - \cos^2 \beta \sin^2 \phi}{Q} \right]^{1/2} \tag{6}$$

where

$$Q = \frac{1}{16\pi^4} \left(\frac{\mu_o e^2}{4m} \right)^2 \frac{\lambda^3}{R_1 R_2 (R_1 + R_2)} G_r G_t S^2 \tag{7}$$

An analysis based on a uniform radiant distribution.--It will first be assumed that the sporadic meteor radiants are distributed uniformly over the entire celestial sphere. An analysis based on this distribution has been previously made by Eshleman and Manning[9], however, the analysis presented here involves fewer approximations. Hines and Pugh[10,11] have also independently performed and reported work equivalent to the analysis presented here[12].

The procedure is to compute the number of observable echoes associated with an arbitrary unit area of the h-surface, which is done by integrating $N(q_o) \cos \zeta$ over those radiants yielding properly-oriented trails. $N(q)$ now refers to the number of trails arriving from a unit solid angle of the celestial sphere. Eshleman and Manning[9] have shown for the uniform distribution that the useful radiants fall within a narrow band of the celestial sphere having an approximate width of $2\psi_m$ (see Figure 1) where

$$\psi_m = \frac{L (R_1 + R_2)}{4 R_1 R_2 \cos \phi} (1 - \sin^2 \phi \cos^2 \beta) \tag{8}$$

Here L is the mean length of the trails and it is assumed that $L \ll R_1$ and R_2. Results equivalent to (8) when L is assumed proportional to sec ζ have been derived in quite different fashions by both Pugh[10] and Meeks[13]. That it is proper to set the mean trail length proportional to sec ζ is indicated by the theory of meteoric ionization[8]. The useful region of the celestial sphere then will be taken to be $2\psi_m$ sec ζ where L is a constant. This band lies on the celestial hemisphere visible to an earth observer and is symmetrical about the intersection of the M-plane with the celestial hemisphere. The M-plane is perpendicular to the bisector of lines along R_1 and R_2 as shown in Figure 1.

As a convenient but good approximation, the surface integration of $N(q_o)$ cos ζ over the relatively narrow $2\psi_m$ sec ζ band will be replaced by a line integration along the center line of the band.

The desired result then for the number, n, of observable echoes associated with an arbitrary unit area of the h-surface is

$$n = \int_{-\epsilon}^{\pi-\epsilon} 2\psi_m \, N(q_o) \, d\beta, \tag{9}$$

where the angles β and ϵ are shown in Figure 1 and defined in the Glossary of Notations and Definitions given in the Appendix.

In principle n can be evaluated for specific cases at points over the h-surface. In practice this computation is very lengthy because of the complexity of the explicit expression for n; in fact closed forms of the integral in (9) have been obtained only for k = 1 and 2. However,

evaluations of n have been obtained by the use of a high-speed digital computer*. Samples of these computations will be shown later.

The computer program for the n-computation was written so that another factor f would be simultaneously computed. This f-factor represents the "duty cycle" of meteor echoes, that is, f is the sum of the durations above noise of individual signals occurring per second from a unit h-surface area. Echo duty cycle is often of more importance than echo rate for the communications engineer, and as will be shown does not vary with h-surface position in the same fashion as does echo rate. The derivation of f proceeds as follows.

The duration above noise of an echo from a single trail is determined from Equation (5) by solving for t with P_r replaced by P_m. This duration time τ is

$$\tau(q) = \frac{\lambda^2 \sec^2 \phi}{16\pi^2 d} \log_e \frac{q}{q_o} \tag{10}$$

Each echo is now multiplied by its duration τ and the integration over the $2\psi_m$ sec ϕ band is performed. The result is expressed as

$$f = -\int_{-\epsilon}^{\pi-\epsilon} \int_{q_o}^{\infty} 2\psi_m \frac{\partial N(q)}{\partial q} \tau(q)\, dq d\beta$$

$$= \frac{\lambda^2}{16\pi^2 d} \frac{\sec^2 \phi}{k} n, \tag{11}$$

---

*The UNIVAC SCIENTIFIC ERA 1101 at the Rich Electronic Computer Center was used.

where $-\frac{\partial N(q)}{\partial q}$ represents the number of trails per unit q. Note that the ratio of f to n will be largest near the path midpoint where ϕ is largest.

A total of nine computations are presented as Figures 2 through 10 to illustrate the uniform-distribution effect on echo rate and duty cycle for various sets of parameters. Contour lines of constant n or f have been drawn over one quadrant of the projected h-surface; the other quadrants are mirror images in the x and y axes. The coordinate system is shown in Figure 1 in which the x-axis is along a straight line between transmitter and receiver and the y axis intersects the x-axis as a horizontal line at the path midpoint. The two stations are at x = D and x = -D respectively.

The contour values in Figures 2 through 10 have been determined for constant values of the parameters λ, d, P_t, P_m, G_r, and G_t. In a particular case, the factor $[G_r G_t]^{k/2}$ can be put back in by integrating the product of this factor with n or f over the illuminated portion of the h-surface. The absolute contour values have so significance.

Figures 2 through 4 show f-contours for a 250 kilometer path, for k = 1.00, and for z = 100 kilometers, which indicates a flat-earth approximation. Figure 2 is for optimum polarization which is had by setting S = 1. Figure 3 applies when one antenna illuminates the point in question with horizontal polarization and the other antenna is adjusted for optimum reception, and Figure 4 applies for horizontal polarizations on both antennas. The contour values in these three figures have been worked out on a consistent basis so that they may be compared. As the polarization is changed from optimum in Figure 2 to horizontal

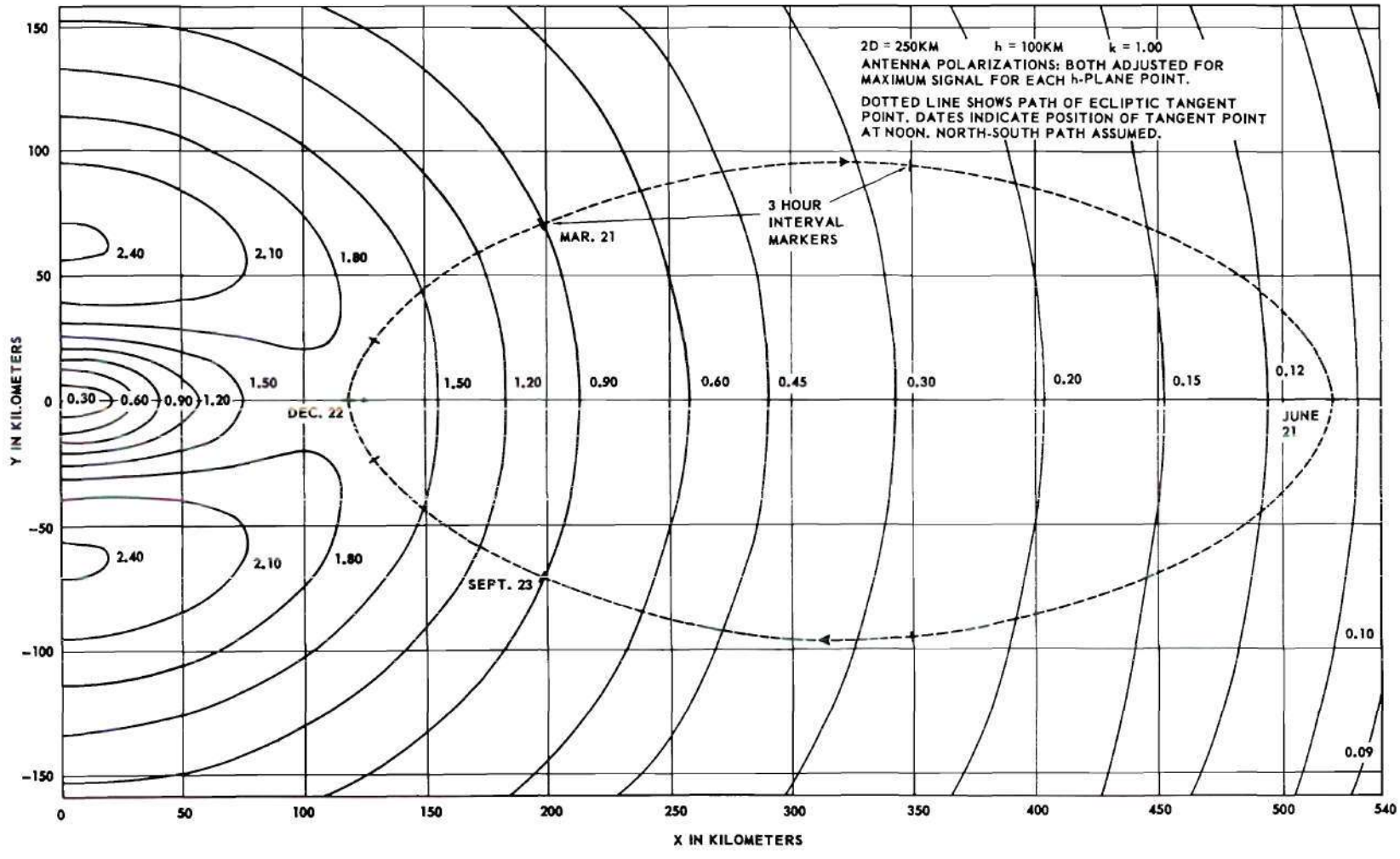

Figure 2. A Distribution of Sources of Signal Duration Above a Given Amplitude Level with Optimum Polarization for Each Illuminated Point.

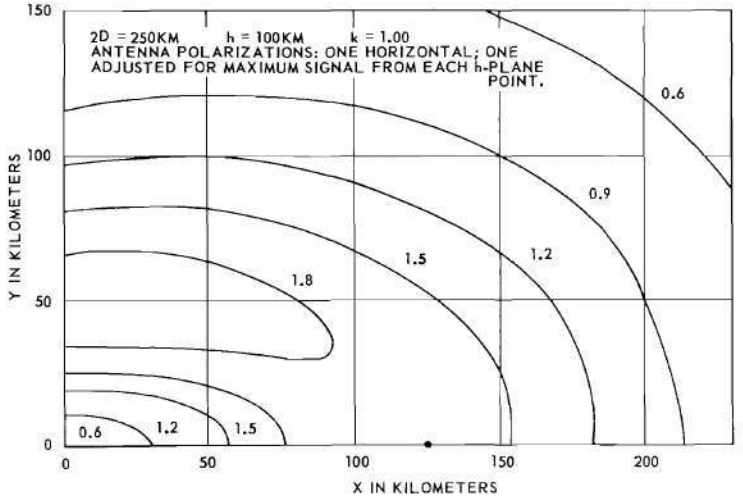

Figure 3. A Distribution of Sources of Signal Duration with Optimum Polarization on One Antenna and Horizontal Polarization on the Other.

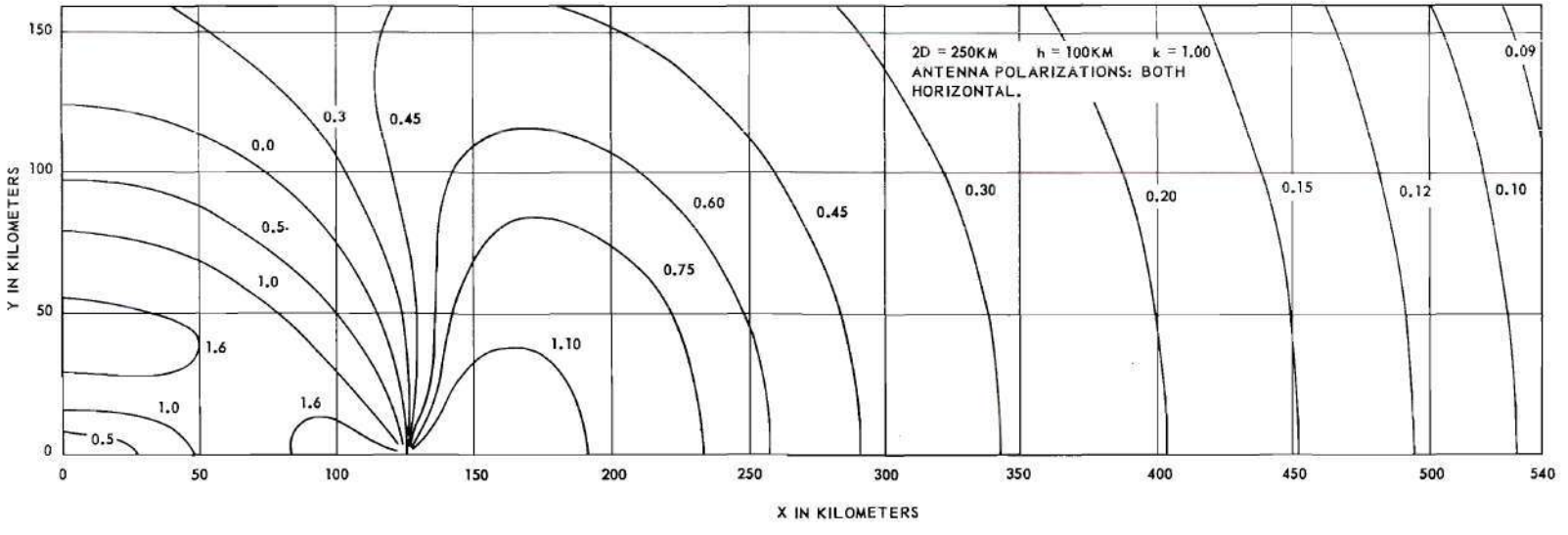

Figure 4. A Distribution of Sources of Signal Duration with Horizontal Polarization on Both Antennas.

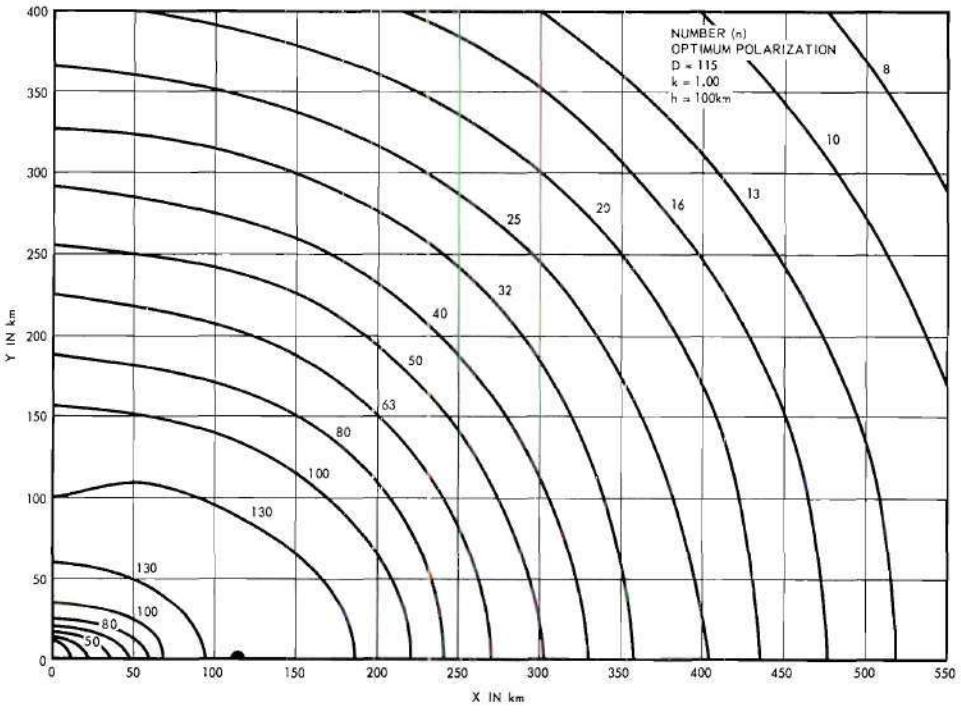

Figure 5. A Distribution of Signal Sources for D = 115 Kilometers.

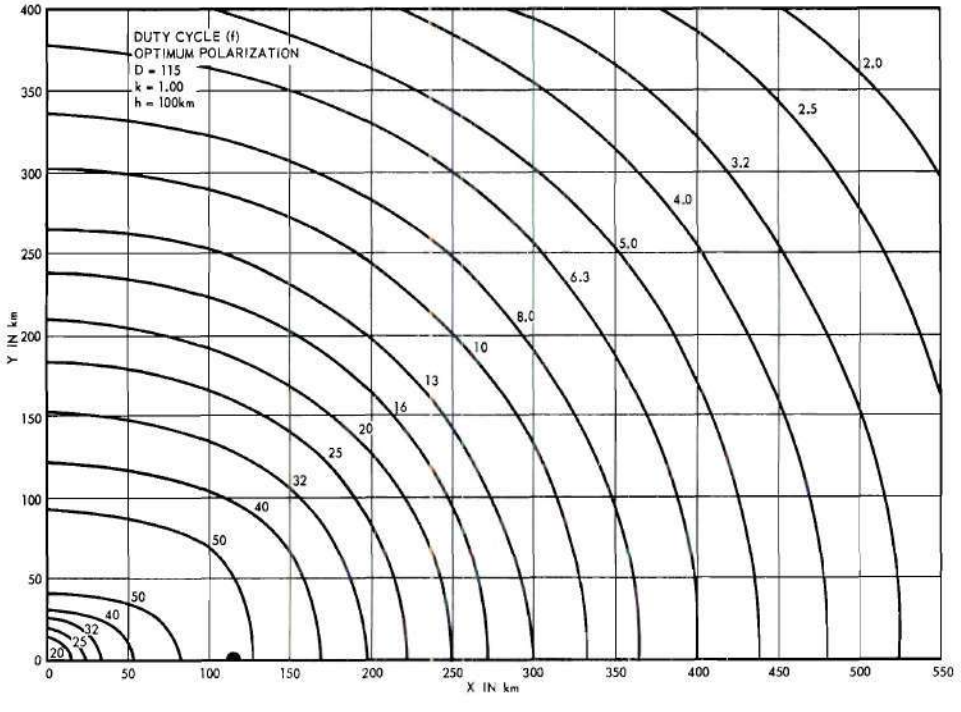

Figure 6. A Distribution of Sources of Signal Duration for D = 115 Kilometers.

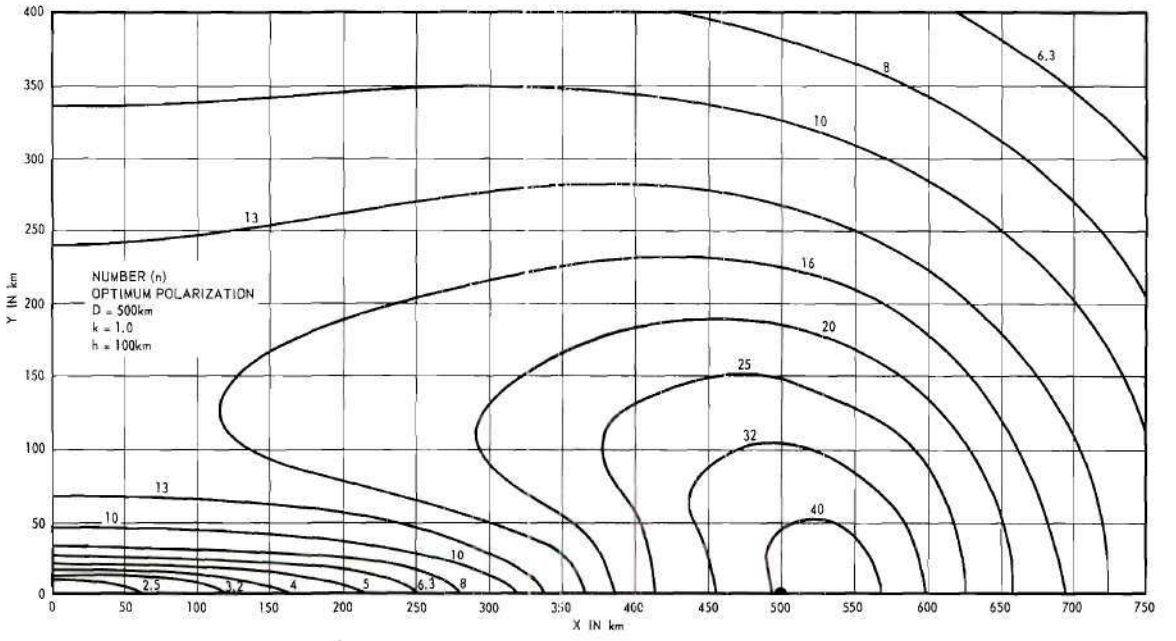

Figure 7. A Distribution of Signal Sources for k = 1.0.

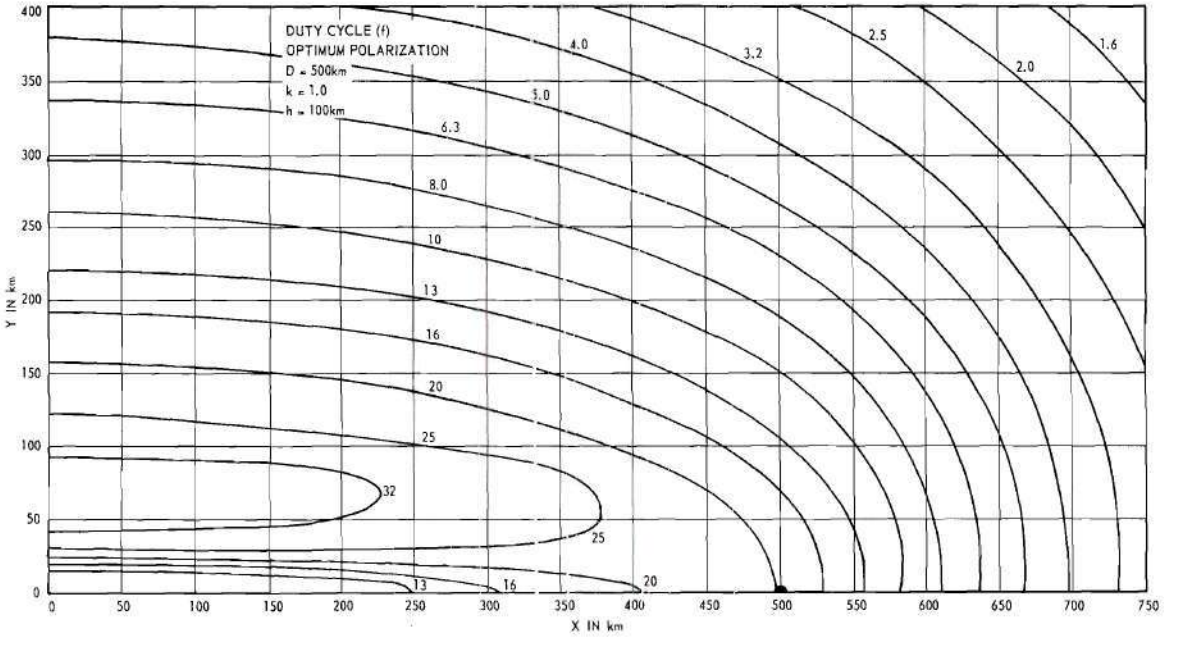

Figure 8. A Distribution of Sources of Signal Duration for k = 1.0.

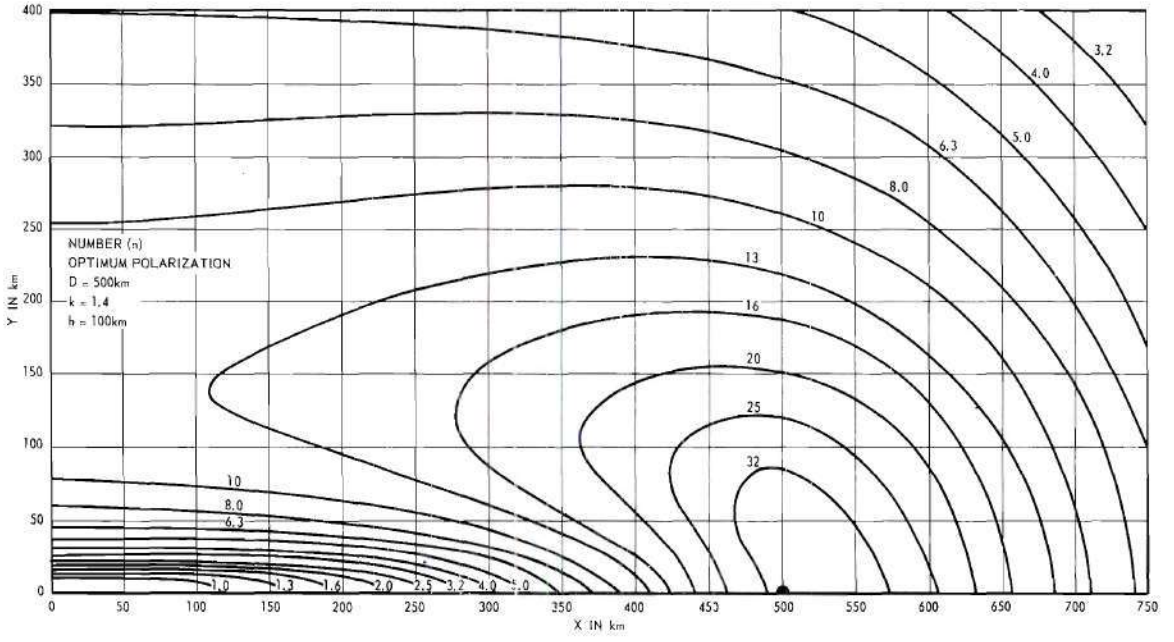

Figure 9. A Distribution of Signal Sources for k = 1.4.

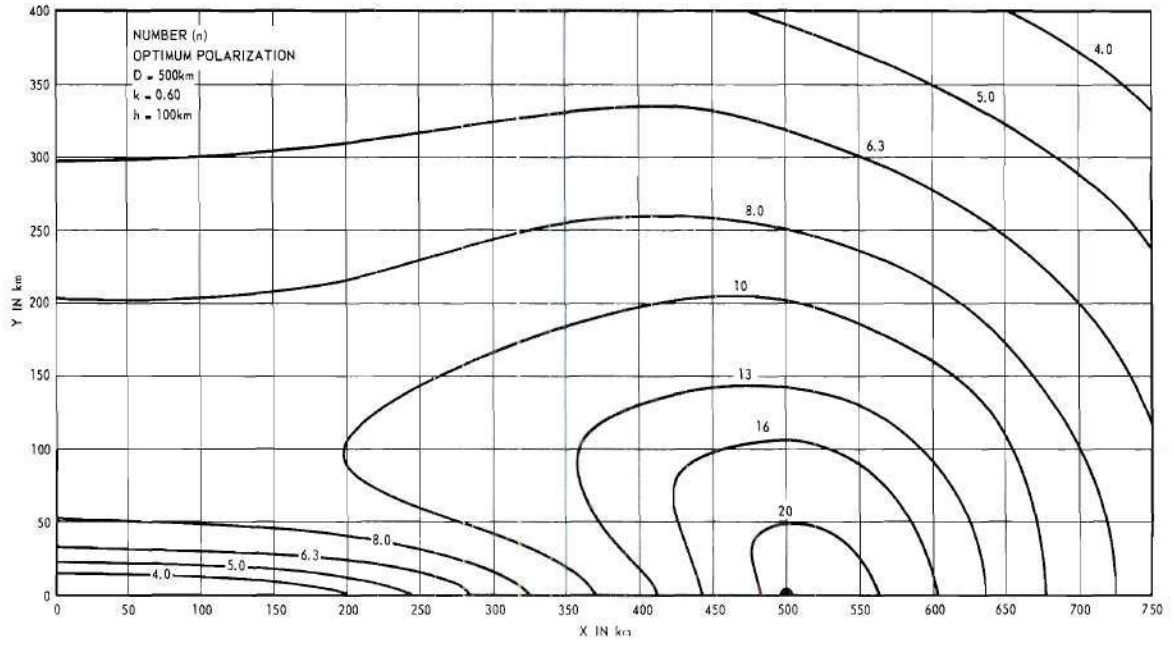

Figure 10. A Distribution of Signal Sources for k = 0.6.

in Figure 4, the contributions at the two maxima (near x = 0, y = $\pm$ 60 km) are cut almost in half. These maxima in Figure 2 are reduced by roughly a quarter in Figure 3. Along the x axis all three combinations of polarizations give the same values for the distribution of sources of signal duration, but well off the x axis, where the uniform radiant distribution predicts the highest duty cycle, the choice of polarization becomes important. When the station separation is relatively small as it is in the present case, the difference between the optimum polarization and horizontal polarization is significant. Figure 4 shows a null on the circle passing through the transmitter and receiver with its center at the path midpoint. This null circle is the locus of points where the polarizations are mutually perpendicular, if each point on the xy plane is assumed to be illuminated and observed with horizontal polarization. The discontinuity which appears in Figure 4 at x = 125 km, y = 0 is a consequence of the fact that horizontal polarization is not uniquely defined for an antenna directed vertically upward.

Figures 5 through 10 show n and f contours for a spherical earth. Therefore for these computations z was made to be a function of x and y according to the approximate expression

$$z = h + \frac{D^2 - x^2 - y^2}{2R_e} , \qquad (12)$$

where R_e is the earth radius. The computations in these figures are all for optimum polarization. These figures serve to illustrate the relation between n and f and the dependence of meteor echo rate on D and k. The particular set of parameters used in each case is shown on the figure.

Except for a scale factor and the antenna gain functions, only those factors that are functions of x and y were used in the f-computations. The relationship between the n and f contours is $n = 4f \cos^2 \phi$. Otherwise all contour values in these figures may be directly compared provided the values for k = 1.4 are divided by 40 and those for k = 0.6 are multiplied by 100.

Even though these curves are based on a radiant distribution that is not completely realistic they do serve to show very well the effect of the geometry on the relative effectiveness of various sky regions. Note in particular that the regions of highest effectiveness as far as echo rate is concerned are generally those regions directly above the transmitter and receiver.

An analysis based on an ecliptic distribution of meteor radiants.--The following analysis serves to emphasize some characteristics of a radiant distribution for which all meteor trails lie in the ecliptic plane. Recent studies indicate an ecliptic concentration for sporadic meteors on the basis of radio, visual, and photographic observations[4,5]. But the observed ecliptic concentration is not sufficiently strong to justify a distribution which is confined precisely to the ecliptic. Thus the strict ecliptic distribution is viewed here as an approximation in much the same sense that the uniform distribution is itself an approximation from a different point of view.

The effect of an ecliptic distribution may be seen by considering the goemetrical requirement for trail reflection. If all radiants are distributed around the ecliptic and if the ecliptic plane itself coincides with the M-plane in Figure 1, then all trails will be properly

oriented to produce reflections*. This situation occurs when the ecliptic plane is tangent to a spheroid having the transmitter and receiver as foci. The point of tangency occurring at some specified height h will be referred to as the "ecliptic tangent point." If h is chosen at the center of the meteor trail zone, then every meteor trail in the neighborhood of the ecliptic tangent point will be properly oriented.

With a strongly ecliptic concentration of radiants, the ecliptic tangent point will be the best point in the sky to illuminate, unless polarization or geometrical factors intervene. The contours in Figures 2 to 10 indicate roughly the combined influence of these factors. For radiant distributions which are less strongly concentrated toward the ecliptic one would expect the ecliptic tangent point to have less significance than before, and other regions with more favorable geometry might become more active than the ecliptic tangent point. This question can be examined by tilting the ecliptic plane slightly in various directions and observing how far the ecliptic tangent point moves from its true position.

The ecliptic plane moves with respect to a fixed observer on the earth in such a way that the ecliptic tangent point describes a simple closed orbit once each sidereal day. The computation of this tangent-point orbit is most easily performed in the cartesian coordinate system of Figure 11. The family of prolate spheroids is described by

$$R_1+R_2 = \sqrt{(x-D)^2 + y^2 + z^2} + \sqrt{(x+D)^2 + y^2 + z^2} = \text{const}, \quad (13)$$

---

*Any plane that intersects the earth and is parallel to the ecliptic is here referred to as an ecliptic plane.

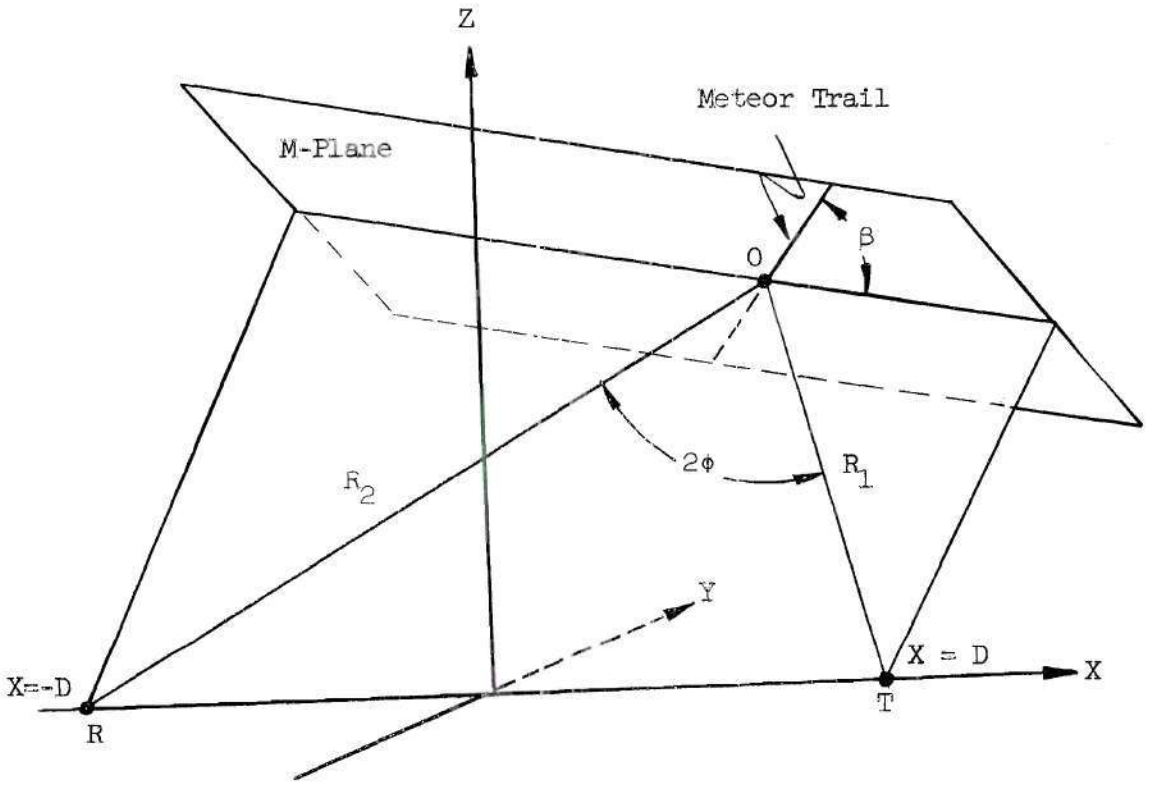

Figure 11. Geometry of the Reflection From a Meteor Trail.

and the unit vector $\underline{n}$ for this family is given by

$$\underline{n} = \frac{\text{grad } (R_1 + R_2)}{\left|\text{grad } (R_1 + R_2)\right|} \quad . \tag{14}$$

The unit normal $\underline{n}$ is used to find the ecliptic tangent point by requiring that $\underline{n}(x, y, z)$ coincide with a unit vector $\underline{m}(t)$ which is normal to the ecliptic plane at a time t. As the earth rotates and moves in its orbit around the sun the normal to the ecliptic, referred to an earth-fixed coordinate system, nutates about a line pointing approximately toward the north star. The angle between $\underline{m}$ and this line is $23^{\circ}27'$, the tilt angle of the earth's axis. The period of the nutation

is one sidereal day. Since the length of a sidereal day is about four minutes less than a mean solar day, the direction of the ecliptic normal is a function of both the time of day and the day in the year.

The determination of the orbit of the ecliptic tangent point for height h above the earth is straightforward but numerically very involved. The components of the spheroid normal are given explicitly by

$$
\begin{aligned}
n_x &= \frac{1}{2\cos\phi}\left[x\left(\frac{1}{R_1}+\frac{1}{R_2}\right) + D\left(\frac{1}{R_1}-\frac{1}{R_2}\right)\right] \\
n_y &= \frac{1}{2\cos\phi}\left[y\left(\frac{1}{R_1}+\frac{1}{R_2}\right)\right] \\
n_z &= \frac{1}{2\cos\phi}\left[z\left(\frac{1}{R_1}+\frac{1}{R_2}\right)\right]
\end{aligned}
\qquad (14a)
$$

in the coordinate system of Figure 11. The corresponding components of the ecliptic normal $\underline{m}(t)$ must be determined in the same coordinate system.

The x, y and z components of the vector $\underline{m}$ can be obtained directly from the transformation matrix relating the earth-fixed, x, y, z coordinate system of Figure 11 to an x', y', z' system fixed with respect to the ecliptic plane. This ecliptic coordinate system is chosen so that z' is normal to the ecliptic plane and x' is along the direction from the sun to the earth at the Autumnal equinox. The transformation from the x, y, z system to the x', y', z' system is made by using two Eulerian transformations*. In the first transformation the Eulerian angles are $\delta - \frac{\pi}{2}$,

---

*H. Goldstein, Classical Mechanics, Addison-Wesley Press, Inc., Cambridge, Mass., 1950, pp. 107-109.

$\theta - \frac{\pi}{2}$, and $-\psi$ respectively, and in the second they are $\frac{\pi}{2}$, σ, and 0 respectively, where

δ is the azimuth angle measured from north clockwise to the x-axis so that $0 \leq \delta < 180^{\circ}$,

θ is the latitude of the midpoint between T and R. (In the northern hemisphere $\theta > 0$ and in the southern hemisphere $\theta < 0$.)

σ is $23^{\circ}27'$, the angle between the earth's axis and the ecliptic normal, and

ψ is the nutation angle which is equal to $\omega_d t_d$ where t_d is elapsed time in solar days since noon of September 23 and ω_d is the rotation of the earth per solar day; ω_d is 360.9856 degrees per day.

The transformation matrix is denoted by A where

$$A = \begin{bmatrix} A_{11} & A_{12} & A_{13} \\ A_{21} & A_{22} & A_{23} \\ A_{31} & A_{32} & A_{33} \end{bmatrix} \tag{15}$$

$$= \begin{bmatrix} \sin\psi \sin\delta + \sin\theta \cos\delta \cos\psi & \sin\theta \sin\delta \cos\psi - \sin\psi \cos\delta & -\cos\psi \cos\theta \\ \sin\sigma \cos\theta \cos\delta - \cos\sigma \cos\psi \sin\delta + \cos\sigma \sin\theta \cos\delta \sin\psi & \cos\sigma \cos\psi \cos\delta + \sin\sigma \cos\theta \sin\delta + \cos\sigma \sin\theta \sin\delta \sin\psi & \sin\sigma \sin\theta - \cos\sigma \sin\psi \cos\theta \\ \sin\sigma \cos\psi \sin\delta + \cos\sigma \cos\theta \cos\delta - \sin\sigma \sin\theta \cos\delta \sin\psi & \cos\sigma \cos\theta \sin\delta - \sin\sigma \cos\psi \cos\delta - \sin\sigma \sin\theta \sin\delta \sin\psi & \cos\sigma \sin\theta + \sin\sigma \sin\psi \cos\theta \end{bmatrix}$$

In the x', y', z' system $\underline{m}$ is a unit vector along z' and by means of the transformation A^{-1} the vector $\underline{m}$ can be written in the x, y, z system as follows.

$$\left[\underline{m}\right] = \begin{bmatrix} m_x \\ m_y \\ m_z \end{bmatrix} = A^{-1} \begin{bmatrix} 0 \\ 0 \\ 1 \end{bmatrix} = \begin{bmatrix} A_{31} \\ A_{32} \\ A_{33} \end{bmatrix} \tag{16}$$

If now the respective components of $\underline{n}$ and $\underline{m}$ as given by Equations (14a) and (16) are required to be equal, the desired expressions for the path of the ecliptic tangent point are obtained. Thus the ratios (n_x/n_z) and (n_y/n_z) are set equal to the respective ratios (m_x/m_z) and (m_y/m_z) which are given in terms of δ, θ, σ, and ψ by Equation (16). Expressions for these ratios are simplified by using two other angles, a and g, where a is the tilt angle of the ecliptic plane with respect to an observer's zenith and g is the angle between the x-axis and the intersection of the ecliptic plane with the earth's surface. The direction cosine of $\underline{m}$ with respect to the z-axis is given by Equation (16) to be A_{33}. The complement of this direction angle is a; hence

$$\sin a = A_{33}. \tag{17a}$$

An expression for angle g is found by working with a unit vector that lies along the intersection of the ecliptic plane with the earth's surface. The x, y, and z components of this vector are cos g, sin g, and zero respectively. By using these components and the transformation A the z' component of this unit vector is found to be

$$A_{31} \cos g + A_{32} \sin g ,$$

but this z' component must be zero because it lies in the ecliptic plane. Hence

$$\tan g = - \frac{A_{31}}{A_{32}} \qquad (17b)$$

and by using a trignometric identity,

$$\sec^2 g = 1 + \tan^2 g = \frac{A_{32}^2 + A_{31}^2}{A_{32}^2} .$$

Matrix A produces only a rotation of axes, therefore

$$A_{31}^2 + A_{32}^2 + A_{33}^2 = 1 .$$

Thus

$$\sec^2 g = \frac{1 - A_{33}^2}{A_{32}^2} = \frac{\cos^2 a}{A_{32}^2}$$

and

$$\cos g = \frac{A_{32}}{\cos a} .$$

Similarly,

$$\sin g = \frac{A_{31}}{\cos a} .$$

Thus

$$\frac{m_y}{m_z} = \frac{A_{32}}{A_{33}} = \frac{\cos g}{\tan a} \tag{18a}$$

and

$$\frac{m_x}{m_z} = \frac{A_{31}}{A_{33}} = \frac{\sin g}{\tan a} . \tag{18b}$$

The corresponding ratios for the unit normal $\underline{n}$ in Equations (14) are as follows:

$$\frac{n_y}{n_z} = \frac{y}{z} \tag{19a}$$

and

$$\frac{n_x}{n_z} = \frac{x}{z} + \frac{D}{z} \frac{R_2 - R_1}{R_2 + R_1} . \tag{19b}$$

When $\frac{n_y}{n_z}$ is equated to $\frac{m_y}{m_z}$ and $\frac{n_x}{n_z}$ is equated to $\frac{m_x}{m_z}$ and Equations (18) are used, the coordinates x and y of the ecliptic tangent point are found to be

$$x = z \frac{\sin g}{\tan a} + D \left(\frac{R_1 - R_2}{R_1 + R_2} \right) \tag{20a}$$

and

$$y = z \frac{\cos g}{\tan a} . \tag{20b}$$

Thus for given values of ψ and z the coordinates x and y of the ecliptic tangent point can be found. For the case of a spherical earth when the height of the reflection point above ground is desired to be kept constant, the correct value of z depends upon the values of x and y as given by Equation (12).

Solutions to Equations (20) and (12) for x and y cannot be easily obtained in closed form, and it was found necessary to use a numerical method of successive approximations to obtain the orbit of the ecliptic tangent point. These computations were also performed on a digital computer.

For a 250 km north-south link, the orbit of the ecliptic tangent point is shown in Figure 2. The position of the ecliptic tangent point for an arbitrary time and date may be obtained by interpolation on the dotted path shown in that figure. The contours shown indicate roughly the effectiveness of the ecliptic tangent point from a geometrical point of view. The effect of spreading out the radiant concentration to within $\pm 10^{\circ}$ of the ecliptic has been considered by tilting the ecliptic by this amount in various directions and observing the calculated displacement of the ecliptic tangent point[12]. The resulting displacements depend strongly on the distance of the ecliptic tangent point from the north station ($x = 125$ km, $y = 0$). For $x < 200$ km in Figure 2, the displacement for a tilt of $\pm 10^{\circ}$ is seldom greater than 50 km. However, far out on the path for $x > 300$ km, the displacement is frequently greater than 100 km. Thus one may regard the ecliptic tangent point as reasonably well defined during the 9-hour period each day when $x < 200$ km.

When the line joining transmitter and receiver is rotated from the north-south direction, the orbit of the ecliptic tangent point is moved over the xy plane and changed in shape. The orbit, however, remains centered roughly north of the midpoint of the transmitter-receiver axis. Figures 12 and 13 each show four computed orbits of the ecliptic tangent point for a short link (250 km between stations) with the transmitter-receiver axis at four different angles δ measured east of north. Figures 14 and 15 show a similar group of orbits for a much longer link (1000 km between stations). Figures 12 and 14 are for a latitude of 35° and Figures 13 and 15 apply to a 45° latitude.

The extent to which the ecliptic tangent point may be regarded as a strong source of scatter signals depends on its position on the orbit. A rough gauge of the effect of broadening the radiant distribution about the ecliptic may be obtained by observing the distance that the tangent point moves during a 2-hour interval. Where this distance is smallest, the assumptions of this section may be expected to remain most appropriate if the radiant distribution spreads out about the ecliptic.

An analysis for meteor-shower radiants.--Roughly 5 per cent of the total meteor influx appears in showers which consist of meteors that strike the atmosphere in a number of well-defined streams[4]. The meteors in a given stream all move with nearly the same velocity and in nearly the same direction. From the standpoint of meteor-scatter communication these showers offer a number of interesting possibilities. Even though the shower meteors form a small fraction of the total meteor influx during the year, they may provide signal rates that are several times

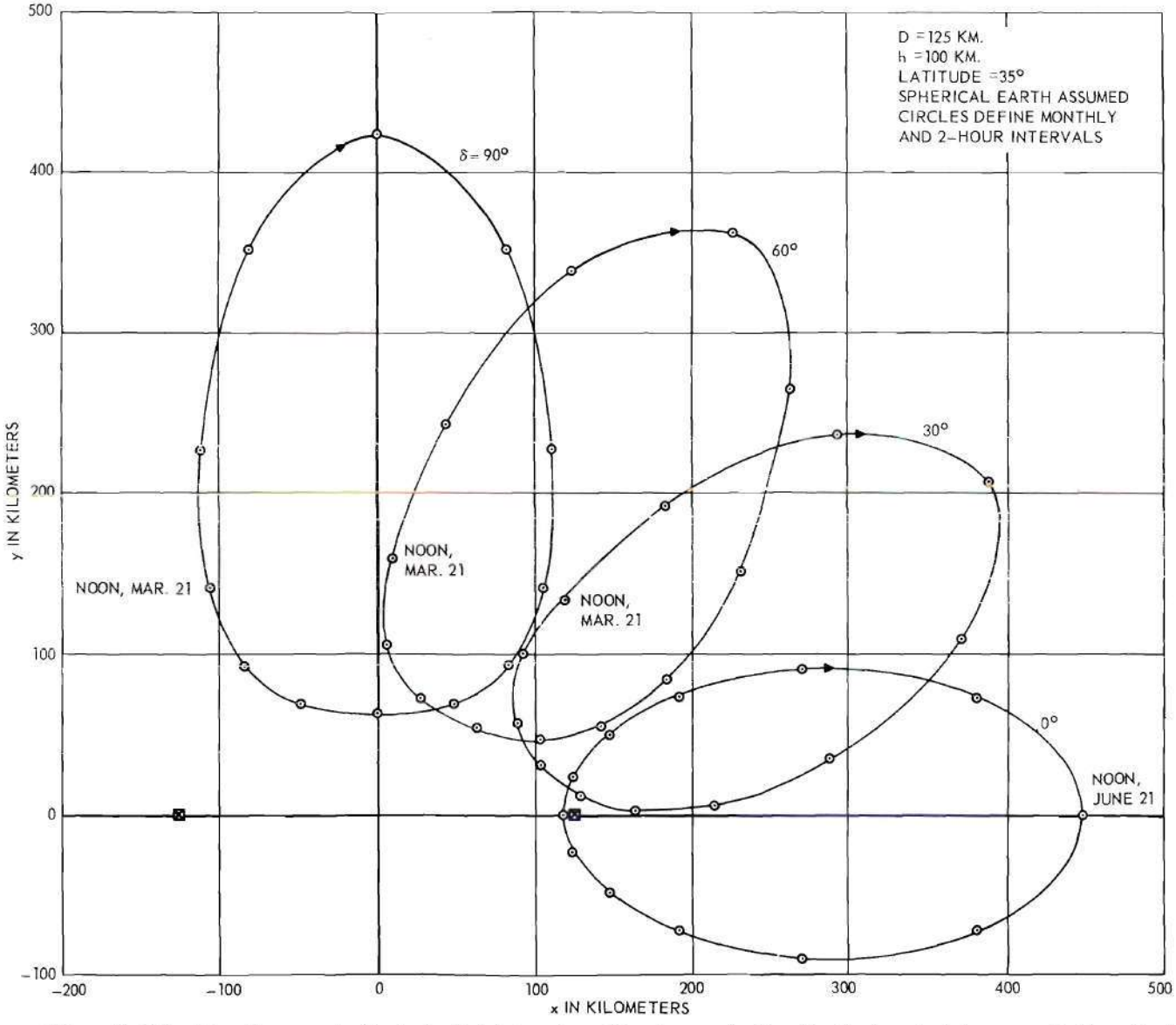

Figure 12. Ecliptic-Tangent-Point Orbits for Various Azimuth Orientations of the X Axis.

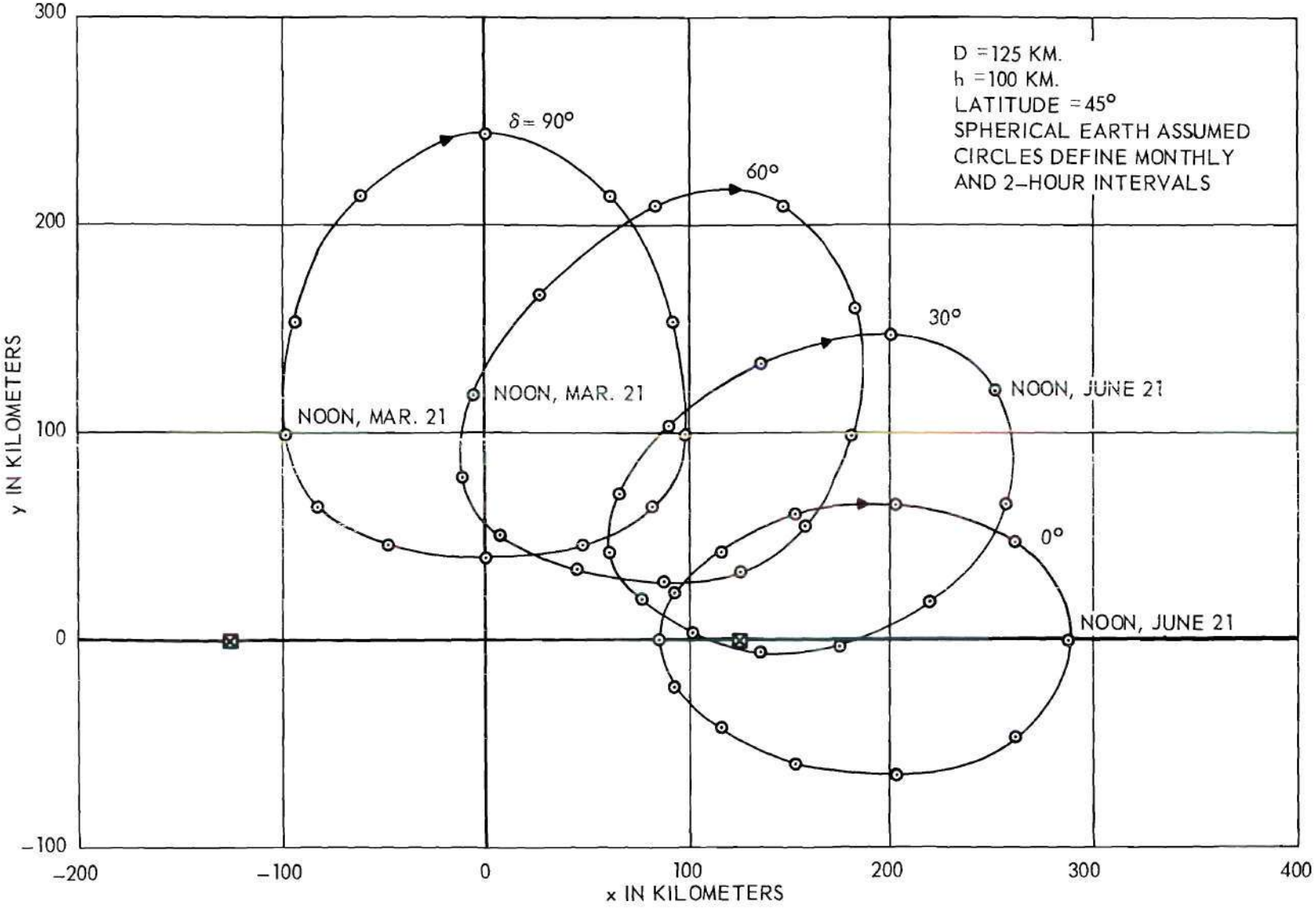

Figure 13. Ecliptic-Tangent-Point Orbits for Various Azimuth Orientations of the X Axis.

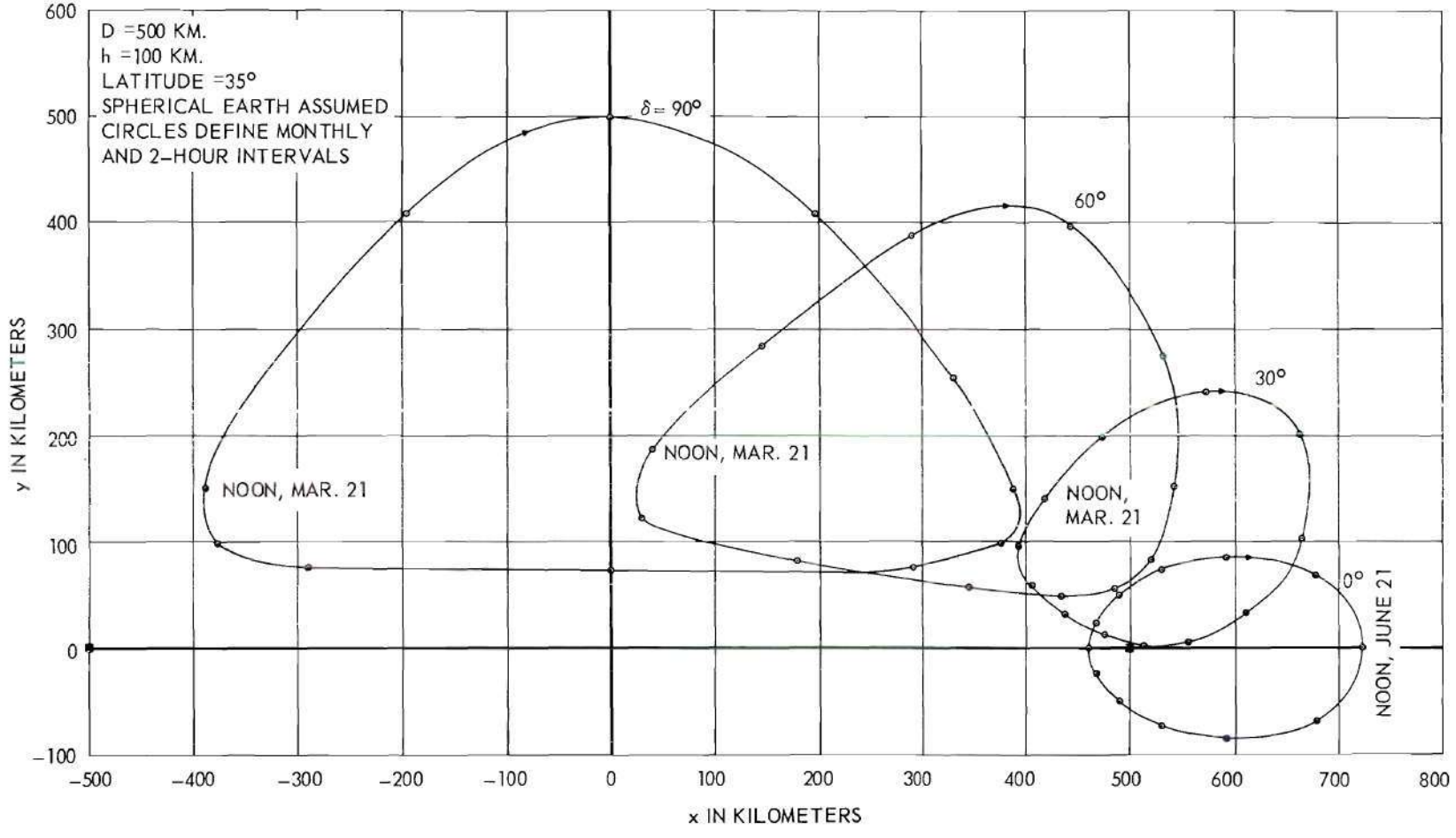

Figure 14. Ecliptic-Tangent-Point Orbits for Various Azimuth Orientations of the X Axis.

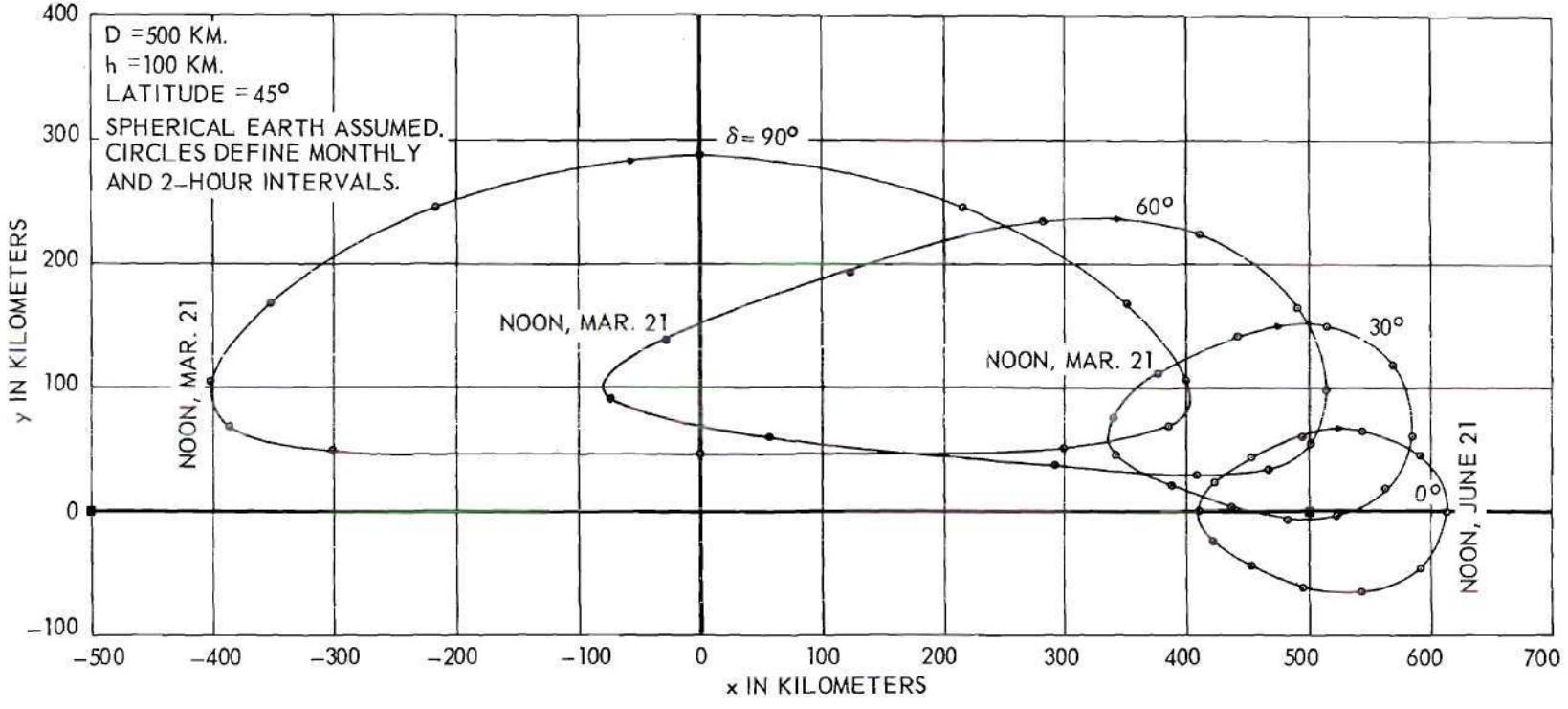

Figure 15. Ecliptic-Tangent-Point Orbits for Various Azimuth Orientations of the X Axis.

the sporadic background at certain intervals when the showers are near their maximum. The shower radiants and periods of occurrence are well known for the larger showers, so it is possible to predict for a given meteor-scatter link the times when showers would make large contributions to the signal rate. Furthermore it is possible to predict the most favorable areas in the sky to illuminate in order to make maximum use of a given shower.

Forward scatter by meteor showers over long transmission paths has been studied experimentally by Canadian workers[14,15]. The associated theoretical treatment has been worked out using an approximation which breaks down if the transmission path is much shorter than 1000 km[16]. It, therefore, has seemed desirable to generalize the theoretical analysis so that it might be applied to transmission paths of arbitrary length*. Theoretical computation of the locations and relative usefulness of reflection points for showers have been made. Because of the complex geometry in such calculations it was again necessary to make use of a high-speed digital computer. The computer code was written in such a way that the geographical position and length of the transmission path for an arbitrary communication link can be inserted. Arbitrary celestial coordinates of the radiant can also be used.

The analysis may be summarized briefly as follows. The problem of scattering by meteor showers is viewed within the framework of previous calculations for sporadic meteors based on uniform and ecliptic

---

*Hines has recently made an independent analysis comparable to that presented here. Both the present work and that of Hines have recently been published. See references 17 and 18 in the Bibliography.

distributions of radiants. The regions in which shower meteors are properly oriented for the desired forward scatter are determined, and the relative effectiveness within these regions is calculated. The results can then be plotted on a series of maps which show the regions of sky which should be illuminated at successive times during the day or, alternatively, the times when a shower will contribute to a given arrangement of antenna beams.

The details of the calculation of the forward scatter from meteor showers proceeds as follows. Consider a system of axes like the one shown in Figure 11. Let $\underline{T}$ be a unit vector directed toward the radiant, so that T_x, T_y, T_z are the direction cosines of a line toward the radiant. The condition that the shower trails be properly oriented for reflection can now be expressed in terms of the unit normal $\underline{n}$ to the spheroid family which is given in (14). This condition is

$$\underline{T} \cdot \underline{n}(x, y, z) = 0, \tag{21}$$

or

$$T_x x + T_y y + T_z z + \frac{R_2 - R_1}{R_1 + R_2} T_x D = 0 \tag{21a}$$

Expressions for T_x, T_y, and T_z in terms of celestial coordinates are given in the Appendix. The coordinates x, y, and z are the components of a vector extending from the origin to the reflection point on a meteor trail. In the flat-earth approximation z would be the height of the meteor trail above the earth and hence z could be set equal to mean height at which the trails occur. In the present calculation a spherical

earth is assumed, so z becomes a function of x, y and the assumed height of the trail. This function is given in (12). If h is specified, (12) and (21a) may be combined so that an implicit function of the form $g(x, y) = 0$ is obtained, which gives a value of y for each value of x, or vice versa.

Now it can be seen that a given shower radiant-point gives rise to a line at a height h above the earth's surface, this line specified by $g(x, y) = 0$ being the locus of points at which shower meteors are properly oriented for the desired forward scatter. If h is allowed to vary between 80 km and 120 km, then a family of loci will result. These curves may be drawn on the xy plane so that a map of the scattering region is obtained. A map such as this is shown in Figure 16. This map would apply to a given link and a given shower at a particular time.

To make the preceding analysis more useful, it is necessary to know something about the relative effectiveness of points along a shower locus. The measure of effectiveness that has been chosen is proportional to the number of observable shower meteors to be associated with the unit length of locus.

Calculation of the measure of effectiveness involves many of the same considerations that were used to analyze the uniform radiant distribution. The number of observable meteors to be associated with a segment of the scattering band shown in Figure 16 is proportional to the h-surface area through which shower meteors can pass with the proper orientation to produce a scattered signal within this segment. The width of this area is determined by a unit length of locus and the direction of the shower radiant. As is shown in Figure 16 this width is designated

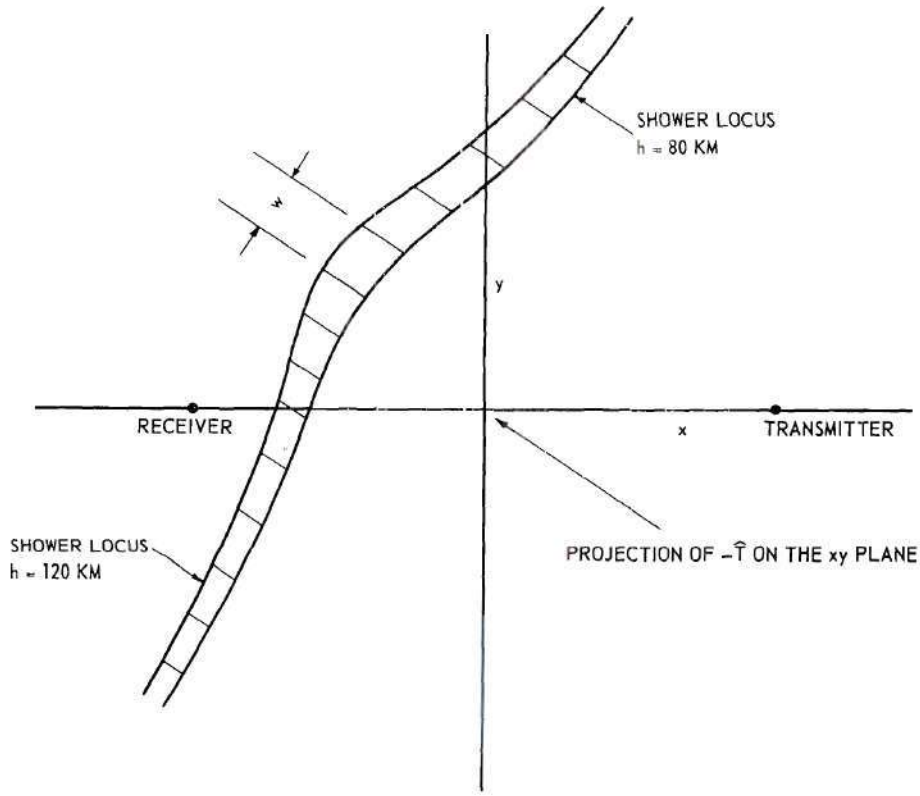

Figure 16. An Example of Shower Loci.

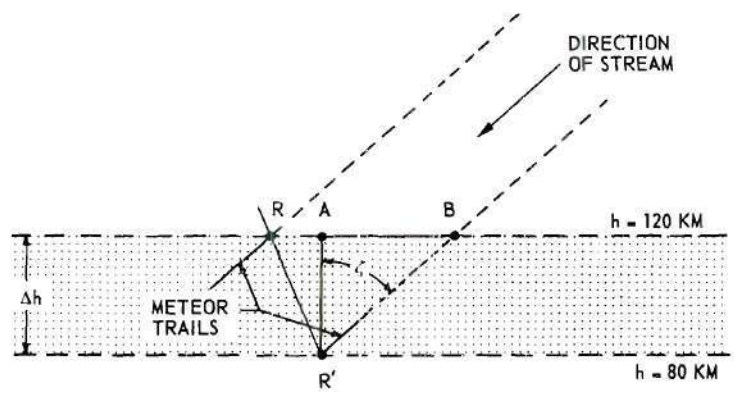

Figure 17. An Illustration of the Surface Through Which Shower Meteors Must Pass to Produce Signals with Reflections Occurring Along Some Line Between R and R'.

w. The depth of this area varies along the band. Figure 17 illustrates the method used in determining this depth which is labeled $\overline{RB}$. The distance $\overline{RA}$ can be measured directly on an xy projection like the one in Figure 16 or it can be computed from the approximate formula

$$\overline{RA} = \frac{\partial y}{\partial z} (\sin a_1 + \cot b_1 \cos a_1) \Delta h \qquad (22)$$

where a_1 and b_1 are respectively the angles from the azimuth direction of the radiant to the positive x axis and the locus. $\frac{\partial y}{\partial z}$ refers to the point of reflection and can be obtained from (21a). The distance $\overline{AB}$ can be calculated knowing the zenith angle ζ of the shower radiant and the distance Δh (taken here to be 40 km). The result is

$$\overline{RB} = \overline{RA} + \Delta h \tan \zeta \, . \qquad (23)$$

The area A_c through which meteors are captured for a given segment then is

$$A_c = w(\overline{RB}) \qquad (24)$$

and the number of meteor signals per second from the segment is then given by

$$n_s = N(q_o) A_c \cos \zeta \, , \qquad (25)$$

where $N(q_o)$ is obtained by combining Equations (4) and (6) as was done for the uniform distribution analysis. A measure of effectiveness F_g which is independent of antenna gains and polarizations can be obtained by writing the preceding equation as

$$n_s = (\text{const}) \left[S \sqrt{G_r G_t} \right]^k F_g, \tag{25a}$$

where

$$F_g = \frac{A_c (\cos \zeta)^{1+k}}{\left[R_1 R_2 (R_1 + R_2) (1 - \cos^2 \beta \sin^2 \phi) \right]^{k/2}} \tag{26}$$

The measure of effectiveness F_g does not take into account the properties of the transmitting and receiving antennas so that it is quite general. Values of F_g can therefore be indicated at intervals along the shower locus. The meteor signal rates for shower meteors with a given arrangement of antennas can be determined by inserting the appropriate values of G_t, G_r and S in (25) and performing a numerical integration along the shower locus.

As an example, computations based on this analysis when k = 1.0 have been made for the Quadrantid Shower with the Atlanta-Knoxville link. Figures 18 through 20 show the loci of properly-oriented trails in the Quadrantid stream for a height h = 100 km at two-hour intervals. Values of the measure of effectiveness F_g are indicated at points along each locus. These loci actually represent roughly the center of narrow bands lying between similar loci for h = 80 km and h = 120 km. The depth of these bands, measured parallel to the projection of the shower direction on the xy plane, varies between zero and 80 km for the loci shown in Figures 18-20. The contribution of the shower to the meteor signal rate is obtained by summing the contributions n_s in (25) along the shower

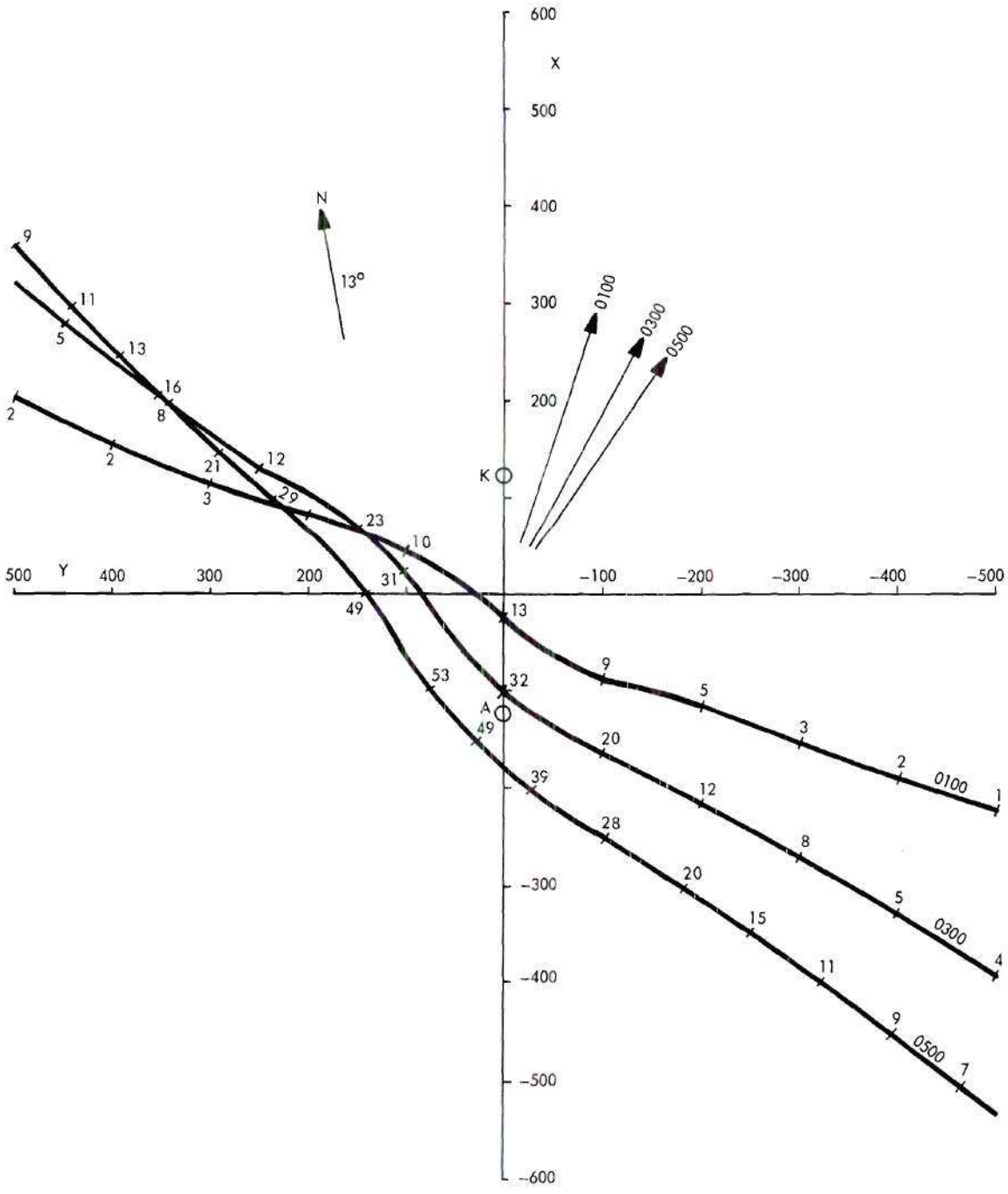

Figure 18. Loci of Properly-Oriented Quadrantid-Shower Meteors for the Atlanta-Knoxville Link.

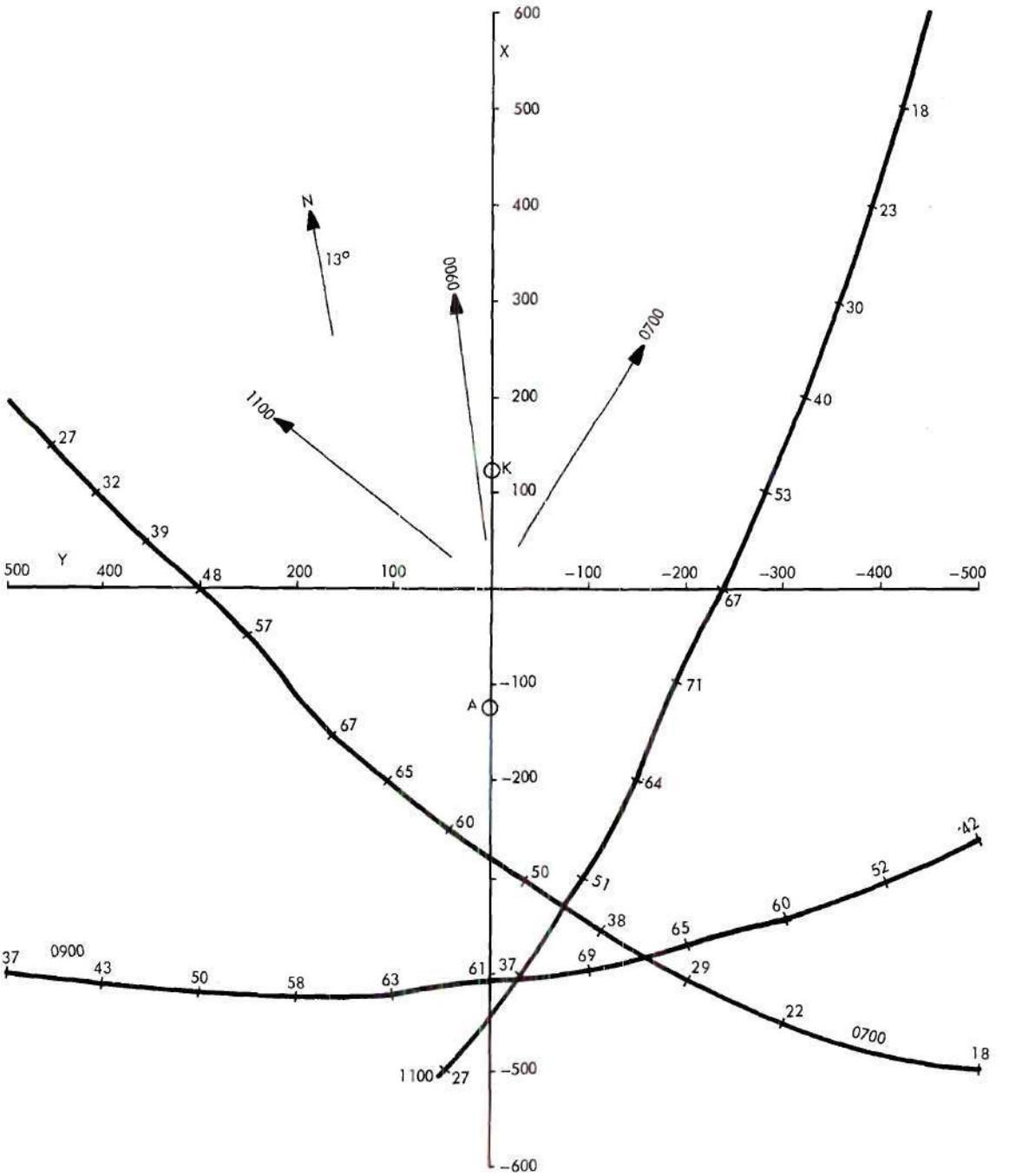

Figure 19. Loci of Properly-Oriented Quadrantid-Shower Meteors for the Atlanta-Knoxville Link.

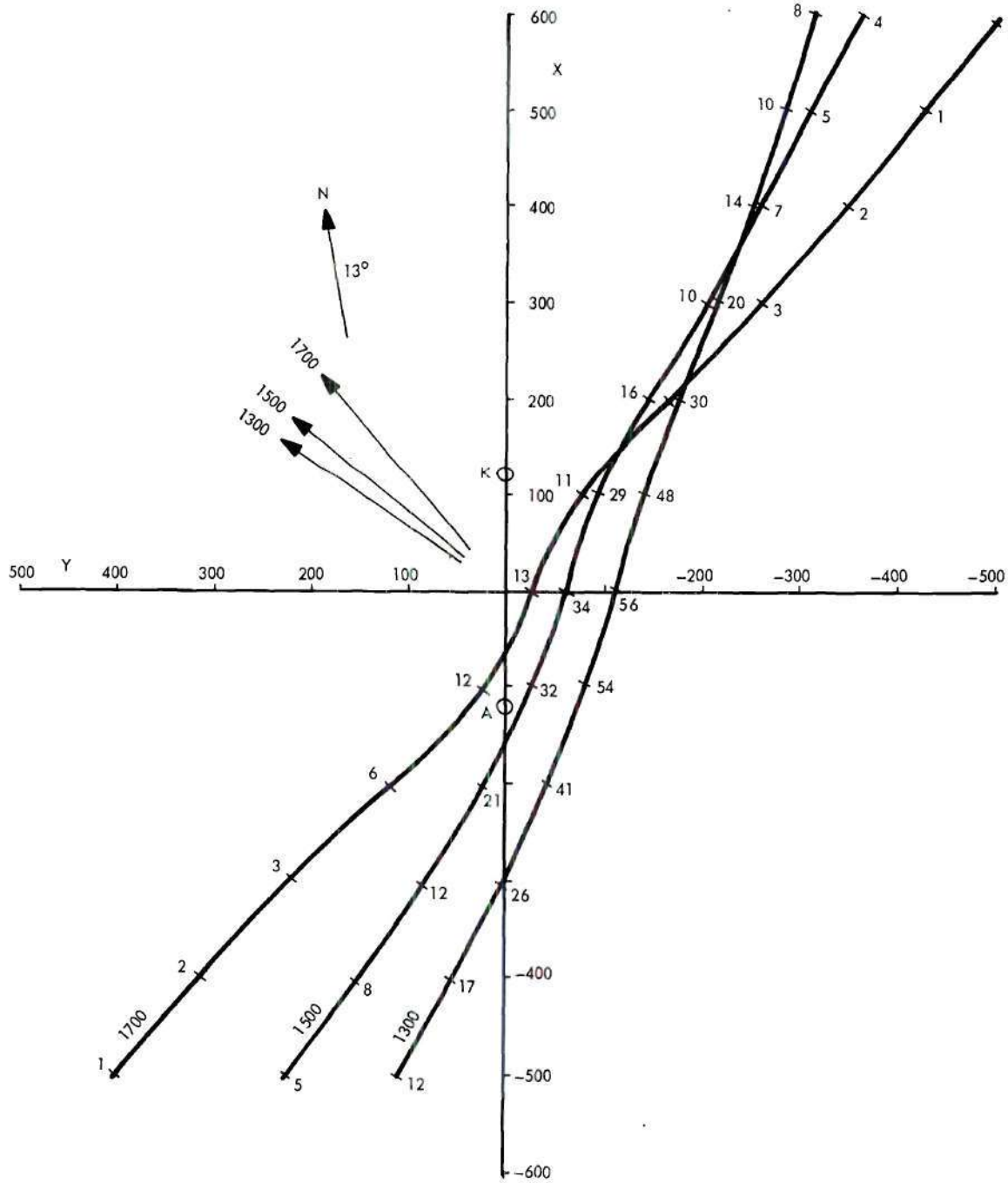

Figure 20. Loci of Properly-Oriented Quadrantid-Shower Meteors for the Atlanta-Knoxville Link.

loci. The contribution to the duty cycle could be obtained from n_s and the relation between rate and duty cycle as given by (11).

The three-point approximation to the sporadic radiant distribution.--In principle any given radiant distribution can be approximated as closely as desired by using a large number of point-radiants. The effect of such a distribution on the meteor signal rate could then be had by computing the effect of each single radiant individually and then summing the results. This is the procedure that will be followed to predict the signal rate due to sporadic meteors except that only three-point radiants are used to represent the sporadic radiant distribution. A representation by a large number of points seems not to be justified at the present time because the actual sporadic distribution is not precisely known. Furthermore, there seems to be a certain amount of day to day variation in the sporadic radiant distribution. Thus it seems wise at the present time to seek a simple model that yields good results rather than an elaborate model that yields perfect results.

The basis for choosing the three points is readily apparent in Figure 21 which is a reproduction of an approximate sporadic radiant distribution as determined by Hawkins[4]. This distribution is based on experimental data and on the assumptions of symmetry about the ecliptic plane and about the apex of the earth's way. Three peaks are shown to occur all in the ecliptic. Three point-radiants are chosen at these three peaks and are given the descriptions Apex, Anti-Sun, and Sun. The Apex radiant is in the direction of the apex of the earth's way, and the Anti-Sun and Sun radiants are respectively plus and minus 65° in ecliptic longitude from the earth's apex. These Sun and Anti-Sun radiants used

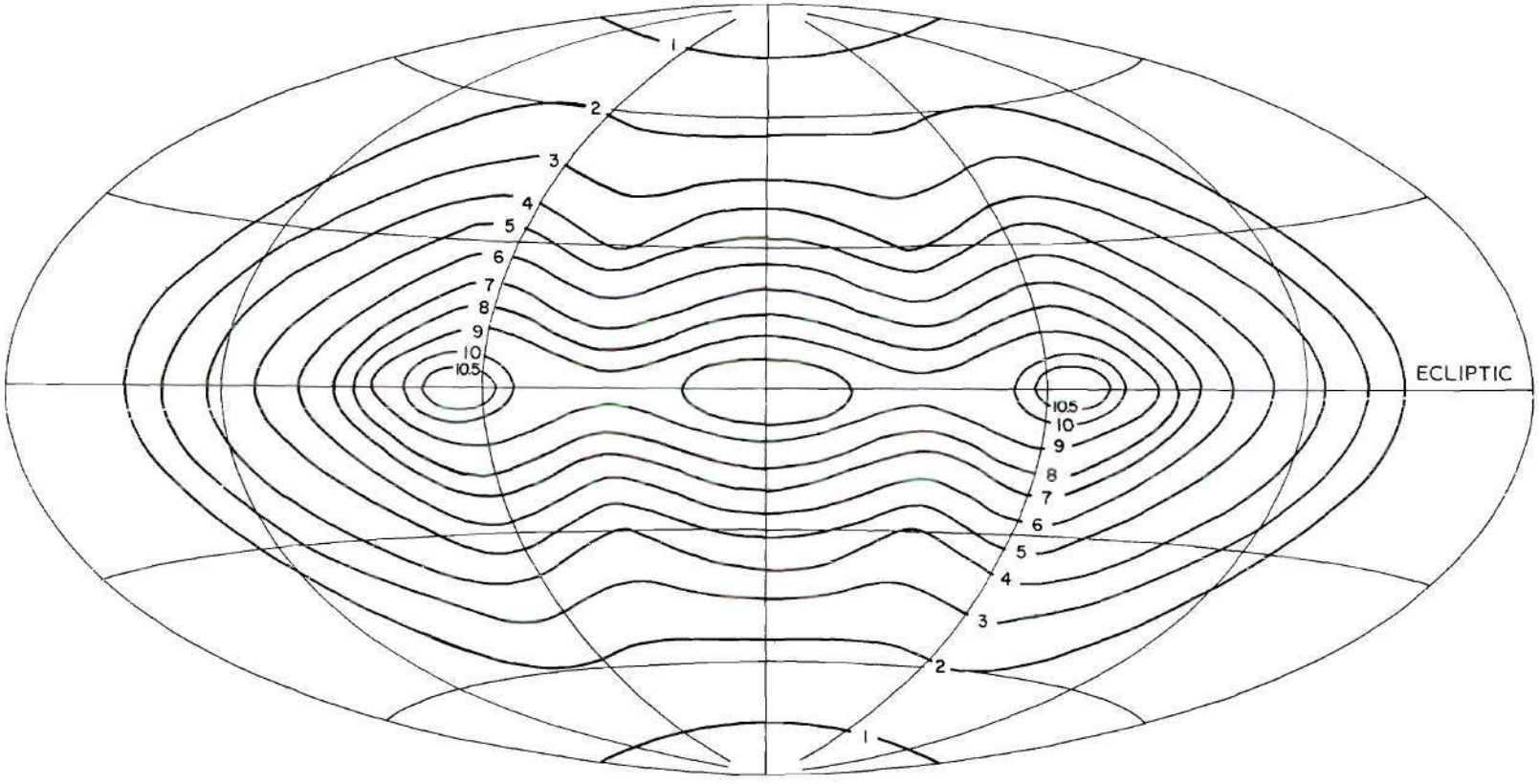

Figure 21. An Approximation for the Sporadic Radiant Distribution as Given by Hawkins[4].

here are not of course exactly at the sun and anti-sun positions because these positions differ in ecliptic longitude from the apex by 90° and not 65°.

Predictions based on this three-point approximation are made by treating each of the three points as a shower radiant and thus following the procedure outlined in the previous section on shower radiants. The results of the three separate computations are then superimposed. The celestial coordinates, right ascension and declination, of the three radiants are computed for a given day in a straightforward manner from the known position of the sun. From these coordinates and the parameters defining a given meteor-scatter link a set of shower-type locus lines are computed for each hour of the day. Figures 22 and 23 show four sample sets of these loci for the Boston-Atlanta link on February 2. The shaded region shows approximately that part of the h-surface illuminated by both antenna beams. The predicted echo rates are determined by performing line integrations along each of the illuminated loci and summing the results. Figure 24 shows the contributions of each of the three radiants and also the total predicted signal rate. Another example of the contribution of each of the three radiants for a different time and a different link is shown in Figure 25. For a given link the general shape of the contributions (plotted vs time) of a radiant is determined by the declination of the radiant. The appropriate declinations are indicated in Figures 24 and 25.

Antenna illumination patterns.--As indicated by the previous theory (i.e., Equations 9 and 25) it is necessary to know the antenna illumination pattern, $\left[S\sqrt{G_r G_t} \right]^k$, in order to predict meteor echo rates.

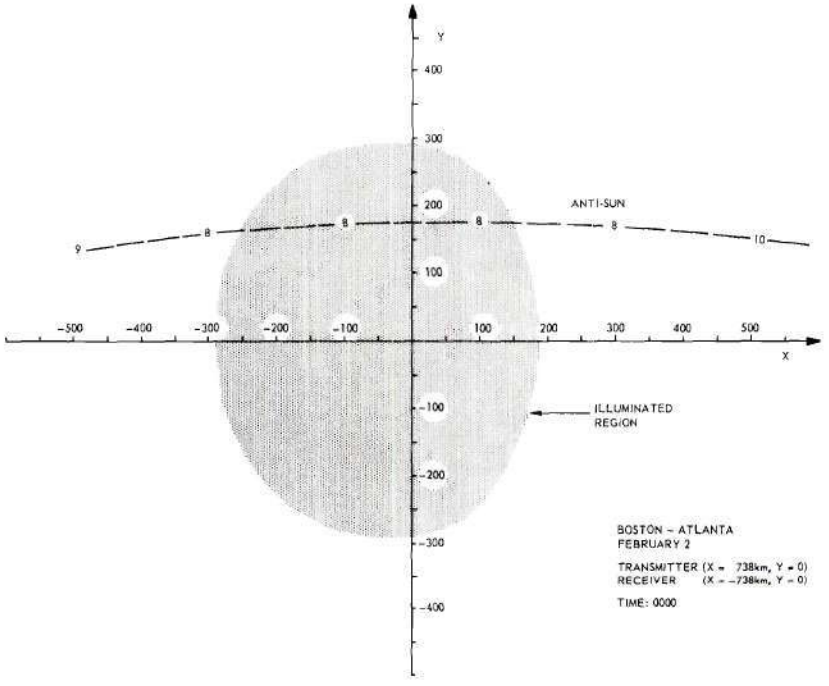

Figure 22a. Sample Loci for the Three-Point Approximation at 0000 on February 2 for the Boston-Atlanta Link.

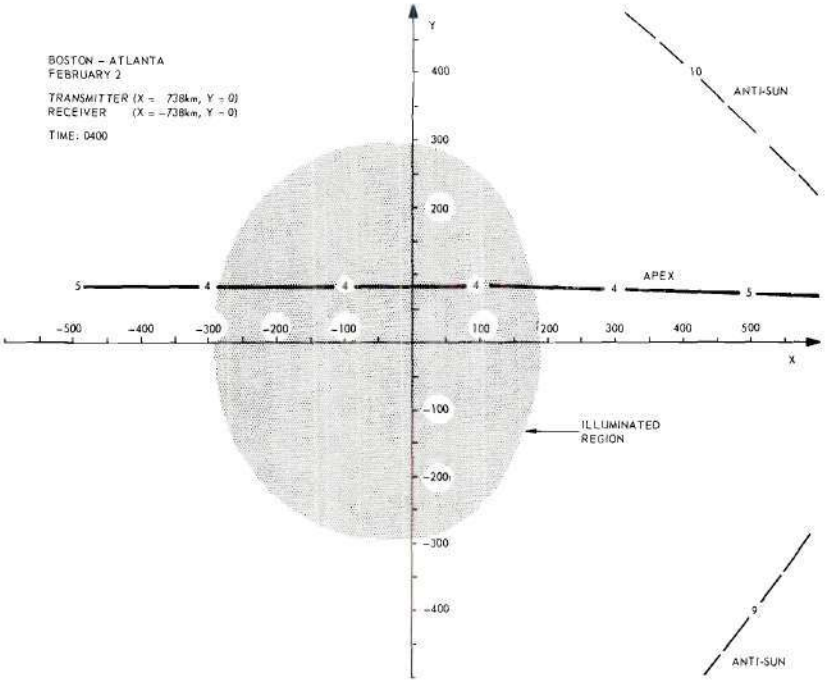

Figure 22b. Sample Loci for the Three-Point Approximation at 0400 on February 2 for the Boston-Atlanta Link.

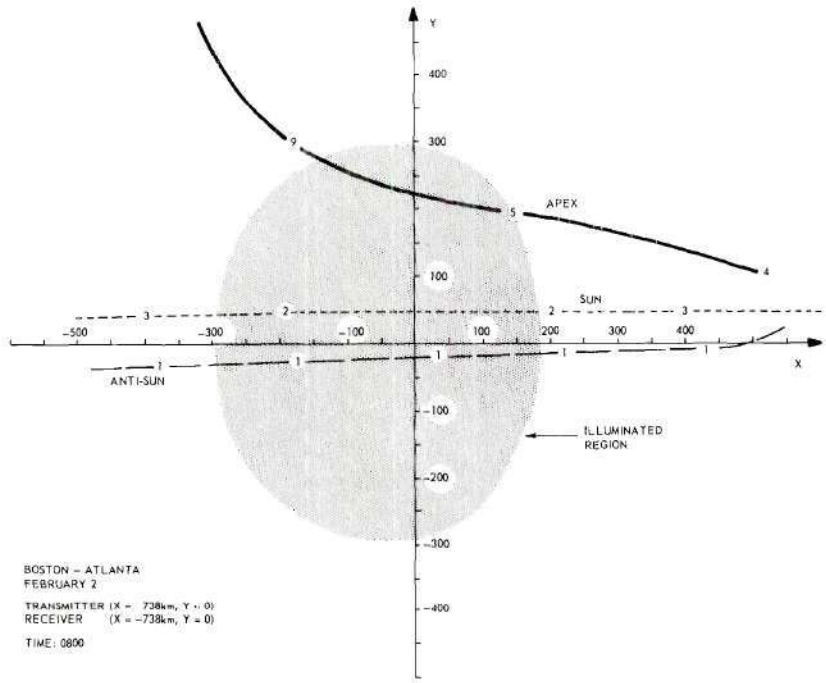

Figure 23a. Sample Loci for the Three-Point Approximation at 0800 on February 2 for the Boston-Atlanta Link.

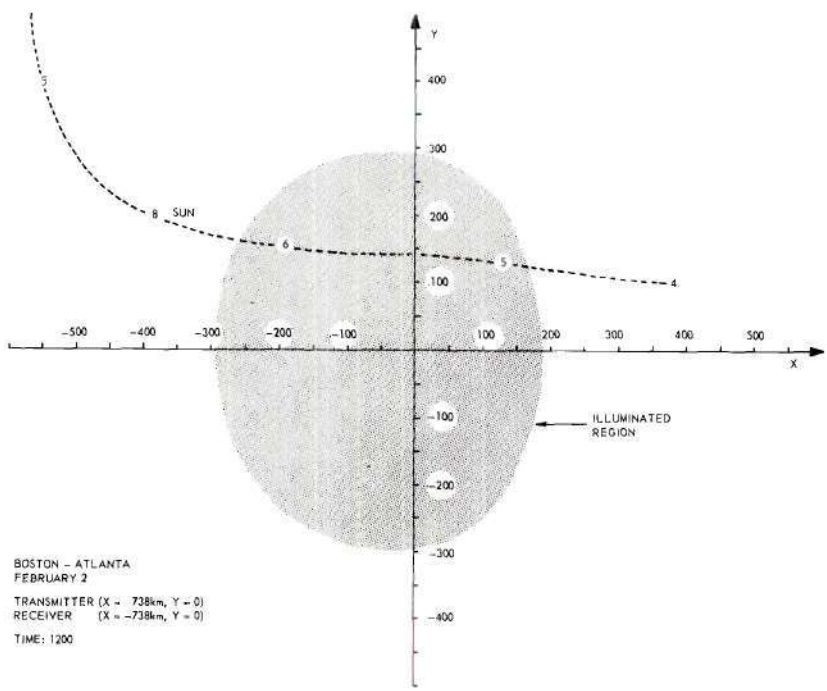

Figure 23b. Sample Loci for the Three-Point Approximation at 1200 on February 2 for the Boston-Atlanta Link.

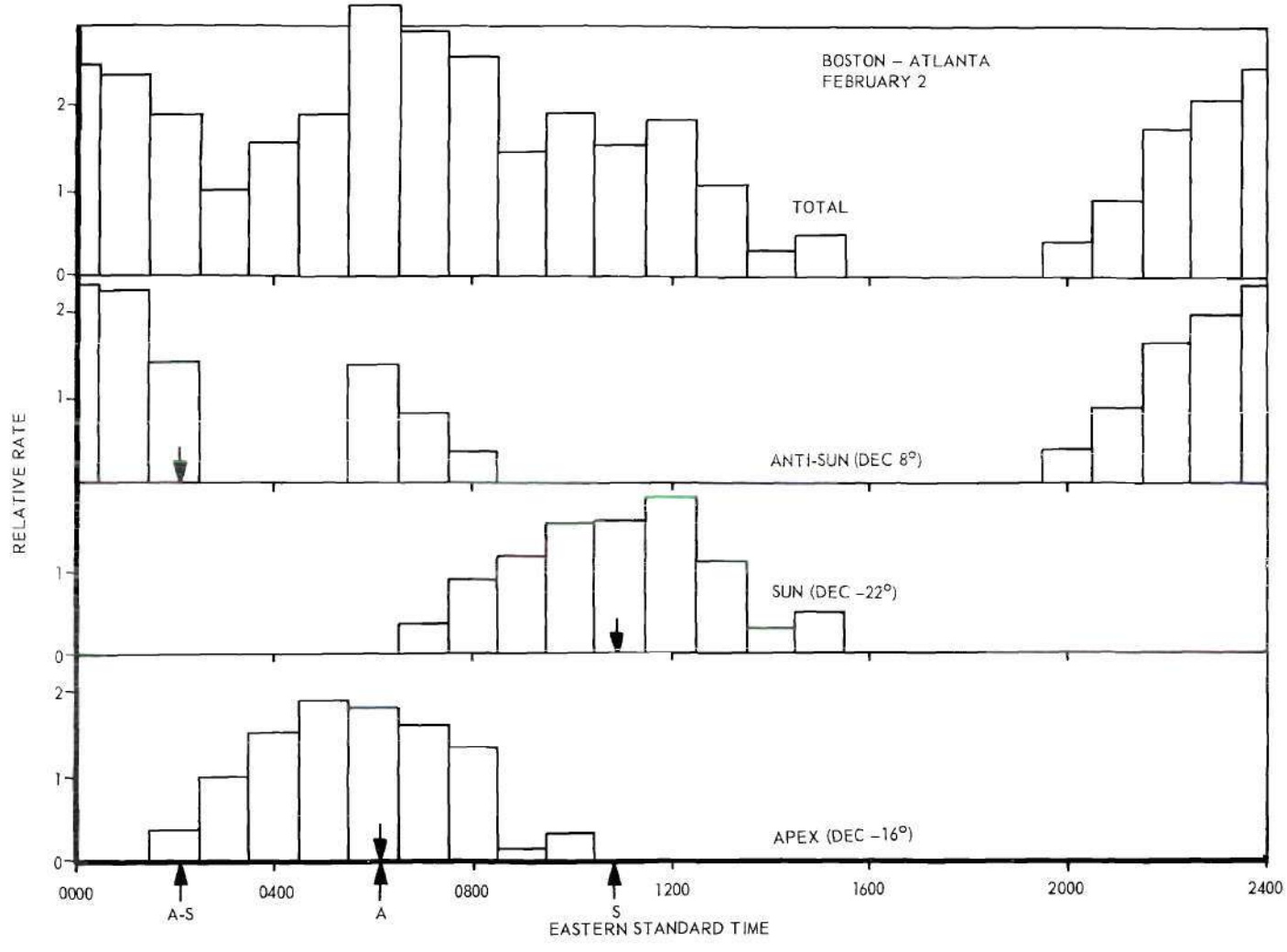

Figure 24. An Example of the Contribution of Each of the Three-Point Radiants to a Predicted Diurnal Curve for the Atlanta-Boston Link.

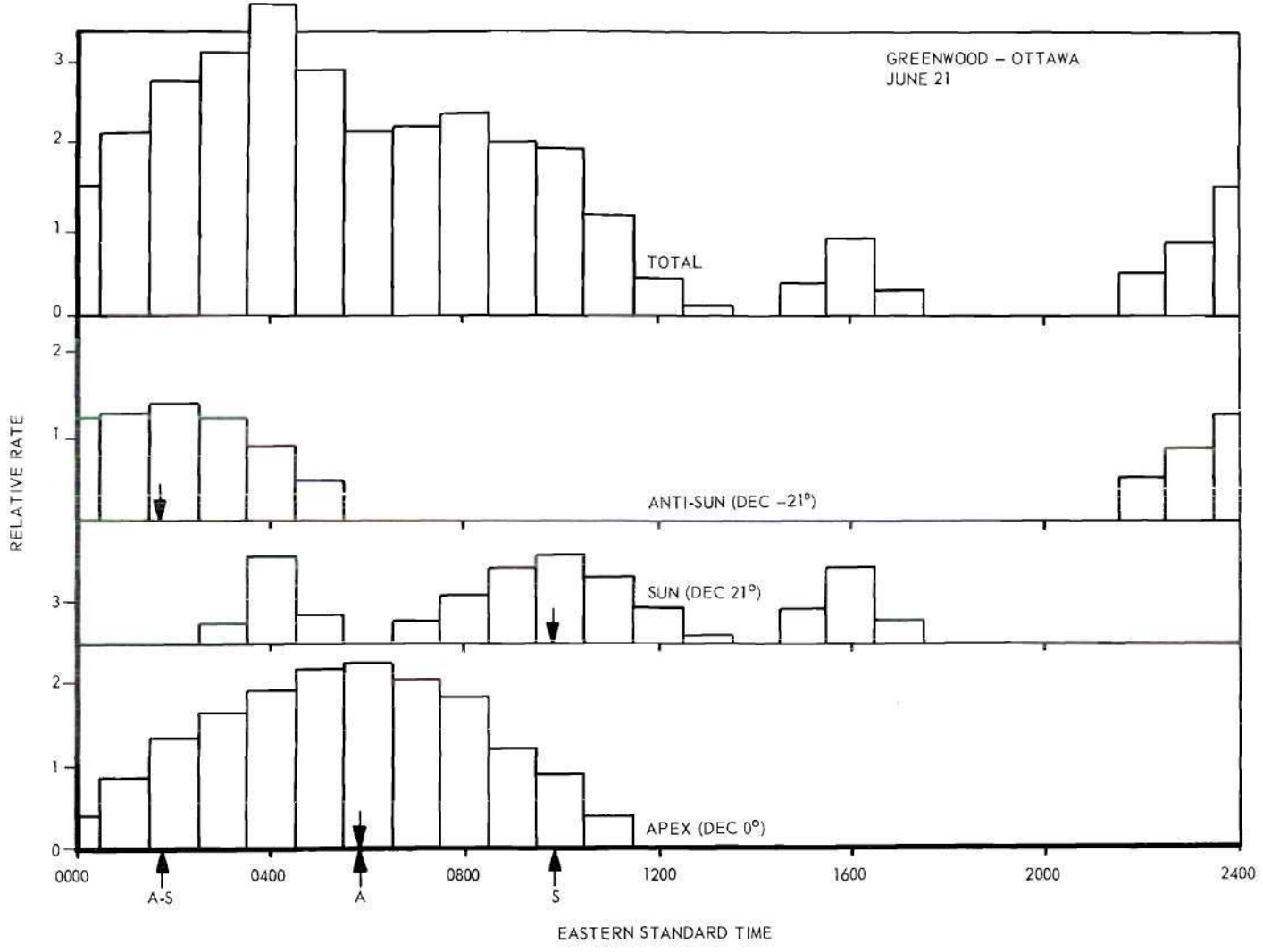

Figure 25. An Example of the Contribution of Each of the Three-Point Radiants to a Predicted Diurnal Curve for the Greenwood-Ottawa Link.

This factor represents the combined h-surface illumination by the two antennas, and can be computed from a knowledge of the free-space antenna patterns, the relative polarizations, and the ground-reflection effects at the antennas. Only a relative antenna pattern is needed because only relative counting rates will be computed. The pattern (for $k = 1$) is simply the vector dot product of two electric-field vectors at the trail. The angle between the vectors is determined by the relative polarization; the amplitudes of the vectors represent the relative field strengths at the trail due to the transmitting and receiving antennas. (It is both convenient and valid here to assume that both antennas transmit.)

The field at the trail due to a single antenna is often the resultant of a direct wave and a ground-reflected wave. When this is the case, for an antenna having a horizontal axis, the field strength is approximately given by the well-known expression $D_1 \sin\left[\frac{2\pi}{\lambda} z_1 \sin \delta_1\right]$, where D_1 is the free-space field strength in some direction having an elevation angle δ_1, and where z_1 is the antenna height above a flat reflecting surface. When there is no ground reflection the field strength is simply D_1 which of course is a function of direction relative to the antenna axis and which can usually be fitted to a simple function. The orientation, or polarization, of the vector representing the transmitted (or received) field strength must satisfy two conditions: The vector must be perpendicular to the direction of travel of the wave and it must be in a plane defined by the direction of travel and the antenna dipole. The polarization factor S results from a straightforward enforcement of these two conditions upon two unit vectors representing the transmitted and received waves, respectively.

Figures 26 and 27 show two sample antenna patterns computed according to the above principles after first fitting the free-space patterns to sin x/x type functions. The algebraic manipulations required for these computations were quite involved and so were performed with a high-speed digital computer*. These patterns are for two meteor-scatter links to be described later and apply specifically for k = 1.0 and h = 100 km. A spherical earth and no atmospheric bending of the waves were also assumed. The antenna heights for Figure 26 were equal and were adjusted so that the main lobes would intersect at 95 kilometers above the earth. The free-space antenna beamwidths were both assumed to be 50° between half-power points in both azimuth and elevation. The antenna heights for Figure 27 were 3.2λ and 2.8λ, respectively, and the free-space antenna beamwidths were both assumed to be 65° in azimuth and 55° in elevation. Horizontal polarization was used in both examples.

---

*The IBM 650 at the Rich Electronic Computer Center was used.

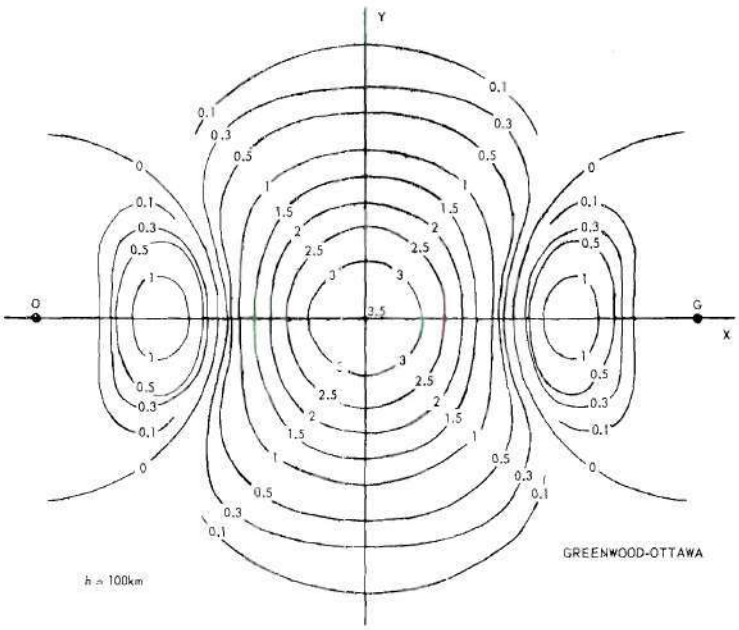

Figure 26. The Computed Antenna Illumination Pattern Used for the Greenwood-Ottawa Link.

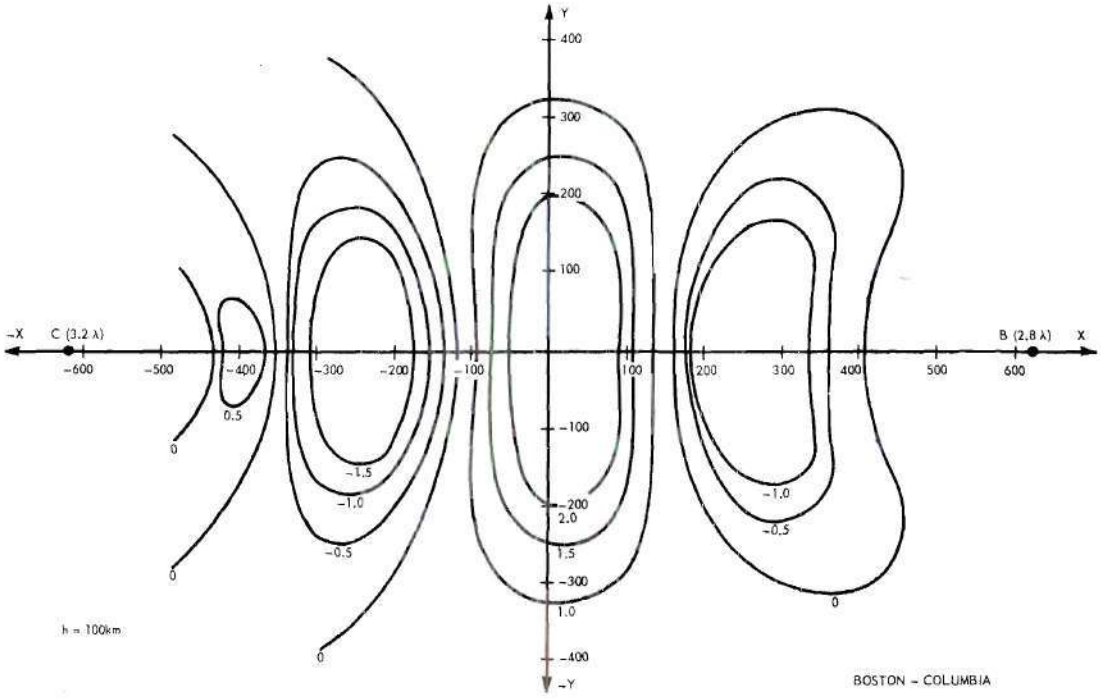

Figure 27. A Computed Antenna Illumination Pattern Used for the Columbia-Boston Link.

CHAPTER III

EXPERIMENTAL EQUIPMENT AND PROCEDURES

The primary purpose of the radio meteor experiments was to procure diurnal distributions of meteor echo rates under various conditions. Data were obtained over three meteor-transmission paths. Each link consisted of a transmitting station and a receiving station separated by a distance of 2D kilometers. The three sets of station locations were Atlanta-Knoxville, Atlanta-Boston, and Columbia-Boston. Table 1 lists some pertinent characteristics of each link. The three parameters A, Δ, and θ are measured at the midpoint of the great-circle path and are respectively: the azimuth bearing of the transmitter-receiver line measured north to east, the number of degrees east of the nearest time-zone meridian, and the number of degrees of north latitude. The transmissions in each case were unmodulated continuous waves with station identifications each half hour and a quiet period of about five minutes each hour. The Atlanta receivers were at Smyrna, Georgia, 12 miles northwest of the Georgia Tech campus. The Columbia receivers were at the Congaree Air Base, 15 miles east of Columbia, South Carolina, and they were operated by radio technicians of the South Carolina Air National Guard. The Knoxville transmitter was 12 miles south of Knoxville, Tennessee, and it was operated by University of Tennessee personnel. The Boston transmitters were at Walpole, Massachusetts, and they were operated by Pickard and Burns, Incorporated. The construction and operation

TABLE 1.
CHARACTERISTICS OF THREE METEOR-SCATTER LINKS FOR WHICH RECEIVERS WERE OPERATED BY GEORGIA TECH PERSONNEL

LINK	FREQUENCY f (MC)	TRANSMITTED POWER P_t (kw)	TRANSMITTER TYPE	STATION SEPARATION 2D (km)	T-R LINE AZIMUTH A (DEG)	TIME-ZONE OFFSET Δ (DEG)	LATITUDE θ (DEG)	ANTENNA BEAMWIDTH AZ-EL (DEG)	RECEIVER TYPE	RECORDER
ATLANTA-KNOXVILLE	41.94	0.5	AN/FRT-1 (MODIFIED)	230	13	−9.0	34.9	40–40	HAMMARLUND SUPER-PRO BC-779B	SANBORN
ATLANTA-BOSTON	49.44	5 to 10	COLLINS 205G-1	1480	51.5	−3.2	38.2	65–55	HAMMARLUND SUPER-PRO BC-779B	EDIN
	73.82	3	RCA BTF-3B (MODIFIED)					65–55	HAMMARLUND SUPER-PRO BC-778	EDIN
COLUMBIA-BOSTON	49.44	5 to 10	COLLINS 205G-1	1250	44.1	−1.4	38.0	65–55	HAMMARLUND SP-600	EDIN
	73.82	3	RCA BTF3-V					65–55	HAMMARLUND SP-600	EDIN

of the receiving stations and all data reductions were under the supervision of personnel of the Engineering Experiment Station of the Georgia Institute of Technology.

The noise figures of the receiving equipment were in all cases less than five db and the intermediate frequency passband was ordinarily three kc.

The Atlanta-Knoxville facility employed at each site a seven-element Yagi antenna mounted on a rotator so that any part of the sky could be illuminated with any polarization. The antennas had a front-lobe to back-lobe gain ratio of 30 db which was desirable because, at times, areas directly behind the transmitter or receiver were illuminated. Figure 28 is a photograph of the antenna and rotator at the receiving station in Smyrna. Figure 29 shows a block diagram of the receiving equipment. The crystal-controlled high-frequency converter, originally designed by personnel at the National Bureau of Standards, had constant gain and low noise figure. The receiver operated at 5 mc and used a separate crystal-controlled local oscillator operating at 5465 kc. The receiver beat-frequency oscillator was adjusted to produce a 1000 cps audio-frequency signal which passed through a 200 cps bandpass filter and was then recorded on a Sanborn paper recorder. The transmitted signal was held within the filter passband by an occasional adjustment of the 5 mc local-oscillator frequency. This filter was followed by the second detector and hence was very effective in improving the signal-to-noise ratio. The Sanborn recorder used paper tape which could be fed at a number of speeds. The frequency response of this recorder was from zero to approximately 80 cps.

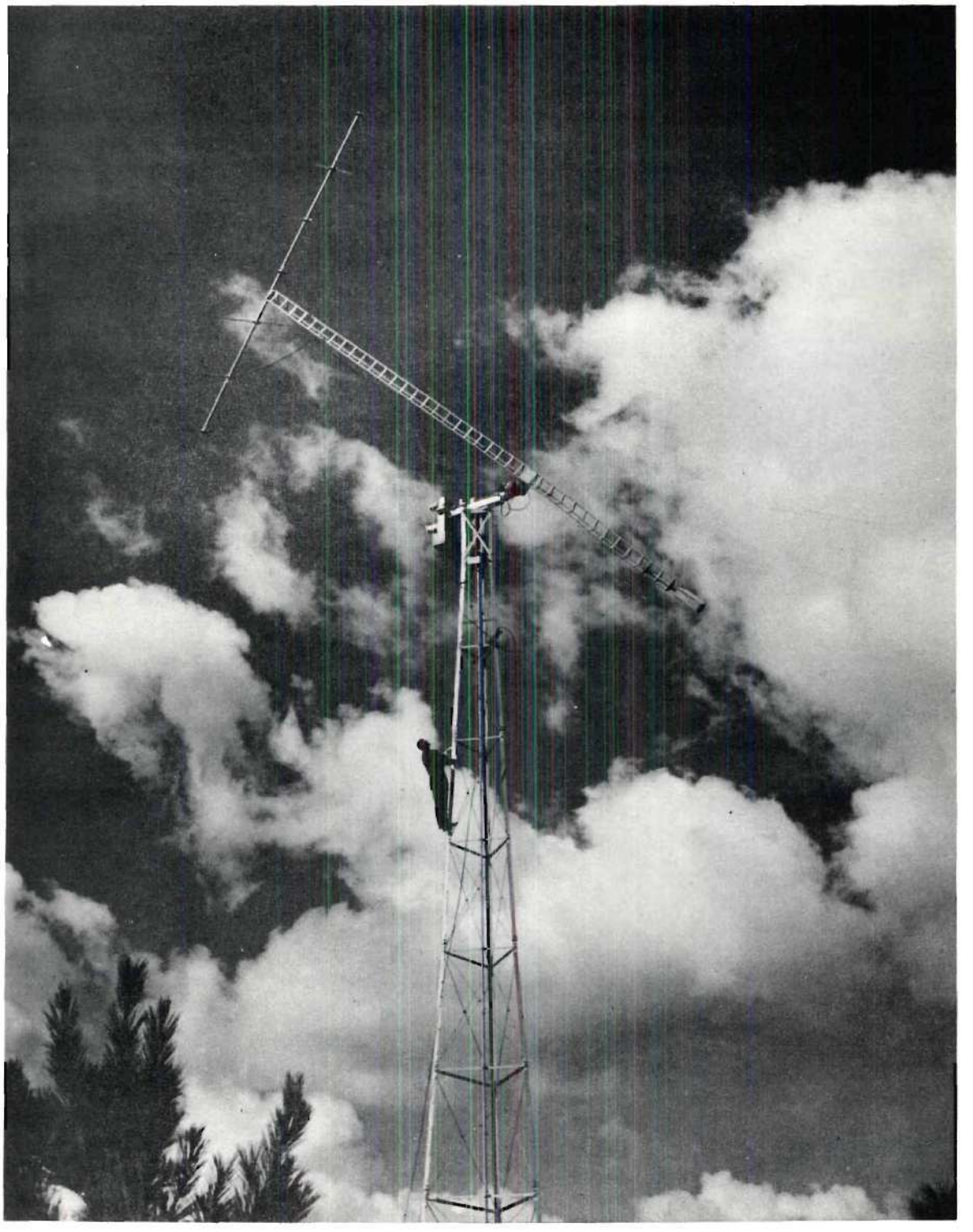

Photograph by Kenneth Rogers

Figure 28. A Photograph of the Antenna, Antenna Rotator, and Tower Used at Smyrna on the Atlanta-Knoxville Link.

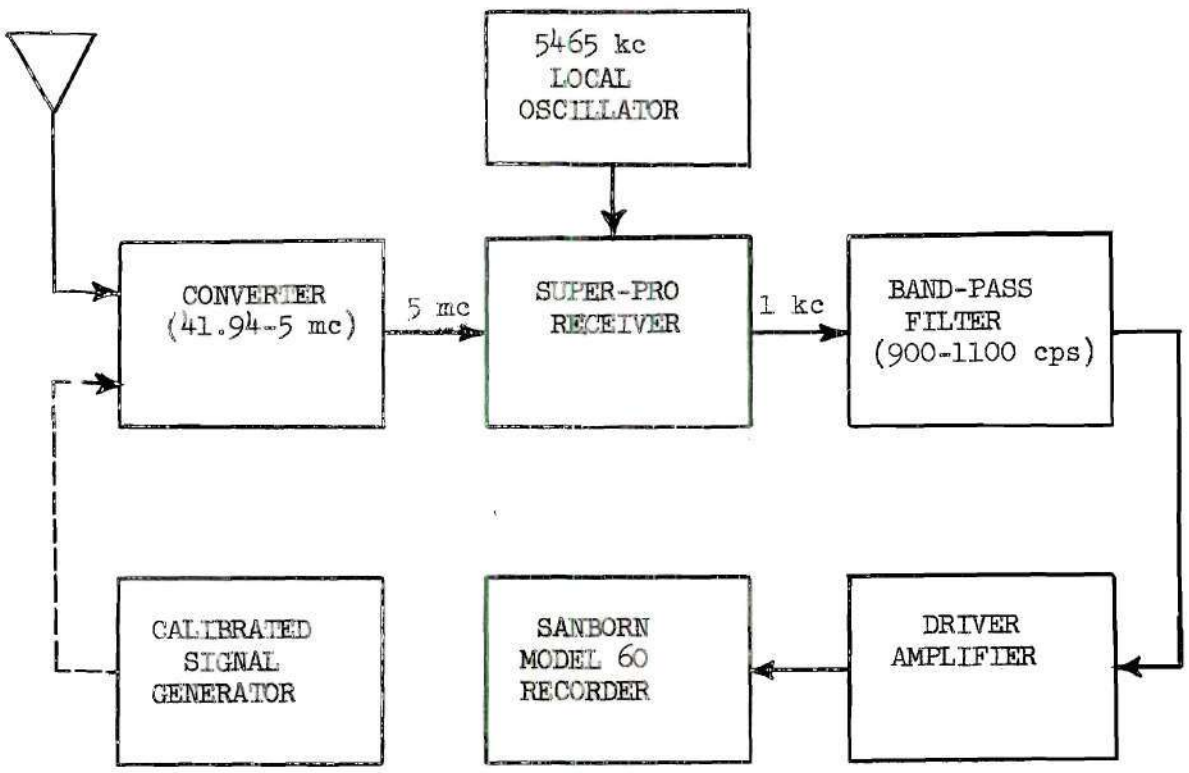

Figure 29. Block Diagram of the Receiving Equipment Used on the Atlanta-Knoxville Link

Figure 30a shows some samples of data taken over the Atlanta-Knoxville path. The amplitude of the pen deflection is approximately directly proportional to the amplitude of the antenna signal. Several types of echoes are illustrated in Figure 30. By far the majority of the echoes are of the underdense type which are characterized by a sharp rise and an exponential-type decay. The overdense or long-enduring echoes may or may not have short rise times and usually decay in a fluctuating manner. Only the sharp-rise echoes above a given threshold were counted; the slow-rise types are attributed to overdense trails that

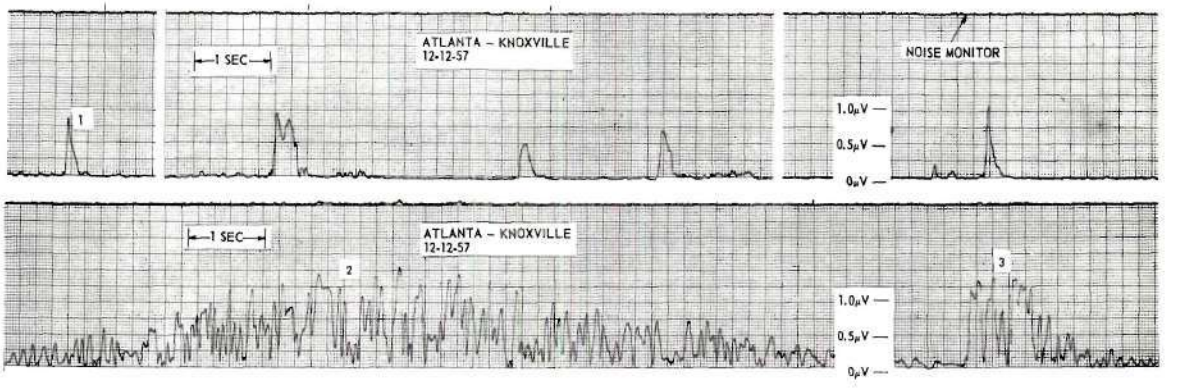

Figure 30a. Samples of Meteor Echoes for the Atlanta-Knoxville Link.

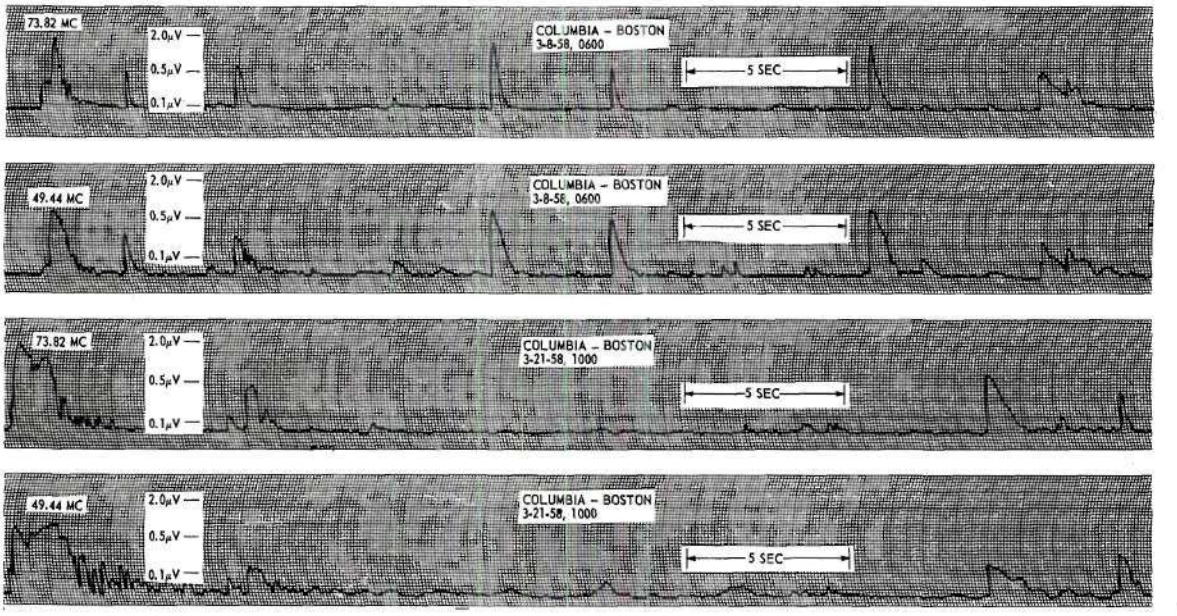

Figure 30b. Samples of Meteor Echoes for the Columbia-Boston Link.

were not oriented properly initially, but were distorted by upper-atmosphere winds. In Figure 30a, echo number 1 is underdense type, number 2 a slow-rise overdense, and number 3 a rapid-rise overdense type. The data were reduced by simply counting the acceptable type echoes that are larger than a given threshold and dividing by the appropriate counting time.

On the Atlanta-Knoxville link there was at certain times a considerable amount of background signal present. This signal is believed to be of tropospheric origin and was larger during the winter months than during the summer months. This signal was usually larger during the daytime when it exhibited a rapidly fluctuating nature; it was so large in fact that during the winter daytime hours very little data were useable. In general one can circumvent the effects of this background signal in either of two ways: (1) by increasing the counting threshold to such a level that the background signal never appreciably affects the meteor-echo amplitude or (2) by adjusting the threshold in accordance with the amount of background signal present so that on the average the meteor counting rate is not affected. Method (1) was not found to be feasible primarily because of the inherently low counting rates on the Atlanta-Knoxville link even under good conditions. Method (2) therefore was used with a threshold of $\sqrt{B^2 + M^2}$, where B is the amplitude of the background signal and M is the desired threshold level in the absence of background. It can be shown that this adjustment is approximately the correct one when meteor amplitudes are distributed according to Equation (1) with a k of unity.

The Atlanta-Boston and Columbia-Boston paths each operated simultaneously on 49.44 mc and 73.82 mc and in all cases employed five-element Yagi antennas. These antennas had axes parallel to the ground but the antenna heights were adjustable (in some cases up to 92 feet). The receiving equipment used was very similar to that for the Atlanta-Knoxville link (see Figure 29) except that no special filter was used and the automatic-volume-control signal was recorded on a six-channel Edin recorder. This Edin recorder had a frequency response of from zero to approximately 30 cps and produced records with curvilinear pen movements on paper tape that could be fed at a number of speeds.

Figure 30b shows some data samples taken over the Columbia-Boston links. The pen deflection for these data is approximately proportional to the logarithm of the antenna signal. Note that the individual time durations are longer than they were for the Atlanta-Knoxville link even though the frequencies are higher. This is due to the larger value of $\sec^2 \phi$ for the longer paths. Note also that for a given path the individual time durations are longer for the lower frequency. These effects are predicted by Equation (5). The counting rates for these longer paths were much larger than the average rate for the shorter Atlanta-Knoxville path due to a much greater coverage of the h-surface by the antenna beams.

The data reduction of the 73.82 mc and 49.44 mc data consisted simply of counting the acceptable echoes above a given threshold level. This level was always at least 10 db above noise or background signal. A considerable amount of ionospheric scatter signal was received on the

49.44 mc channel but very little was present at 73.82 mc. Care was always taken to distinguish noise pulses that might be present.

CHAPTER IV

A COMPARISON OF PREDICTED AND MEASURED ECHO RATES

The purpose of this chapter is to show comparisons between predicted variations in meteor echo rate and experimental data. The theories on which the predictions are based were presented in Chapter II. The experimental data are from two sources, namely from field stations of the Georgia Institute of Technology and from published results of Vogan and Campbell[19]. The experimental facilities used by personnel of the Georgia Institute of Technology were described in Chapter III. The data of Vogan and Campbell were taken over a Canadian link between Greenwood, Nova Scotia, and Ottawa, Ontario. This path was almost exactly east-west (N 93° E) with a station separation of 860 kilometers. The transmitted power was 100 watts at 49.98 mc, and the antennas were five-element Yagis (beamwidth 50°) for which the h-surface illumination was shown in Figure 26. The experimental data from these various sources will be shown later plotted adjacent to the predicted results.

The predicted results of the analysis based on a uniform distribution do not show a variation in echo rate with time. For this reason no comparisons of diurnal variations in echo rate can be made with these results; however, they are quite useful in several ways, especially for indicating the most effective h-surface regions as far as geometry is

concerned. On the other hand the ecliptic radiant distribution does predict a time variation in counting rate but the analysis based on this distribution only shows qualitative variations in the effectiveness of various h-surface regions. Therefore comparisons of these results with experiment will be made only in a qualitative fashion. The point-radiant studies described in Chapter II lead to predicted results that can be compared directly with measured diurnal variations of echo rate. The quantitative comparisons in this chapter therefore will be between experimental data and either predicted data for shower meteors or predicted data for sporadic meteors based on the three-point approximation.

A Geminid shower study.--The Atlanta-Knoxville link is particularly well suited for the study of meteor showers because of the small separation of stations and because of the antenna mounts that permit the antennas to be rotated with three degrees of freedom. Several showers have been studied and some results for the August Perseid shower have previously been reported[17].

Figure 31 shows a plan view of the Atlanta-Knoxville link together with some sample locus lines due to the December Geminid shower. The shaded area indicates the illuminated region of the h-surface on the night of December 12-13, 1957. The locus line moves slowly into the shaded region at about 2100 and then rapidly out of it after 0000. A predicted rate due to the Geminid shower for this experiment was computed according to the procedures discussed in Chapter II. This predicted rate is shown in Figure 32 along with the measured echo rates.

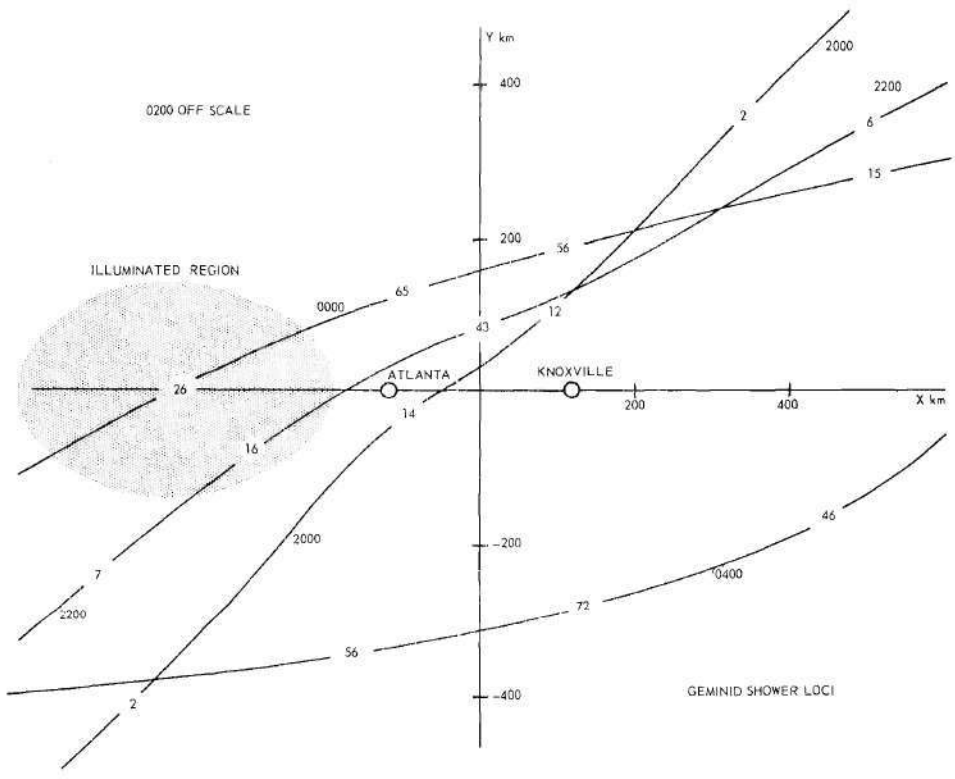

Figure 31. Geminid-Shower Loci for the Atlanta-Knoxville Link.

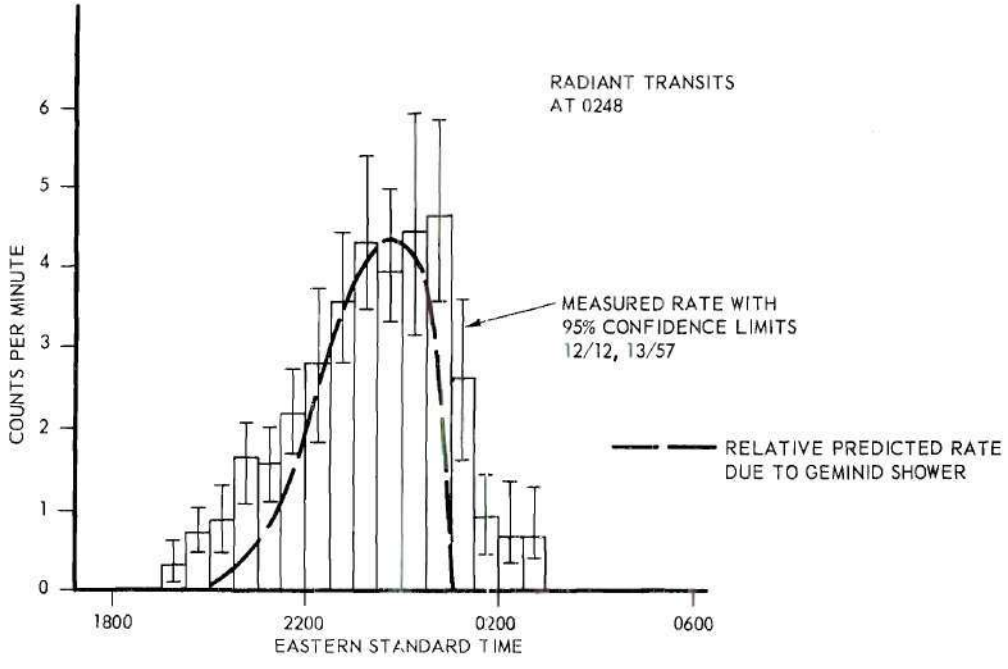

Figure 32. Comparison of Predicted and Experimental Results for a Geminid Shower Experiment on the Atlanta-Knoxville Link.

The experimental data include both shower and sporadic meteors; however, on the basis of tests made December 4 the sporadic background is expected to be less than one count per minute during the interval of the test. From about 0030 until 0300 there were a large number of echoes of the slow-rise, long-enduring type which were not counted. These echoes are attributed to overdense trails that occur in the illuminated region with an orientation that differs very little from the proper orientation for reflection. It is surmised that upper-atmosphere winds distort and break up these trails so that sections of them become properly oriented a short while after the trail is formed.

The agreement of predicted and measured results in Figure 32 is very good. This and similar results for other showers indicates that the procedures used in making point-radiant computations are correct and that good results should always be had if the correct radiant point is used.

Three-point approximation comparisons.--These comparisons will be made between predicted results on the basis of the three-point approximation described in Chapter II and experimental data taken on the Greenwood-Ottawa, Atlanta-Knoxville, Atlanta-Boston and Columbia-Boston links. The predicted results were computed according to the procedures outlined in Chapter II.

The comparisons between predicted and experimental results for the Greenwood-Ottawa link are shown in Figures 33 through 38. In each case the predicted results for these comparisons were made for the fifteenth day of the month except for the June results which are an average of June 7 and June 21 predictions. The amplitudes of the

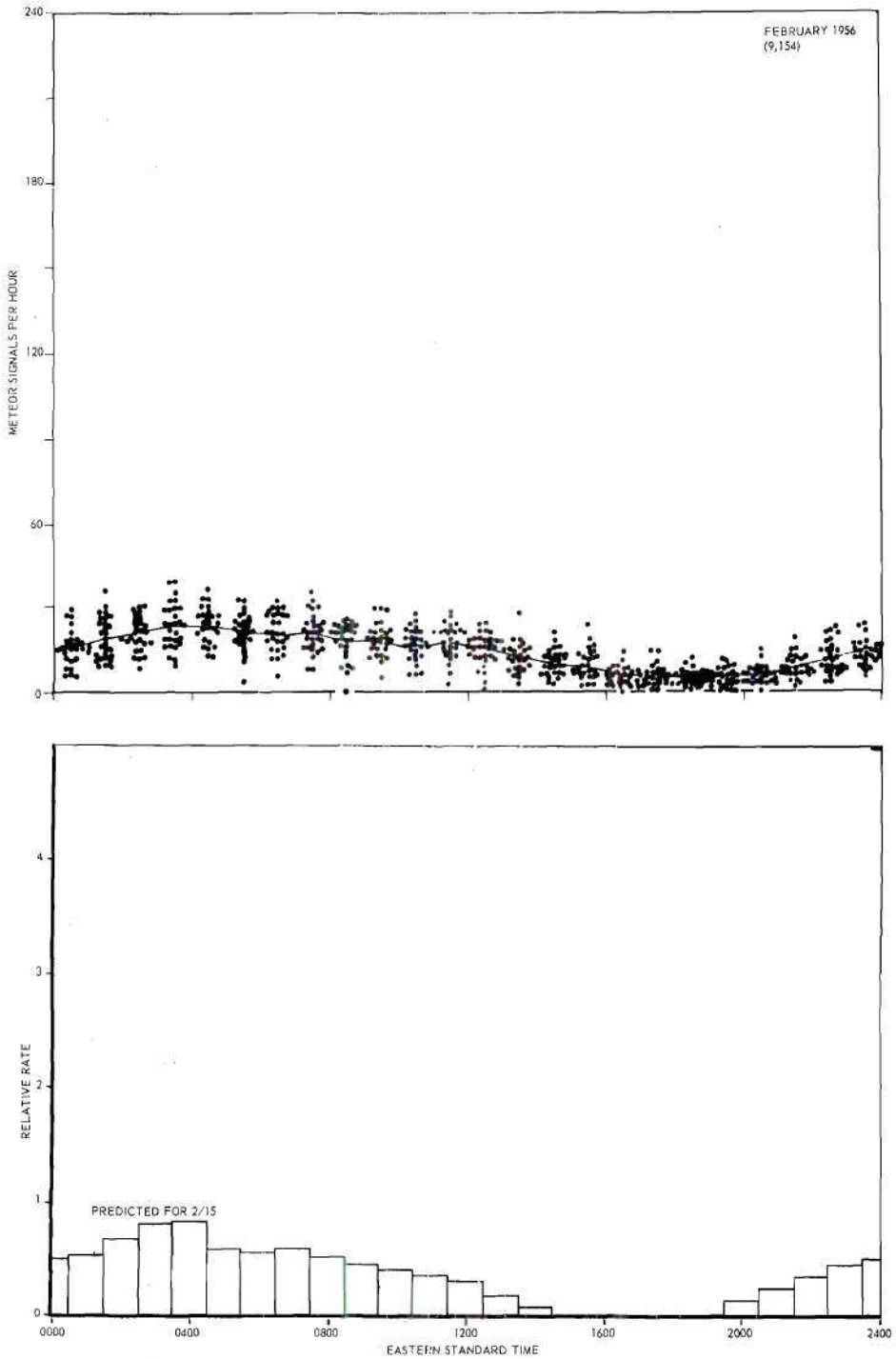

Figure 33. A Comparison of Experimental and Predicted Results Using the Three-Point Approximation for the Greenwood-Ottawa Link.

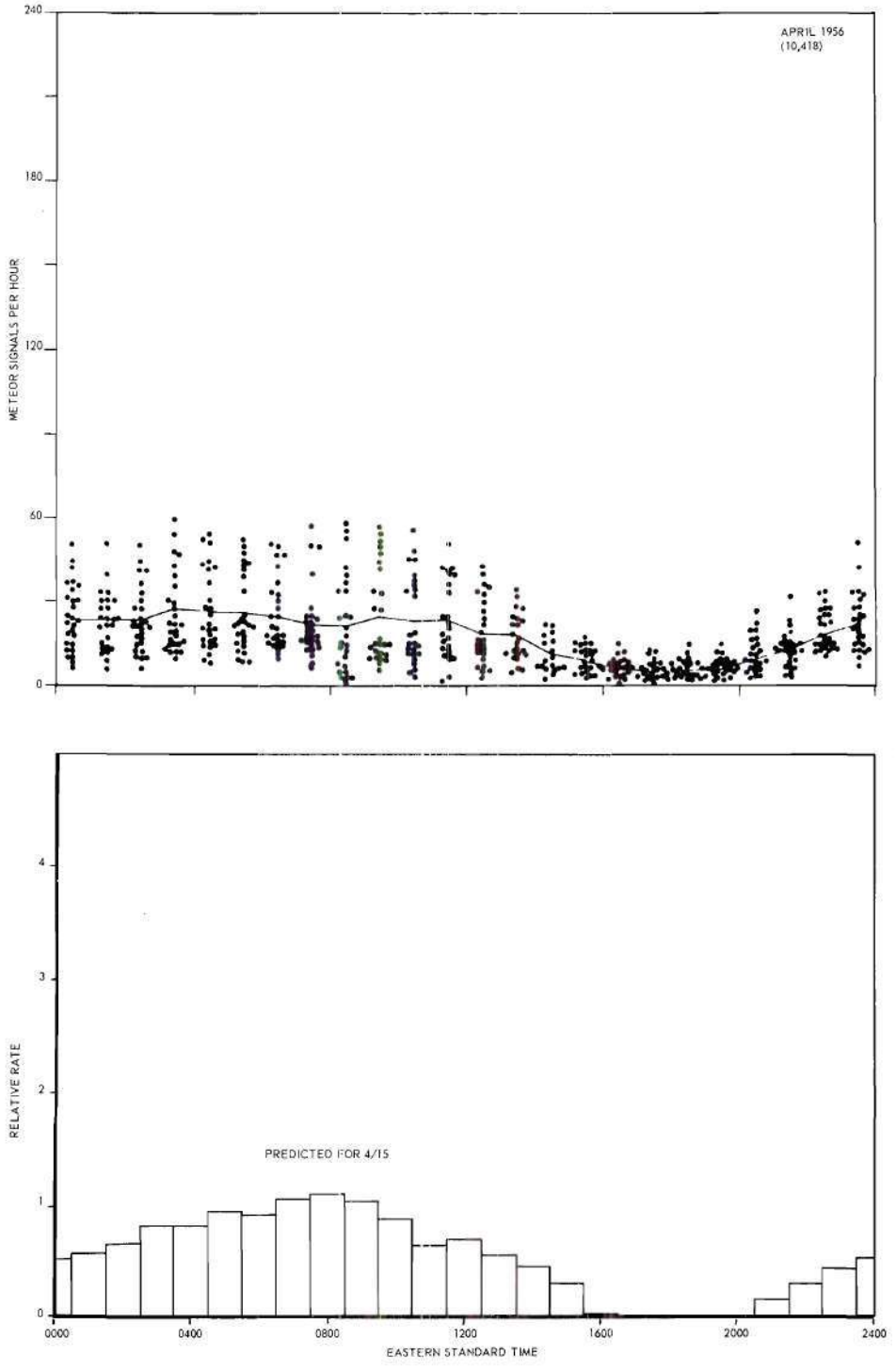

Figure 34. A Comparison of Experimental and Predicted Results Using the Three-Point Approximation for the Greenwood-Ottawa Link.

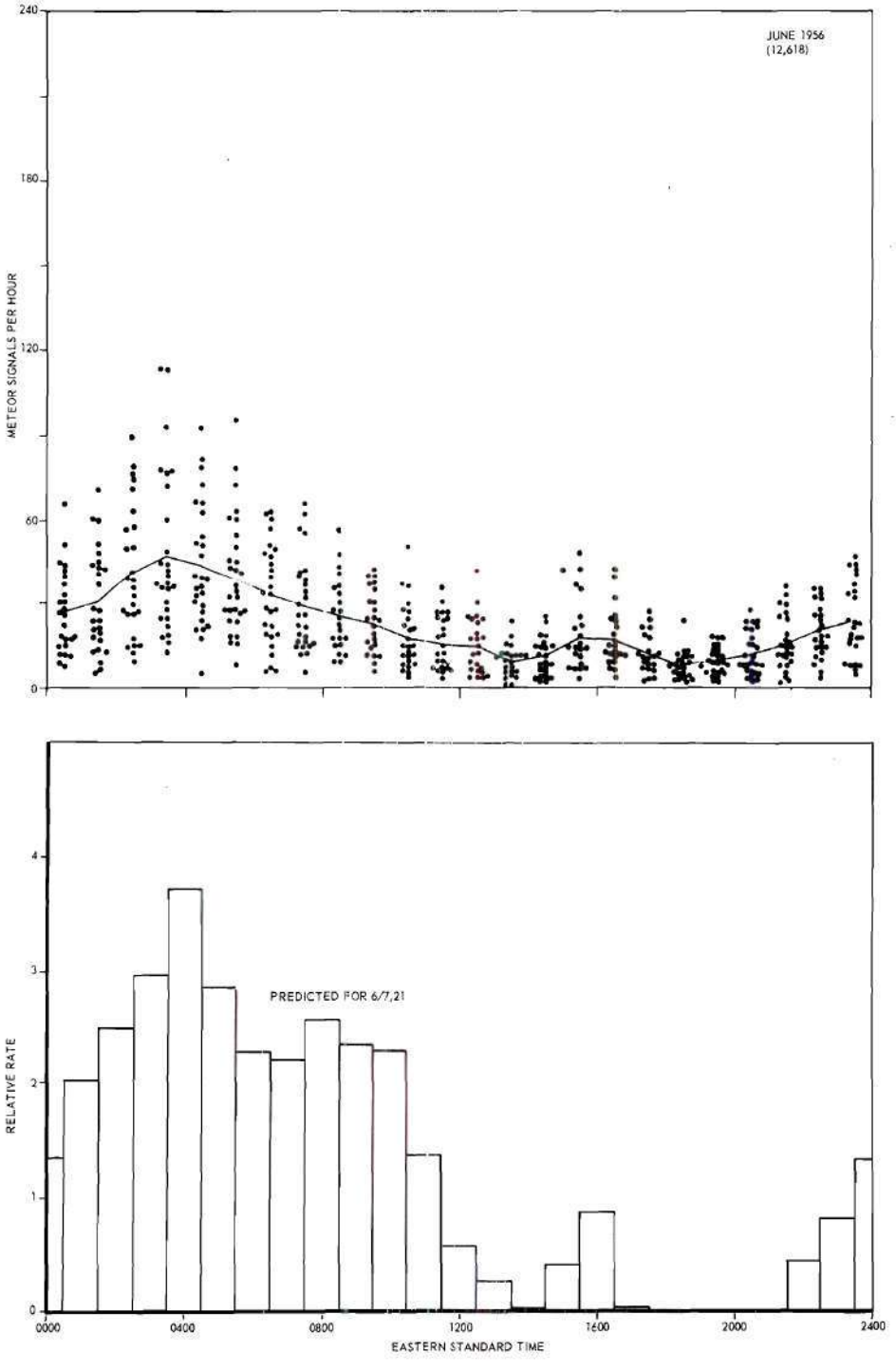

Figure 35. A Comparison of Experimental and Predicted Results Using the Three-Point Approximation for the Greenwood-Ottawa Link.

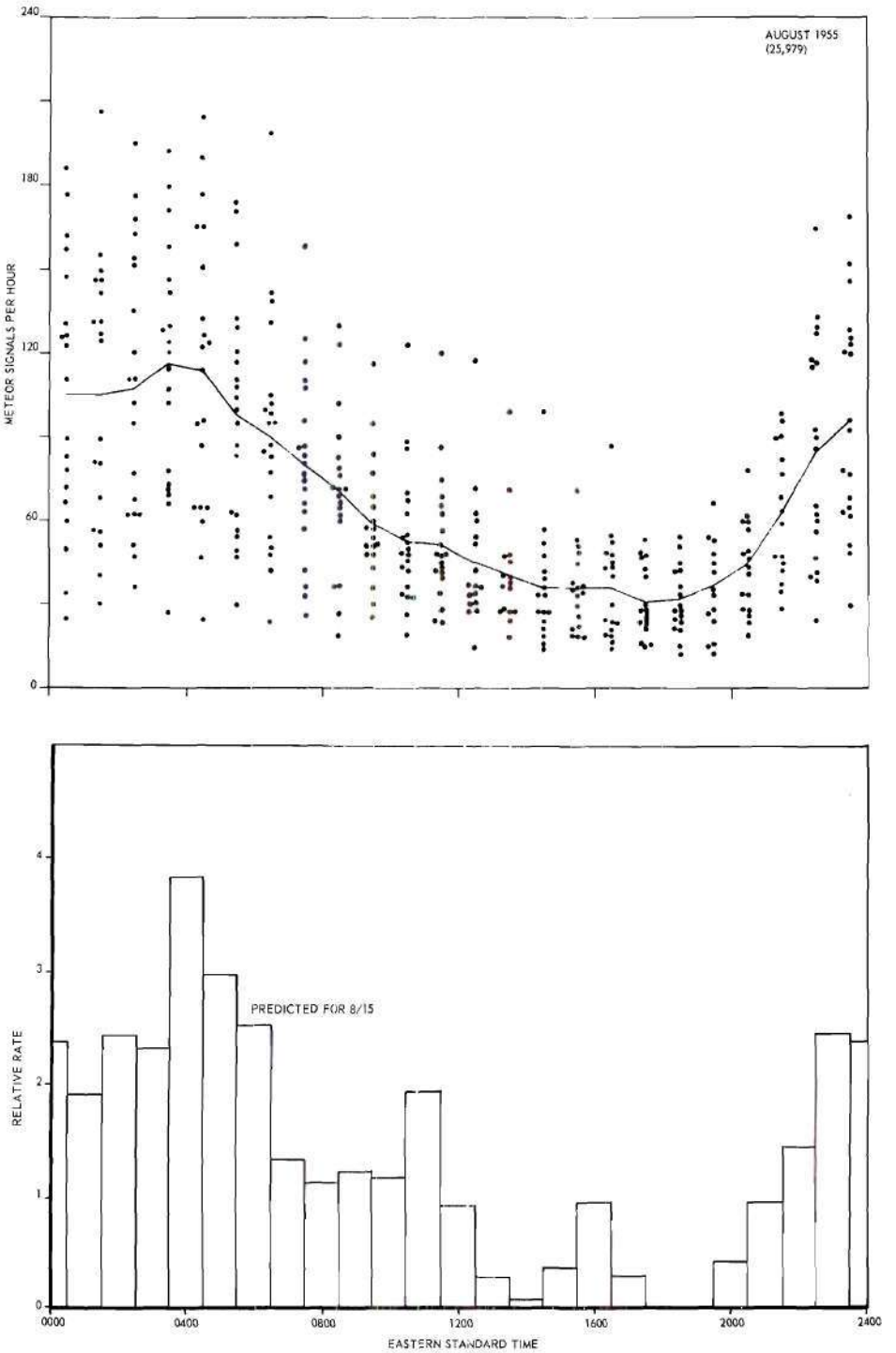

Figure 36. A Comparison of Experimental and Predicted Results Using the Three-Point Approximation for the Greenwood-Ottawa Link.

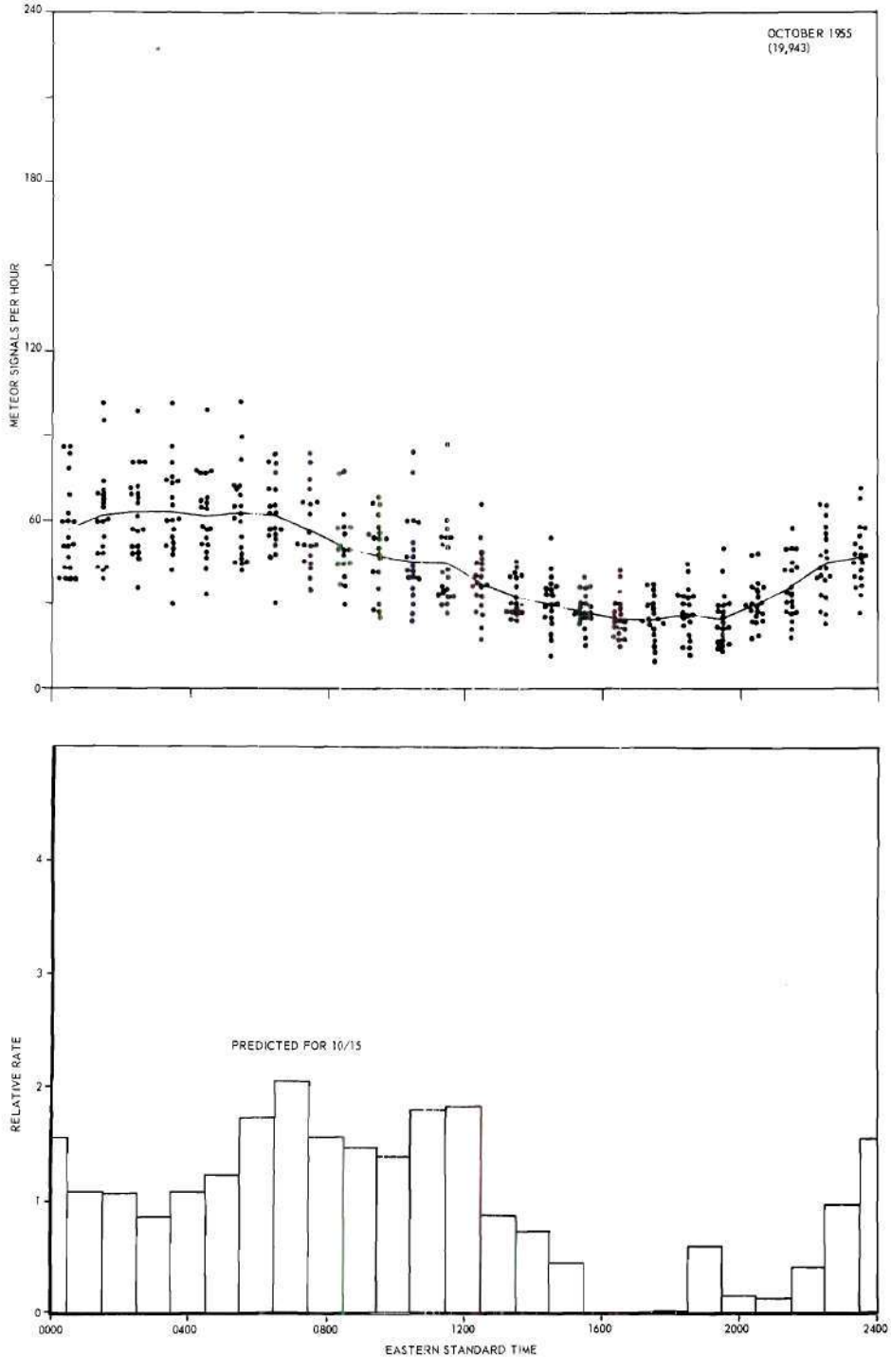

Figure 37. A Comparison of Experimental and Predicted Results Using the Three-Point Approximation for the Greenwood-Ottawa Link.

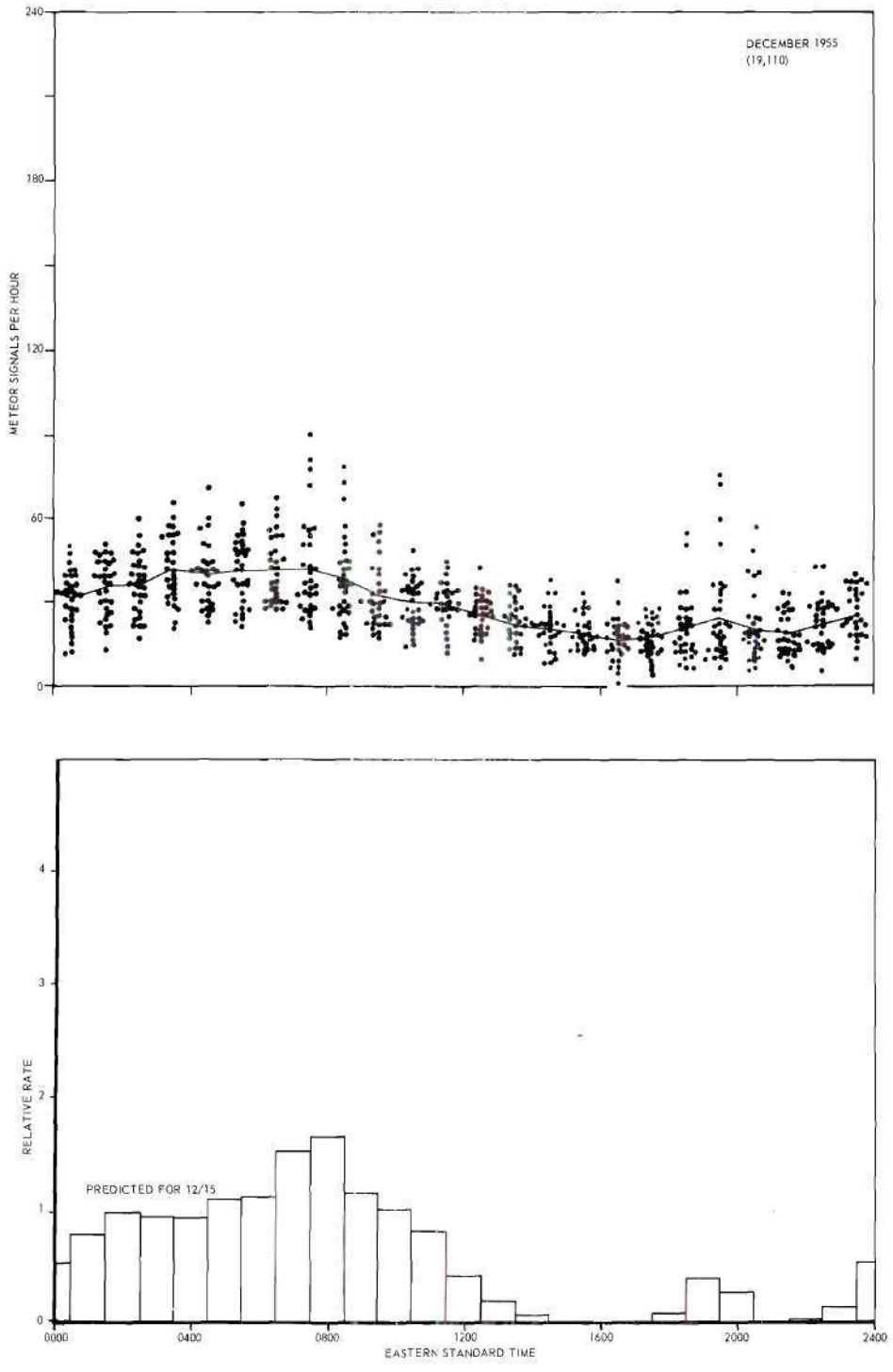

Figure 38. A Comparison of Experimental and Predicted Results Using the Three-Point Approximation for the Greenwood-Ottawa Link.

predicted results for each month have been normalized to agree with the monthly average echo rates as reported by Hawkins[4]. Thus on this basis the relative amplitudes of all the predicted results for the Greenwood-Ottawa link can be compared among themselves.

The published data of Vogan and Campbell for the Greenwood-Ottawa link are in the form of twelve monthly averages of the diurnal distributions of echo rates. There is one averaged curve for each month of the year and on each curve is shown the total number of echoes from which the average was taken and an indication of the hourly spread about the mean. Six of these twelve plots have been reproduced in Figures 33-38.

The results in Figures 33-38 show generally good agreement. Figure 33 shows a broad maxima at 0400 on both predicted and experimental results and in general the two curves match very well. The predicted result in Figure 34 shows a broad maxima at 0800 and the experimental results show essentially a constant rate from 0000 to 1200 hours. Figure 35 shows a sharp peak at 0400 and an interesting sub-peak at 1600 on both predicted and experimental curves. This predicted sub-peak is due to the Sun radiant and thus it seems that the experimental results confirm a concentration of radiants about this location. The plots of Figure 36 both show a high activity at midnight and a sharp peak at 0400 but the predicted sub-maxima at 1100 and 1600 do not show up very strongly in the experimental results. However, the agreement is generally good. The experimental data of Figure 37 do not show a relative minimum at 0300 as predicted but the relatively high rate on the experimental data at 1130 is present as predicted. The results in Figure 38 show very good agreement

with peaks on both predicted and experimental curves appearing at 0800 and 1900. These peaks are more pronounced on some days than on others as indicated by the spread of points about the averaged curve.

Atlanta-Boston comparisons of prediction and experimental results are shown in Figures 39 through 42. The experimental data were taken simultaneously for the two frequencies for a total of two to five days within the time interval shown on each figure. The total number of echoes used for each average plot is also shown. Note that the 49.44 mc and 73.82 mc plots do not agree perfectly even though the antenna illumination patterns were nominally equivalent. The main source of difference between the two experimental curves is believed to be due to a difference in the relative threshold levels used for making the two counts.

The agreement of theory and experiment is in general good for these data. The better agreements are generally found for the experimental data with the better statistics. The December comparisons in Figure 42 are particularly good. The relative minimum that occurs on all the predicted results around 0200 to 0400 is due to the Anti-Sun locus moving northward out of the antenna pattern at about this time. The experimental data do not in all cases show this minimum. Except for this variance the February comparisons in Figure 39 are particularly good. The two sets of comparisons shown by Figures 40 and 41 have poorer statistics and, although the comparisons are not bad, they are not as good as those in Figure 39 and 42.

Figures 43 and 44 show two sets of predicted and experimental comparisons that have been made for the Columbia-Boston link. The

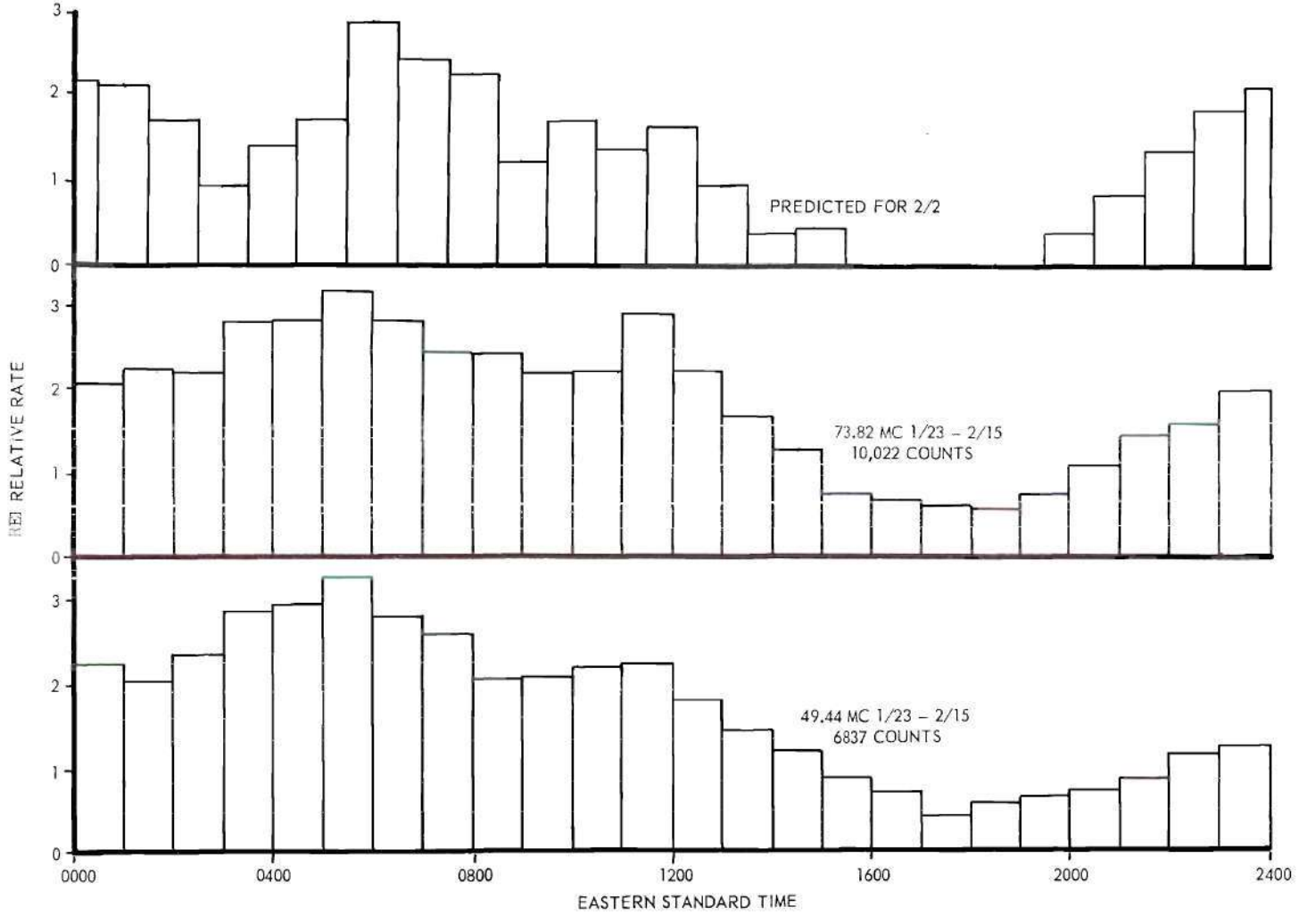

Figure 39. A Comparison of Experimental and Predicted Results Using the Three-Point Approximation for the Atlanta-Boston Link.

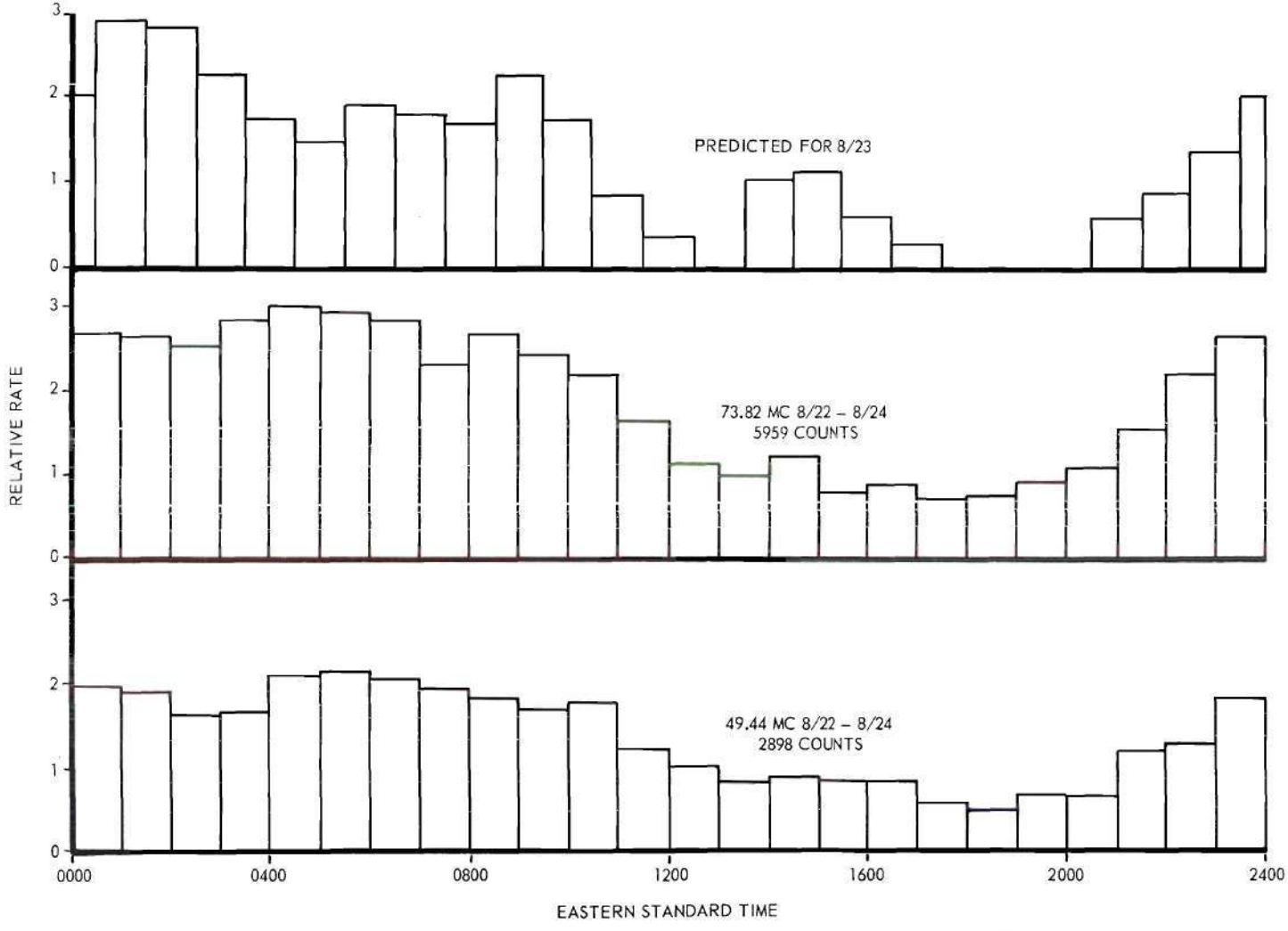

Figure 40. A Comparison of Experimental and Predicted Results Using the Three-Point Approximation for the Atlanta-Boston Link.

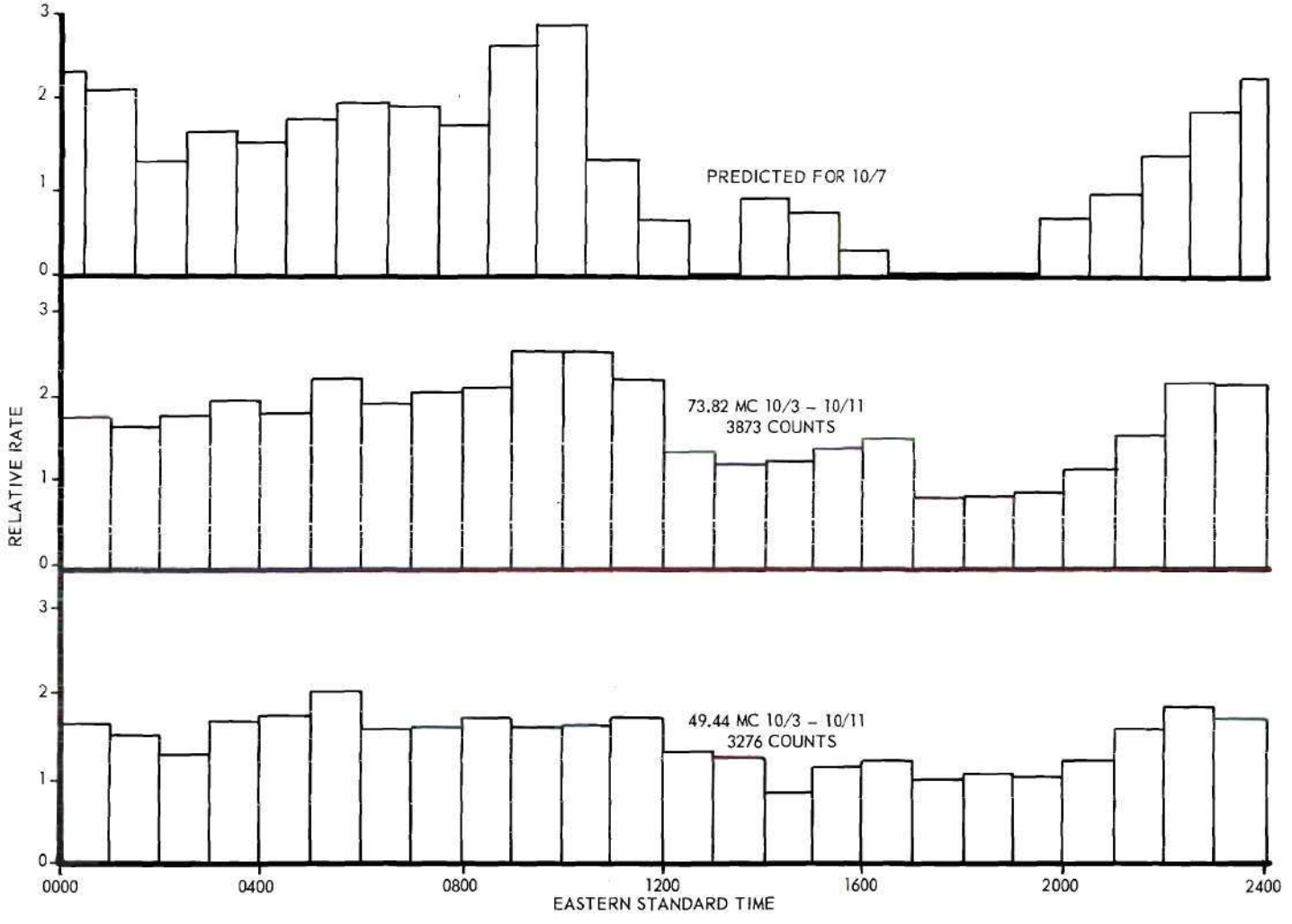

Figure 41. A Comparison of Experimental and Predicted Results Using the Three-Point Approximation for the Atlanta-Boston Link.

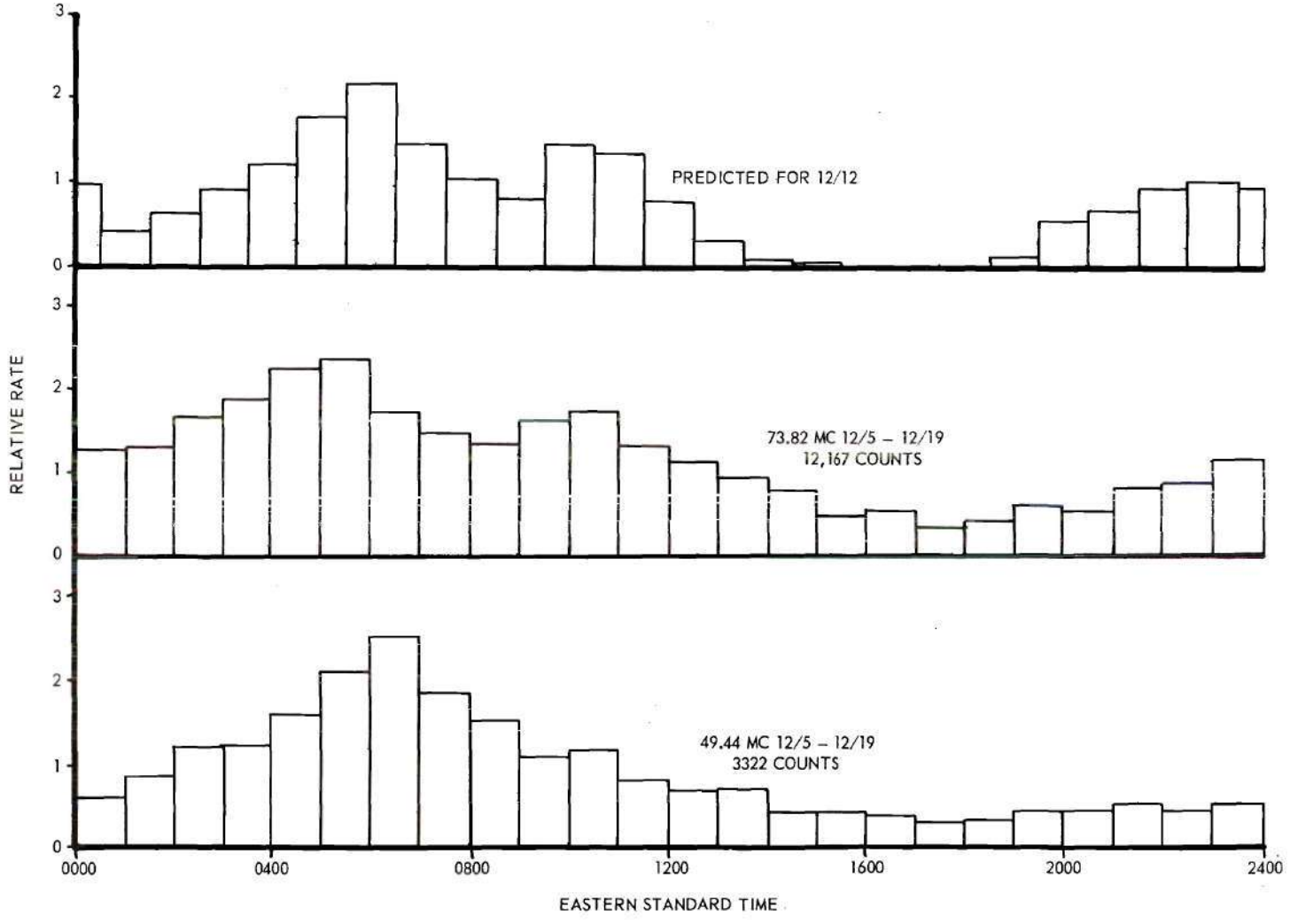

Figure 42. A Comparison of Experimental and Predicted Results Using the Three-Point Approximation for the Atlanta-Boston Link.

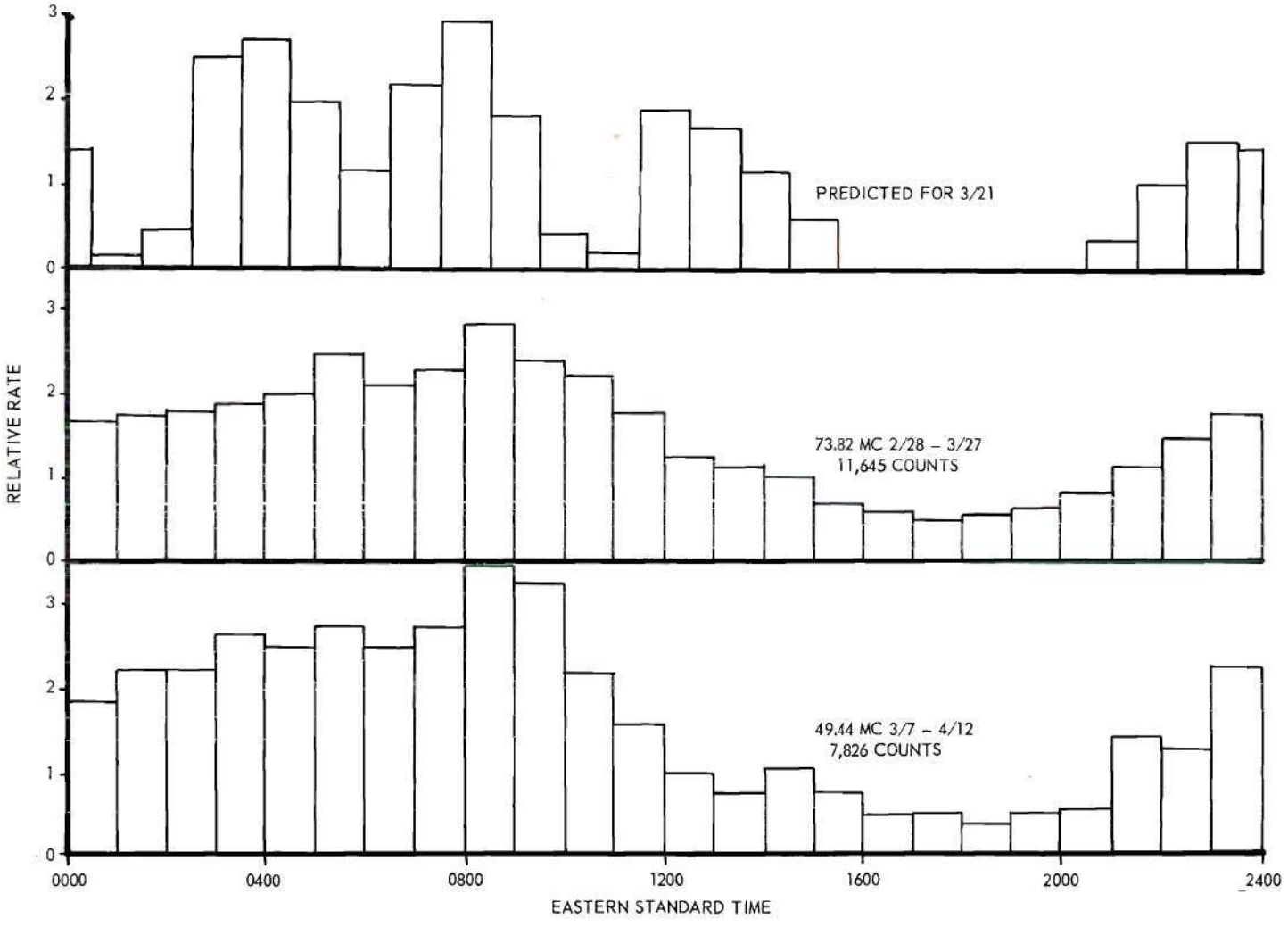

Figure 43. A Comparison of Experimental and Predicted Results Using the Three-Point Approximation for the Columbia-Boston Link.

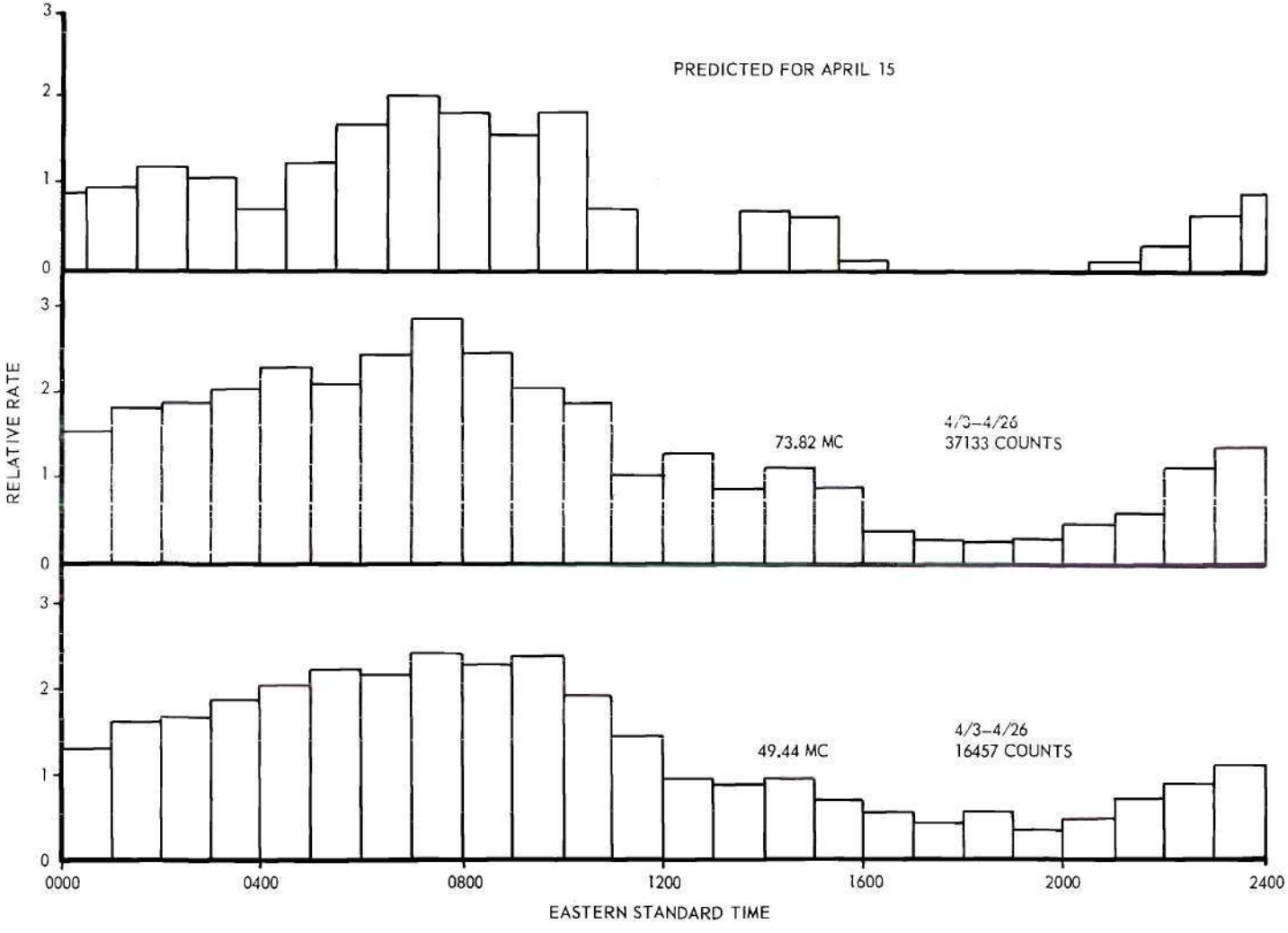

Figure 44. A Comparison of Experimental and Predicted Results Using the Three-Point Approximation for the Columbia-Boston Link.

antenna pattern used for the predicted results in these two figures has been shown as an example in Figure 27. The predicted and experimental rates of Figure 44 show better agreement than those of Figure 43. However, if one would permit a smoothing of the predicted data in Figure 43 so that the relative maxima and minima were not as severe, the agreement would be much better with a slow increase in counting rate before 0800 and a slow decrease after 0800 with a minimum occurring around 1800.

Three sets of comparisons using Atlanta-Knoxville data are shown in Figures 45, 46 and 47. Each figure shows both a predicted and a measured diurnal distribution of echo rates. For the experimental data in these figures the antenna beams were in each case directed alternately to intersect with optimum polarization at two geometrically equivalent points on the h-surface. In Figure 45 these two points are A(x = 200 km, y = 75 km) and B(x = 200 km, y = -75 km). In Figure 46 they are A(x = 0 km, y = 60 km) and B(x = 0 km, y = -60 km), and in Figure 47 they are A(x = 115 km, y = 0 km) and B(x = -115 km, y = 0 km). The computed results are shown plotted for 30-minute intervals but in each case the computations were made to apply on the hour.

The regions of the h-surface illuminated by the antennas for this relatively short link are much smaller in absolute magnitude than the illuminated region for the Greenwood-Ottawa link. The illuminated region applicable to Figure 47, when areas directly above Atlanta and Knoxville were alternately searched, is very small indeed. For this case the gain factor, $S\sqrt{G_r G_t}$, decreases to approximately one-half of peak value on a circle of radius 50 km about the center of the illuminated zone. In computing the predicted rates for this case (Figure 47) an analytical

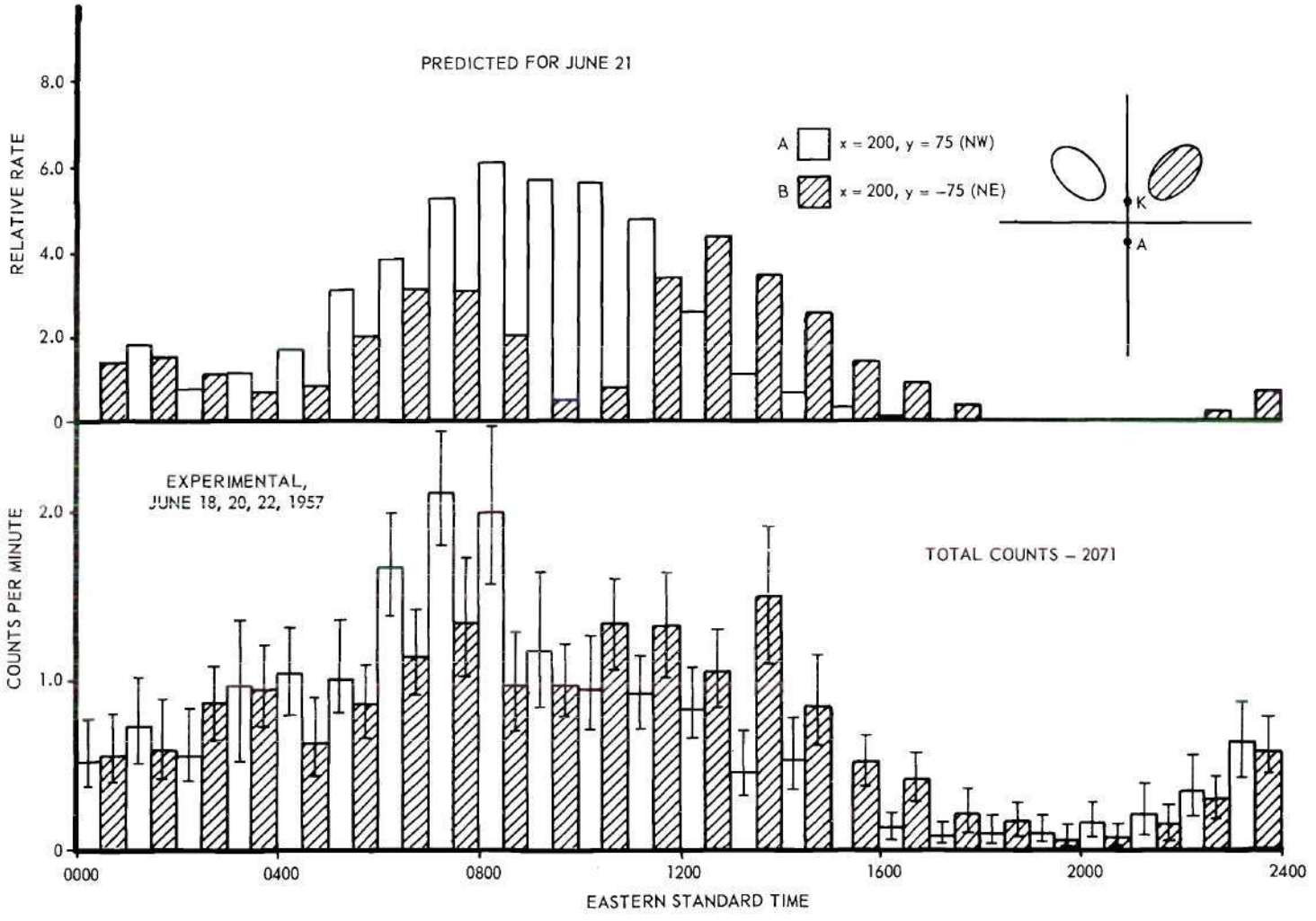

Figure 45. A Comparison of Experimental and Predicted Results Using the Three-Point Approximation for the Atlanta-Knoxville Link.

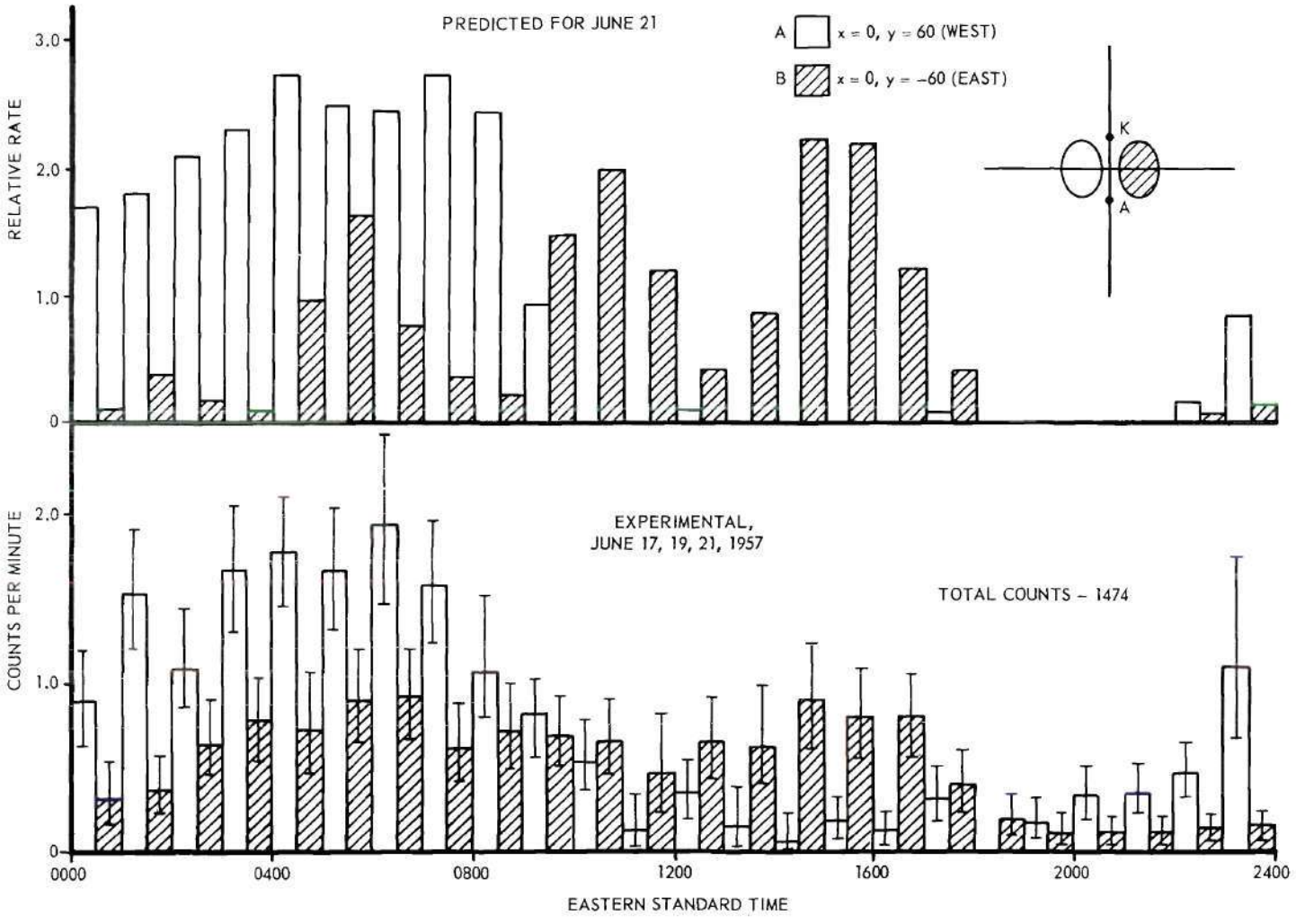

Figure 46. A Comparison of Experimental and Predicted Results Using the Three-Point Approximation for the Atlanta-Knoxville Link.

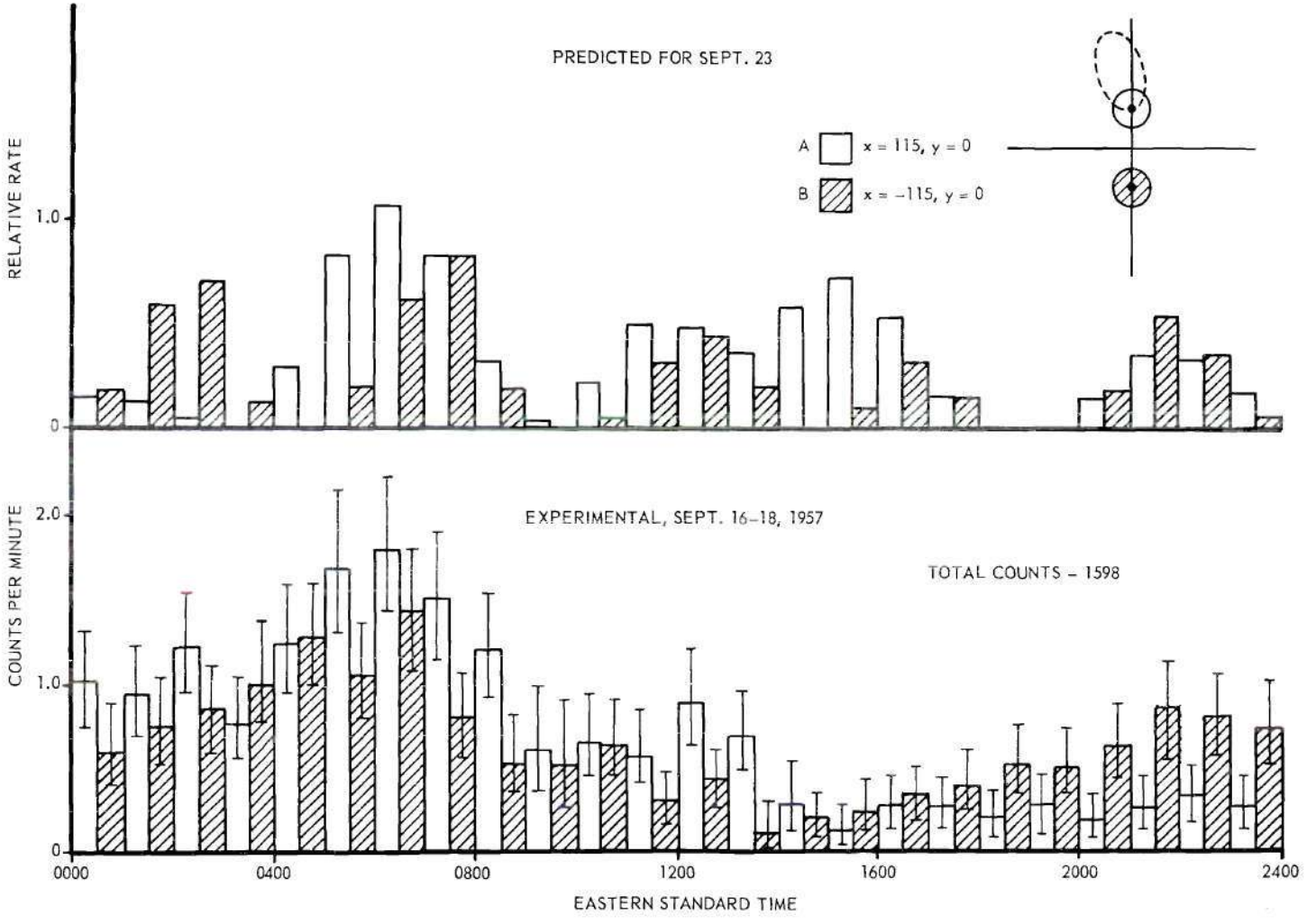

Figure 47. A Comparison of Experimental and Predicted Results Using the Three-Point Approximation for the Atlanta-Knoxville Link.

procedure was used in which the width of each locus line was taken to be 100 km. The magnitudes of the predicted results are, however, comparable among the Figures 45, 46 and 47. The magnitudes of the experimental rates are believed to be comparable; however, no attempt to make rigorous absolute calibrations was made.

The agreement of predicted and experimental results for these Atlanta-Knoxville data is not as good as was obtained for the Greenwood-Ottawa data. There are at least two reasons for this: (1) The Atlanta-Knoxville statistics are, by comparison, poor. A total of only 2071, 1474, and 1598 echoes were used to obtain the averaged data in Figures 45, 46 and 47, respectively, while the Greenwood-Ottawa curves in each case are the results of averages made using 9,000 to 28,000 echoes. Furthermore, appreciable day-to-day variations in the shapes of diurnal distributions of echo rates even for data with good statistics have sometimes been observed. This means that experimental data obtained by averaging over many days as well as over many echoes should be expected to show better comparisons with predictions. (2) A large antenna illumination pattern has a smoothing and averaging effect on the discrete nature of the three-point approximation. That is, a large antenna pattern has the general effect of replacing each point-radiant by a distribution of radiants in the vicinity of the point, as far as the predicted results are concerned.

The data in Figures 45, 46 and 47, however, show several points of agreement. For example, the experimental data of Figure 45 show a higher count for point A at 0700 and a higher count for point B at

1400 as predicted. Points of agreement in Figure 46 are the higher count for point A from 2200 until 0800, the higher count for point B from 1200 until 1800, and the very low count for point A from 1200 until 2200. The points of agreement in Figure 47 are the peaks at about 0600 with the rate for A being larger than the rate for B, and the larger relative rate for B at about 2200.

The predictions on the basis of the three-point approximation that have been shown here for the four links represent all such predictions that have been made. They are not a selected sample from a larger number of such computations.

Some predictions of diurnal variations of meteor echo rates have been made previously by Hines[20]. He used a symmetric radiant distribution centered on the apex of the earth's way to make sample predictions for days near the solstices. Good agreement was claimed but no comparisons with experimental data were shown.

Ecliptic-tangent-point comparisons.--The significance of the ecliptic tangent point will be deduced on the basis of comparisons of the Greenwood-Ottawa and Atlanta-Knoxville data with the appropriate tangent-point paths shown in Figures 12-15. For the Greenwood-Ottawa link, which has a station separation of 860 kilometers, the curve labeled $\delta = 90^{\circ}$ in Figure 15 is the most appropriate of the orbits shown. When the appropriate tangent-point orbit is determined and superimposed on the antenna pattern given in Figure 26 it can be seen that the ecliptic tangent point moves through the central region of this pattern for about four hours each day. For each succeeding month this four-hour interval appears two hours earlier in the day. In

June, for example, this interval appears at midnight, in September at 1800, in December at 1200, and in March at 0600 hours. When the proper four-hour interval is in this manner associated with each of the Figures 33-38 and the relative experimental rates during these four-hour intervals are noted, there seems to be little correlation between high relative echo rates and the movement of the ecliptic tangent point. This is especially true around 1800 hours. However, during the morning hours, the movement of the ecliptic tangent point is correlated with a shift in the time of maximum echo rate for the experimental data from about 0800 in December to about 0400 in June. Hence these data indicate that the ecliptic tangent point may have some significance during the morning hours.

Figures 45 and 47 show two sets of data taken on the Atlanta-Knoxville link that can be compared with the ecliptic-tangent-point results. For the experimental data of Figure 45 the antennas were directed alternately toward two points on the orbit of the tangent point. These points were A(x = 200 km, y = 75 km) and B(x = 200 km, y = -75 km). From the standpoint of scattering geometry these points are mirror images about the path axis, and any difference in counting rate can therefore be assigned to the radiant distribution. Points A and B were observed alternately every thirty minutes and Figure 45 shows the average meteor signal rate for a period of three days. When the antenna beamwidths are taken into account, one would expect on the basis of the orbit shown in Figure 12 that point A should receive a contribution from the ecliptic tangent point from about 0500 until 1000, and point B should receive a contribution from about 1500 until

2000. Figure 45 shows a significantly higher counting rate for A from roughly 0530 until 0900. The degree by which the two counting rates differ may be judged by observing the 95 per cent confidence limits which have been indicated for each counting period. The meteor signal rate for point B in Figure 45 shows higher values during the entire afternoon period until roughly 1930. The experimental data show clearly a higher activity for point B from 1530 until 1730 as predicted. The low counting rate during the period 1730-2000 does not permit a clear statistical distinction between the rates at points A and B. Thus, one finds good agreement between the measurements and predictions based on a rather diffuse concentration of radiants near the ecliptic. The comparatively high counting rate observed at point B during the interval 1330-1400 is, however, not expected on this basis.

For the data of Figure 47 the antennas were directed alternately toward a point on the tangent-point orbit and a geometrically equivalent point off the orbit. These points were A(x = 125 km, y = 0 km) and B(x = -125 km, y = 0 km). Figure 47 shows the meteor signal rate averaged for a period of two days. On the basis of the orbit shown in Figure 12, and the computed antenna coverage, point A should receive a contribution from about 1700 until 2100 and point B should receive no contribution at all from the ecliptic tangent point. However, Figure 47 shows a higher counting rate for point B from 1700 until 2100, which is just the reverse from what is predicted on the basis of the ecliptic tangent point, and therefore again no evidence of the effect of this ecliptic tangent point is observed around 1800 hours.

CHAPTER V

CONCLUSIONS

The effect of radiant distributions on meteor-trail communication has been demonstrated by a number of computations based on several different radiant distributions. An analysis based on a uniform distribution of meteor radiants over the celestial sphere shows that the relative effectiveness of various regions of the sky is a function of many geometrical factors and also of k. This parameter k, which is defined in Equation (1), is determined by the size distribution of the meteoroids incident upon the atmosphere. The results of several sets of computations based on different values of k, station separation, and antenna polarization are shown in Figures 2-10. The uniform distribution plots in Figures 2-4 serve to show that the antenna polarizations are important for meteor-scatter links having small station separations. The effect of increasing k is to intensify the relative differences in the effectiveness of various regions of the meteor-trail zone.

The relative-effectiveness computations have been performed for two parameters that are of interest and that can be measured for a given meteor-scatter link. These parameters are meteor signal rate and duty cycle. The relationship between the two is proportional to $\sec^2 \phi$ as shown by Equation (11). Duty cycle is more difficult to measure directly but is perhaps of more value to the communications engineer.

The predictions based on a uniform radiant distribution are not time dependent and are symmetrical about both the x and the y axes. These predictions indicate that the regions of the largest potential contribution to the meteor signal rate are those regions directly above the transmitter and receiver and that the regions having the largest potential duty-cycle contribution are to either side of the midpoint of the transmitter-receiver line. It is convenient to think of the contribution of a given region of the meteor-trail zone as being due to the product of three factors: an antenna illumination factor, a geometrical factor, and a factor determined by the radiant distribution. To a first approximation the prediction based on the uniform radiant distribution is the geometrical factor; however, the geometrical and the radiant distribution factors cannot be completely separated.

A radiant distribution in which all radiants are near the ecliptic has been investigated and it was found that a region of high activity, as far as the radiant distribution factor is concerned, moves over a fixed path on the h-surface once each sidereal day. This region of high predicted activity, called the ecliptic tangent point, becomes diffuse when all radiants are not exactly on the ecliptic. When these results were compared with experimental data no evidence of an ecliptic distribution was found for the evening hours around 1800. However, some indication of an ecliptic distribution was found for the morning hours. Just how strong the ecliptic concentration is cannot be determined from this analysis because no provision is made for the computation of the relative effectiveness at all points on the h-surface.

An analysis based on a single radiant has been made, and the results show that a line across the h-surface represents the locus of points at which the meteor trails are properly oriented for a reflection at a height h. When account is taken of the variation of h, from about 80 km to 120 km, this locus becomes a long narrow band. A measure of effectiveness at points along the locus has also been determined. This analysis applies directly to meteor-shower studies and is basic to studies of arbitrary radiant distributions that are represented by a number of point-radiants.

The validity of the single-radiant analysis has been verified experimentally with data taken over the Atlanta-Knoxville link during strong meteor showers. The agreement of predicted and experimental results for these showers has always been good. This implies that computations for sporadic meteors based on this analysis will agree with experiment provided the correct radiant distribution is used.

An approximation to the sporadic radiant distribution has been made by using three point-radiants placed respectively at the apex of the earth's way and $\pm 65^{\circ}$ in ecliptic longitude from the apex. This selection of three points was suggested by an approximate sporadic radiant distribution determined by Hawkins[4]. Numerous comparisons have been made between predicted results made on the basis of this three-point approximation and experimental data. Some of the experimental data used for these comparisons were measured over the Atlanta-Knoxville, Atlanta-Boston and Columbia-Boston meteor-scatter paths. Comparisons were also made with data published by Vogan and Campbell for a path between Greenwood, Nova Scotia, and Ottawa, Ontario[19]. The comparisons,

Figures 33 through 47, in some cases show remarkably good agreement. All comparisons show at least reasonably good agreement except for one comparison for the Atlanta-Knoxville path shown in Figure 47. The poor agreement in this case is perhaps due to the relatively small illuminated region of the h-surface which tends to emphasize the discrete nature of the assumed three-point radiant distribution. Also the experimental data for this comparison were statistically very poor.

The good results obtained with the three-point approximation imply that this approximation can be used in further research as a basis for determining where in the sky the antenna beams should be oriented in order to make the most effective use of specular reflections from the meteor trails. These predictions would be in terms of average signal rates, however, and should not necessarily be expected to apply to any one particular day. Furthermore the choice of k in the distribution of signal amplitudes may in some cases influence the best region to illuminate and more experimental work needs to be done on this problem.

APPENDICES

I

GLOSSARY OF NOTATIONS AND DEFINITIONS

English letters

a	the angle between the ecliptic plane and a vertical line
D	one-half the straight-line distance between transmitter and receiver
d	the gaseous diffusion coefficient in the region where reflections occur
f	the sum of the durations above noise of individual signals occurring per second from a square kilometer of the h-surface. The duty cycle is obtained by integrating f over the h-surface and applying a statistical correction for the overlapping of signals.
G_r and G_t	the receiving- and transmitting-antenna power gains over an isotropic radiator
g	the angle between the x-axis and the intersection of the ecliptic plane with the earth's surface
h	the height of the h-surface in kilometers above the transmitter and receiver

English letters

k	an exponent used in the formula giving the assumed distribution of trails as a function of their ionization densities
L	the assumed length of the meteor trails
$\underline{m}$	a unit normal to the ecliptic plane equal to $\underline{i}\, m_x + \underline{j}\, m_y + \underline{k}\, m_z$.
N	the number of meteor trails incident on a square kilometer of the h-surface per second having a line density greater than q electrons per meter of trail length
$\underline{n}$	a unit normal to an ellipsoid having the transmitter and receiver as foci. $\underline{n} = \underline{i}\, n_x + \underline{j}\, n_y + \underline{k}\, n_z$.
n	the number of individual signals above noise level arising from a square kilometer of the h-surface per second
n_s	the number of meteor signals per second from that part of the meteor trail zone represented by a unit length of shower locus
P_m	the minimum detectable power in the receiver
P_r and P_t	the received and transmitted powers, respectively

English letters

q	the ionization density of a trail in electrons per meter of trail length
q_o	the line density of the trail that produces the minimum detectable signal when the trail is oriented to produce a reflection to the receiver; q_o is a function of transmitter power, minimum detectable power, antenna gains and polarizations, receiving antenna aperture, frequency, and the location and orientation of the trail
R_1 and R_2	the respective distances from the reflection point on the meteor trail to the transmitter and receiver
S	the dot product of a unit incident electric vector and a unit vector of the reflected wave in the direction of the polarization of the receiving antenna. When both antennas are oriented for the maximum signal for each h-surface point, S is unity.
t	the elapsed time since the formation of a trail
w	the width of an area through which meteors that contribute to the effectiveness of a shower locus line must pass

English letters

x, y and z — the variables of a right-handed cartesian coordinate system such that the origin is at the midpoint of the straight line between transmitter and receiver, x is along the direction of this line and z is vertical

Greek letters

β — the angle between the axis of the meteor trail and the plane defined by the transmitter, receiver and the reflection point on the trail

γ — the angle between a vertical line and the M-plane. A useful formula for γ is

$$\arcsin\left[\frac{z^2(R_1 + R_2)^2}{R_1R_2(R_1 + R_2)^2 - 4R_1R_2D^2}\right]^{1/2}$$

Δ — the distance in degrees longitude from a time-zone meridian to the midpoint of the transmitter-receiver line. Eastward distances from the meridian are positive and westward distances are negative.

ϵ — the angle between the intersection of the M-plane with the h-surface and the intersection of the M-plane with the plane

Greek letters

determined by lines along R_1 and R_2. A useful formula for ϵ is

$$\arccos \frac{y}{\sqrt{y^2 + z^2 \sin^2(\phi - \lambda_1)}}$$

where

$$\lambda_1 = \arccos \frac{\sqrt{z^2 + y^2}}{R_2} .$$

ζ the angle between a vertical line and the axis of the meteor trail.

$\cos \zeta = \cos \gamma \sin (\beta + \epsilon)$.

δ the azimuth angle measured eastward from north to the direction of the transmitter-receiver line.

$0 \leq \delta < 180^\circ$

θ earth latitude of the midpoint of the transmitter-receiver line

λ the free-space wavelength of a radio wave

σ $23^\circ 27'$, the angle between the earth's axis and the ecliptic normal

τ the duration above noise of a signal from a single meteor trail

ϕ one-half the included angle between lines along R_1 and R_2

Greek letters

ψ	the nutation angle of the unit vector $\underline{m}$ as it precesses around a line parallel to the earth's axis at the midpoint of the transmission path; ψ is equal to $360.9856\ t_m$ where t_m is elapsed time in solar days since midnight of March 21 or noon of September 23.
ψ_m	a factor that determines the width of a narrow band on the celestial sphere where the radiants of the meteors piercing a given unit area of the h-surface must lie in order to be properly oriented to produce a reflection between two stations

Terms

Celestial sphere	a sphere of arbitrary radius with center at the earth and upon which the stars appear to lie
Declination	the angular distance of a point from the celestial equator. Points in the northern hemisphere have positive declinations.
Duty cycle	the fraction of time that a signal is received by meteor-trail reflection
Echo	a term referring to a burst of radio signal due to a meteor-trail reflection

Terms

Echo rate	the number of individual signals received per unit time. One signal is assumed to result from each properly oriented meteor trail of sufficient ionization.
Ecliptic	the great circle of the celestial sphere which is the apparent path of the sun
Ecliptic plane	the plane defined by the center of the sun and the path of the earth's center around the sun. This term is also used to refer to any plane which intersects the earth and which is parallel to the true ecliptic plane.
Ecliptic tangent point	a point of the meteor-trail zone at which an ecliptic plane is tangent to a spheroid having the transmitter and receiver as foci
Ecliptic-tangent-point path	the path described on the h-surface by the ecliptic tangent point as the earth rotates
First Point of Aries	a reference point on the celestial sphere which moves less than 0.014 degrees per year with respect to the stars. The sun passes through this point when moving from south to north of the equator.

Terms

h-surface	a shell h kilometers above and concentric with the earth. This surface is used to represent the meteor-trail zone.
Hour angle	the interval of sidereal time that has elapsed since a radiant (or star) was on the meridian
M-plane	the plane in which a trail must lie to present a principal Fresnel zone to a given transmitter and receiver
Meteor	a transient fiery streak in the sky produced by a meteoroid passing through the earth's atmosphere
Meteoroid	a small heavenly body that produces a meteor when it plunges into the atmosphere
Meteor scatter	a term referring to the scattering or reflecting of radio energy by means of meteor trails
Meteor-trail zone	that region of the atmosphere from about 80 to 120 kilometers above the earth's surface in which meteor trails are formed
Observable meteor	a meteor large enough to produce a radio signal of sufficient size to be observed in the presence of noise
Radiant	a point on the celestial sphere from which a meteor appears to come

Terms

Radiant distribution	a term referring to the density of meteor radiants over the celestial sphere
Right-ascension	the angular distance measured eastward along the celestial equator from the First Point of Aries to the meridian line of a point
Shower locus	a line drawn across the h-surface that represents the locus of points at which trails due to a given shower (or single radiant) are oriented to yield reflections
Shower meteors	meteors occurring on certain dates that result when the earth moves through a stream of particles all traveling approximately along the same path around the sun
Sidereal day	the length of time it takes the earth to make one complete revolution with respect to the First Point of Aries
Specular reflection	a mirror-type reflection that is essentially the resultant of reflected wavelets from the principal Fresnel zone
Sporadic meteors	meteors that have not been associated with meteor showers. These meteors account for most of the meteor influx.

II

THE DIRECTION COSINES, T_x, T_y AND T_z, OF A UNIT VECTOR IN THE DIRECTION OF A METEOR RADIANT

The direction cosines T_x, T_y and T_z of a meteor radiant can be written in terms of the azimuth angle, A (measured north to east), and the zenith angle, Z, of the meteor radiant, and in terms of the azimuth angle, B, of the transmitter-receiver line as follows:

$$T_x = \sin Z \cos (B - A)$$

$$T_y = \sin Z \sin (B - A)$$

$$T_z = \cos Z$$

If the "hour angle," H, and "declination," Dec, of the radiant are given, A and Z may be found by the formulae of spherical trigonometry. These angles may be expressed as follows where θ is the earth latitude of the midpoint of the transmitter-receiver line.

$$\cos A = \frac{1}{\cos \theta \sin Z} \left[\sin (\text{Dec}) - \sin \theta \cos Z \right]$$

$$\cos Z = \sin \theta \sin (\text{Dec}) + \cos \theta \cos H \cos (\text{Dec})$$

The coordinates of a radiant (or star) are customarily given as "right ascension," RA, and declination. The relation between RA and H is

$$H = 99.4C^{\circ} + \Delta + 0.9856\ d + 15.041\ n - RA$$

where d is the number of days since January 1, n, the number of hours since midnight, and Δ, the number of degrees that the path midpoint is east of the standard time meridian.

BIBLIOGRAPHY

1 Lovell, A. C. B., "Meteoric Ionization and Ionospheric Abnormalities," The Physical Society Reports on Progress in Physics, vol. 11, 1948; pp. 389-401.

2 Hey, J. S., "Radio Reflections from Meteoric Ionization," Nature, vol. 160, July 19, 1947; p. 74.

3 Prentice, J. P. M., "Meteors," The Physical Society Reports on Progress in Physics, vol. 11, 1948; pp. 389-401.

4 Hawkins, G. S., "Variations in the Occurrence Rate of Meteors," Astronomical Journal, vol. 61, November, 1956; pp. 386-391.

5 Hawkins, G. S., and Prentice, J. P. M., "Visual Determination of the Radiant Distribution of Sporadic Meteors," Harvard University, Cambridge, Massachusetts, Radio Meteor Research Program, under Air Force Contract No. AF 19(122)-458, Progress Report No. 19, March, 1957.

6 Whipple, F. L., "Meteors and the Earth's Upper Atmosphere," Reviews of Modern Physics, vol. 15, 1943; pp. 246-264.

7 Herlofson, N., "The Theory of Meteor Ionization," The Physical Society Reports on Progress in Physics, vol. 11, 1948; pp. 444-454.

8 Kaiser, T. R., "Radio Echo Studies of Meteor Ionization," Advances in Physics, Philosophical Magazine Supplement, vol. 2, October, 1953; pp. 495-544.

9 Eshleman, V. R., and Manning, L. A., "Radio Communication by Scattering From Meteoric Ionization," Proceedings of the Institute of Radio Engineers, vol. 42, March, 1954; pp. 530-536.

10 Pugh, R. E., "The Number Density of Meteor Trails Observable by the Forward-Scattering of Radio Waves," Canadian Journal of Physics, vol. 34, April, 1956; pp. 997-1004.

11 Hines, C. O., and Pugh, R. E., "The Spatial Distribution of Signal Sources in Meteoric Forward-Scattering," Canadian Journal of Physics, vol. 34, April, 1956; pp. 1005-1015.

12 James, J. C., and Meeks, M. L., "On the Relative Contributions of Various Sky Regions to Meteor-trail Communication," Georgia Institute of Technology, Atlanta, Georgia, Engineering Experiment Station, under Office of Naval Research Contract No. NOnr-991(02), Technical Report No. 1, June, 1956.

13 Meeks, M. L., and James, J. C., "The Effect of Radiant Distributions on Meteor-scatter Communication," Georgia Institute of Technology, Atlanta, Georgia, Engineering Experiment Station, under Office of Naval Research Contract No. NOnr-991(02), Technical Report No. 2, July, 1957.

14 Forsyth, P. A., Hines, C. O., and Vogan, E. L., "Diurnal Variations in the Number of Shower Meteors Detected by the Forward-Scattering of Radio Waves," Canadian Journal of Physics, vol. 33, October, 1955; pp. 600-606.

15 Hines, C. O., and Vogan, E. L., "Variations in the Intrinsic Strength of the 1956 Quadrantid Meteor Shower," Canadian Journal of Physics, vol. 35, June, 1957; pp. 703-711.

16 Hines, C. O., "Diurnal Variations in the Number of Shower Meteors Detected by the Forward Scattering of Radio Waves," Canadian Journal of Physics, vol. 33, September, 1955; pp. 493-503.

17 Meeks, M. L., and James, J. C., "On the Influence of Meteor-radiant Distribution in Meteor-scatter Communication," Proceedings of the Institute of Radio Engineers, vol. 45, December, 1957; pp. 1724-1733.

18 Hines, C. O., "Diurnal Variations in the Number of Shower Meteors Detected by the Forward-scattering of Radio Waves," Canadian Journal of Physics, vol. 36, January, 1958; pp. 117-126.

19 Vogan, E. L., and Campbell, L. L., "Meteor Signal Rates Observed in Forward-scatter," Canadian Journal of Physics, vol. 35, October, 1957; pp. 1176-1189.

20 Hines, C. O., "Diurnal Variations in Forward-Scattered Meteor Signals," Journal of Atmospheric and Terrestrial Physics, vol. 9, No. 4, 1956; pp. 229-232.

VITA

Jesse Clopton James was born in Florence, Alabama, on February 29, 1924. He is the son of Edward N. and Ira Denton James. He was married in 1947 to Miss Barbara Hayman of Jemison, Alabama, and has three children.

He attended public schools in Florence, Alabama, where he graduated from Coffee High School in 1941. He attended the Alabama Polytechnic Institute at Auburn, Alabama, as an undergraduate and after a year in the U. S. Army received the Bachelor of Electrical Engineering degree in 1945 and the Bachelor of Engineering Physics degree in 1946. He attended the William M. Rice Institute at Houston, Texas, for two years and received the Master of Arts in Physics degree there in 1950. His master's thesis was in the field of nuclear physics. He has attended the Georgia Institute of Technology at Atlanta, Georgia, since 1952.

His experience includes nine months as an engineer's aid with the Reynolds Aluminum Company at Sheffield, Alabama, while a cooperative student with the Alabama Polytechnic Institute. He worked two years from 1946 to 1948 for the Southern Research Institute, Birmingham, Alabama, on x-ray diffraction and spectrographic analysis and in electronic circuit development. From 1950 to 1951 he worked as a physicist for the U. S. Navy Mine Countermeasures Station at Panama City, Florida, and from 1951 to 1952 he worked at Redstone Arsenal, Huntsville, Alabama, as an electronic engineer. Since 1952 he has

worked for the Engineering Experiment Station at Georgia Institute of Technology, where he has engaged in analysis of radar systems and studies of meteor-scatter communication.